Dissertation

zur Erlangung des akademischen Grades
des Doktors der Naturwissenschaften

(Dr. rer. nat)

An Indoor Positioning Strategy based on Inertial Sensors

eingereicht
am Institut für Informatik
des Fachbereichs Mathematik und Informatik
der Freien Universität Berlin
von

Yi Sun

Berlin, 2016

Gutachter:

Prof. Dr. Jochen Schiller
Institut für Informatik
Freie Universität Berlin, Germany

Prof. Dr. Bettina Schnor
Institut für Informatik und Computational Science
Universität Potsdam, Germany

Tag der Disputation: 25. Mai 2016

Eidesstattliche Erklärung

Ich versichere, dass ich die Doktorarbeit selbständig verfasst, und keine anderen als die angegebenen Quellen und Hilfsmittel benutzt habe. Die Arbeit hat keiner anderen Prüfungsbehörde vorgelegen. Ich habe niemals zuvor ein Promotionsverfahren gehabt.

Mir ist bekannt, dass bei Verwendung von Inhalten aus dem Internet ich diese zu kennzeichnen und einen Ausdruck mit Angabe des Datums sowie der Internet-Adresse als Anhang der Doktorarbeit anzugeben habe.

Author's Declaration

I hereby declare to have written this thesis on my own. I have used no other literature and resources than the ones referenced. All text passages that are literal or logical copies from other publications have been marked accordingly. All figures and pictures have been created by me or their sources are referenced accordingly. This thesis has not been submitted in the same or a similar version to any other examination board. I never had a PhD procedure before.

Yi Sun

Berlin, den 9. Mai 2016

Abstract

The indoor scenario is also called the GPS-challenged environment due to the obstruction and accuracy reasons of the satellite based positioning methods. The current solutions to this problem are primarily resorting to the local communication networks. In this dissertation an autonomic positioning strategy is proposed, which relies solely on inertial sensors. Because of the interference immunity and unobtrusiveness of the Inertial Measurement Units (IMUs) the reliability and invulnerability of the system deserves to be enhanced substantially.

In reality certain body impulses are prompted when a pedestrian is walking. This sort of impulses would be recorded by the accelerometer in user's smartphone. Associated with the extra data sampled by other built-in inertial sensors, the motion patterns of the pedestrian are recognized, in which the length and azimuth of each step are estimated. Accordingly the current position is supposed to be updated in real-time.

Previously all of the collected data are processed by Zero Velocity Compensation Algorithm and Moving Average Filter in order to reduce the noises in advance. Subsequently, the heading angles derive from the fusion of the gyroscope and magnetometer data so that both of their advantages are produced concurrently. On the basis of the variance analysis for the azimuth and acceleration data, the stop and turning actions are detected, by which the entire walking process are divided into separate segments. In each segment the comparatively uniform step patterns are processed with the specified parameters exclusively. In addition Kalman Filter is employed to further remove the jitters in the acceleration signals. After that the steps are recognized by the successive peak-trough pairs.

Particularly, the step lengths are estimated according to two self-developed mathematical models, for walking and running respectively. The relations between the step length, frequency and variance are revealed after a multitude of experiments. The average deviation rates of both the estimation models are 10.99% and 19.66% which are superior to all of the related works.

With respect to the map matching problem, particle filter is utilized to constrain the moving trajectory to the physical surroundings. Moreover, the uncertainties caused by gesture changing are

expected to be eliminated by this probabilistic algorithm to a great extent. In the same experiment scenario by applying particle filter, the average deviation declined from 1.96 m to 1.21 m. Therefore the accuracy is improved by 38.27%. With the physical layout information, the positioning results would be rectified as well.

Eventually the digital barometer is selected for floor detection. In comparison this scheme demonstrates stronger operability than the previous solutions. On the basis of the statistics, the effectiveness of the approach reckoning the relative altitude from atmospheric pressure is able to maintain for more than 10 minutes. As a result, with a few calibrations the indoor positioning system is extended to the multi-storied scenarios.

Zusammenfassung

Das indoore Szenario wird die GPS-herausgeforderte Umwelt genannt wegen der Nachteile z.B. die Blockierung und Genauigkeit in den satelite-bezogenen Positionierungsmethode. Die aktuelle Lösungen der Probleme sind sich an die lokalen Kommunikationsnetzwerke zu wenden. In dieser Dissertation wird eine autonome Positionierungsstrategie hervorgebracht, die sich lediglich auf die Inertialsensoren stützt. Wegen der Störfestigkeit und Unaufdringlichkeit der Inertialsensoren, werden die Zuverlässigkeit sowie Unverwundbarkeit des Systems sich erheblich verbessert.

Tatsächlich werden einige Impulse des Körpers angeregt während ein Fußgänger geht. Diese Impulse werden von dem Beschleunigungssensor im Smartphone des Benutzers verzeichnet. Mit den Daten aus anderen eingebauten Inertialsensoren, werden die Bewegungszustände des Fußgängers erkannt, damit die Länge sowie der Azimut jedes Schritts errechnet werden. Demgemäß wird die Echtzeitposition kontinuierlich aktualisiert.

Zuallererst werden alle sammelnde Daten vom Zero Velocity Compensation Algorithmus und gleitenden Durchschnitt-Filter bearbeitet, um das Rauschen im Voraus zu reduzieren. Anschließend stammen die Steuerkurswinkel aus der Datenverschmelzung vom Gyroskop und Magnetometer, um beide Vorteile gleichzeitig auszunutzen. Nach der Varianzanalyse für die Azimute und Beschleunigungen, werden die Bewegungen z.B. die Stopps und Abbiegungen detektiert, damit der ganze Ablauf des Gehens in getrennten Abschnitte geteilt wird. In jedem Abschnitt werden die relative gleichförmige Schrittmuster mit den spezifizierten Parametern bearbeitet. Außerdem bürgert Kalman Filter sich ein, um die Grate im Beschleunigungssignal weiter zu entfernen. Danach werden die Schritte anhand von den aufeinanderfolgenden Gipfel-Tal Paare erkannt.

Insbesondere, jeweils für Gehen und Laufen werden die Schrittlänge mit zwei selbst-entwickelten mathematischen Modelle errechnet. Die Beziehungen zwischen die Schrittlänge, Frequenz und Varianz werden nach einer ansehnlichen Menge Experimente entdeckt. Die durchschnittliche Abweichung-Raten von beiden Modelle sind jeweils 10.99% und 19.66%, die vorzüglicher als alle bisherige Modelle sind.

In Hinsicht auf das Problem über die Kartenanpassung, wird Particle Filter verwendet, um die Bewegungsbahn auf die physikalischen Umgebungen zu schränken. Ferner werden die Ungewissheiten von diesem Wahrscheinlichkeitsalgorithmus in großem Maße abgebaut, die von den Gesteveränderungen verursacht werden. Beim Experimentalszenario, mit Particle Filter anzuwenden verringert die durchschnittliche Abweichung sich von 1.96 m auf 1.21 m. Deshalb erhöht die Genauigkeit sich um 38.27%. Die Informationen über den Grundriss und die Einrichtung können auch behilflich sein, die Positionierungsergebnisse zu berichtigen.

Zum Schluss wird der digitale Barometer für die Geschosse zu erkennen ausgewählt. Im Vergleich zu den vorherigen Lösungen zeigt das Verfahren mit Barometer die bessere Bedienbarkeit. Nach den Statistiken kann die Validität der Verfahrensweise für länger als 10 Minuten behalten, die relative Höhe mit dem Luftdruck einzuschätzen. Infolgedessen, mit einigen Kalibrierungen kann das Indoorpositionierungssystem sich auf den mehrgeschossigen Szenarios ausbreiten.

Acknowledgements

Almost 5 years have passed by, I can still very clearly remember the moment I received the offer from Prof. Dr. Jochen Schiller on Dec 29th 2010. After 8 months, with full of hopes and expectations I stepped my foot on the land of Berlin. The first a few days in a new country were always filled with freshness and excitements. Among the university and German language school a whole new stage of my life was opened up. Gradually some questions arose in my mind: what is the key factor makes Germany to be a highly developed country? In other words, as a super industrial powerhouse, which trait in Germany is the most worthy of our learning?

Over 100 years ago a reputable Chinese philosopher, Hu Shih, wrote an article titled “Discussion about the disadvantages of studying abroad”. The answer could be partly summarized from his analyses. Besides, a couple of problems in the academic circle 100 years ago are also found in China today: quite a few Chinese students never have any through in the long run. They choose the foreign institutes whose requirements for Degrees are lower; engage in the research topics on which it is easier to publish papers. Their aim is not to learn the most advanced and frontier knowledge from the western countries but to get the foreign certifications as convenient as possible and exchange for decent lives in China.

I tried my best to avoid that disgraceful situation. For study, I chose a less theoretical subject: analyzing the human’s kinetic characteristics with inertial sensors and applying it in the positioning field. I considered it has more practical significance. But this is an application-oriented topic, hence, on one hand, there is less mathematical reasoning, so comparatively it is not apt to produce papers; on the other hand, it needs a great deal of experiments as well as programming. In life, I attached German course in the first 2 years and employed any chance to integrate into the local community, even made a presentation in German in my research group. From my point of view, it is quite lamentable for the international students to stay in Germany for 4 years but speak no German. They restrict themselves within their own cycle, graduate and return as soon as possible, and the solely gain is the diploma.

To live a more meaningful life, one must try something different. Surely the expenses were also greater. The German course took me every evening in the first 2 years which could be used to read literatures. In order to implement a real app on smartphone so that my research findings would be easier available and serve the public well, I had to spend several months on learning Swift (a new programming language for iOS). During this period my peers were writing their dissertations. Particularly to develop my own mathematical models I performed a multitude of experiments. These experiments lasted for 5 weeks and the data processing cost me 3 entire months! The amount of exercises for all kinds of walking, running and stair climbing experiments were around 100 km in all! I'm fully aware, that should be the right way doing research: only after a huge amount of experiments the true principle might be revealed. The procedure was extremely lonely, helpless and a little desperate, especially for a middle age in a foreign country far from hometown. One must undergo it and there is no way to avoid. Only with full concentration in the long term, never being conceited and impetuous, it would be possible to open the door to the truth. I argue that it is the main deficiency in the current Chinese academic circle. According to the statistics that at present all over the world more than 70% SCI papers' first author are in Chinese names. Obviously Chinese academicians are numerous and good at publishing papers. But that is not equivalent to a high scientific and technological level in China. The similar reason applies to the weaknesses of the advanced manufacturing area and football as well. With perseverance and tolerance, refusing complaint or explanation, is the indispensable trait to get great achievement. Frankly speaking I'm gratified that I had the opportunity to experience the real scientific research once.

I'm lucky that the results of the experiences were positive. Although they were not so wonderful to draw an overwhelming conclusion or apply a patent, fortunately a dissertation could be based on them adequately. Due to the time-consuming works mentioned above, my first paper was accepted in the 3rd year. But after my self-developed models were finished, I published 4 papers this year. Especially in June I showed my demo app at the presentation of ICL-GNSS in Gothenburg Sweden. Although I had worked around the clock continuously for several months, the appreciations from the audiences convinced me that all of these efforts were worthy. Here I wish to express my gratitude to my supervisor Prof. Schiller again. Thank him for so kindly supporting me to participate in 4 conferences this year.

Generally I'm a slow starter. The majority of my fruits were born in the final phase. When I first arrived I had much confusion. Thank Prof. Dr. Katinka Wolter and Prof. Dr. Marcel Kyas. They are other professors in my research group and also offer me lots of beneficial guidance. Thank my colleagues Jialu Hu, Yubin Zhao, Yuan Yang, Huaming Wu, Qiushi Wang, Norman Dziengel, Marco Ziegert, Martin Seiffert, Stephan Adler, Alexandra Danilkina and Simon Schmitt (the sequence is

according to the first time we met). They provided me valuable advices when I had troubles and always help me conquer the difficulties, either in life or in study. With their effective assistances I avoided many detours. In my research, a multitude of algorithms together with mathematical models about human activities recognition were studied in detail. Together with the skill of developing apps on iOS devices, a whole new horizon in the field of the wearable smart consumer electronics has already been opened up in front of me. By means of the endeavors and attempts during these years, I'm fully confident that I could achieve more in this really promising field. In view of the fact that my study program in Germany is about to end, I feel a little sorry. At this moment the lyric of the soundtrack in an Indian movie "3 Idiots" comes to my mind:

Give me some sunshine

Give me some rain

Give me another chance

I wanna grow up once again...

With respect to my personal life, I'd like to thank my dear parents. But unlike others who only thanks with words, I thank them with actions. In the summer of 2014, I invited my parents to visit Germany. Someone felt that was unnecessary. Formerly I heard a few words from an elder. He said to the Chinese youths: "If you came from countryside and found a job in big cities like Shanghai, Beijing or Shenzhen. I suggest you invite your parents from village to visit the city you work once. For you it doesn't cost a lot time and money. You can never rewrite your destiny. But for your parents it would be a treasurable memory in their whole lives." After some experiences, I cannot agree more. Correspondingly I invited my parents to Berlin. Although it spent a whole month during the key period of my research, I regard it as the most right decision I've ever made in these 4 years.

In China there was an influential historian named Ji Xianlin. During WWII he studied in Göttingen. Afterwards he wrote his stories from 1935 to 1945 in a book "The ten years studying in Germany". In my college days I was fascinated by his interesting, marvelous, and though-provoking experiences. Fortunately I also had my own opportunity to spend several years studying abroad, which has opened a new window in my brain. I desire to thank China Scholarship Council (CSC) and Prof. Schiller again, thank them for giving me this precious chance to see the world, so that I could get more profound and insightful understandings toward certain issues than people who never saw outside or only spent several weeks or months for visit or exchange.

During these 4 years I have grown up a lot, not only in academics but also in all aspects. Studying abroad is about so much more than improving my own future. It's also about shaping the future of my country and of the world we all share. I also want to say thanks to the memorable and adventurous experiences during these years. They gave me a clear perspective of what I ought to do

with my life and why. Finally I'd like to post a photo taken at the fjord in north Europa. I hope it can inspire the people in struggles: when you feel like giving up, remember why you held on so long in the first place. I'm a great believer in luck, and I find the harder I work, the more I have of it.

Maybe the journey is really long, maybe the journey is uncommonly arduous, but the world in my eyes is unimaginable fabulous.

Sun, Yi
on Oct 28th 2015 in Berlin

Contents

Abstract i

Acknowledgements v

1 Introduction 1

1.1 Background . . . 1
1.2 Related Works . . . 2
1.3 Inertial Measurement Units . . . 4
1.4 Dissertation Structure . . . 7

2 Design of the Positioning System 9

2.1 System Architecture . . . 9
2.2 Pre-process for Sensor data . . . 12
2.2.1 Accelerometer . . . 13
2.2.2 Gyroscope . . . 16
2.2.3 Coordinate Transformation . . . 20

3 Step Recognition 23

3.1 Sensitive Component . . . 23
3.2 Zero Velocity Compensation (ZVC) . . . 25
3.3 Moving Average Filter . . . 28
3.4 Divide and Conquer . . . 30
3.4.1 Recognition for Start-up and Stop Actions . . . 31
3.4.2 Recognition for Turn Actions . . . 33
3.4.3 Evaluation . . . 37
3.5 Kalman Filter . . . 41

3.6 Step Recognition . . . 48
3.6.1 Related Works . . . 48
3.6.2 Peaks and Troughs Detection . . . 49
3.7 Alternative Scheme . . . 54
3.7.1 Model Wave Simulation . . . 54
3.7.2 Evaluation . . . 56

4 Walking Step Length Estimation Model **57**
4.1 Related Works . . . 57
4.1.1 Static Models . . . 57
4.1.2 Dynamic Models . . . 58
4.2 Walking Step Length Estimation Model . . . 61
4.3 Evaluation for the Model . . . 75
4.4 Implementation of the Application . . . 79

5 Running Step Length Estimation Model **83**
5.1 Related Works . . . 84
5.2 Running Step Length Estimation Model . . . 88
5.3 Evaluation for the Model . . . 98

6 Particle Filter **103**
6.1 Background . . . 103
6.2 Map Matching . . . 104
6.3 Evaluation . . . 106

7 Enhancement of the Functions **109**
7.1 Distinguish between Walking and Running . . . 109
7.2 Altitude Detection . . . 111
7.2.1 Related Works . . . 111
7.2.2 Accelerometer based Solution . . . 113
7.2.3 Barometer based Solution . . . 117
7.2.4 Evaluation . . . 121

8 Conclusion and Future Works **123**
8.1 Contributions and Conclusion . . . 123
8.2 Future Works . . . 124

Bibliography **126**

List of Figures **135**

List of Tables **142**

List of Publications **144**

About the Author **146**

Chapter 1

Introduction

1.1 Background

Nowadays a wide variety of positioning techniques change our modern life dramatically. The popularization of the portable devices has brought this area new opportunity. Together with navigation, a growing number of smartphone applications in terms of Location Based Service (LBS) received a considerable success. With respect to outdoor navigation, Global Navigation Satellite Systems (GNSS) such as GPS, Galileo, GLONASS and Beidou [1], along with cellular techniques are current common solutions.

However, as far as indoor or underground scenarios are concerned, these techniques appear to some degree inadequate. Normally the accuracies of satellite or cellular network based techniques are more than 10 meters which is completely unacceptable. With so rough a precision to track a target within a building and distinguish among rooms is not in any way realistic. Not merely the sensitivity is less than satisfactory, but also the signals from them are either blocked by building or ground, or severely affected by multipath propagation.

Meanwhile, indoor positioning receives more and more attentions in recent years. Statistics show human averagely spends over 70% time on indoor activities in modern life. Along with the booming of various terminal devices, indoor positioning becomes a really promising field and the relevant applications based on smartphones, tablets, and other wearable objects are sprouting up in every aspect of the informative life. For example, electronic guidance in a museum or an exhibition hall cannot merely display the information according to visitors' real-time location, but also show the way to where they would find, such as ATM, WC, lift or exit [2] [3] [4]. In the area of smart living and office, the attendances for a meeting, etc., can be identified and registered unobtrusively. When

people arrive at a certain room or area, the projector and lighting or any other supporting facilities could be activated automatically. Commercially it would also make advertising in a shopping mall more targeted and efficient. With the app installed in customers' smartphones or on shopping carts, the sale information could be provided for the potential customers directly according to the location data. In the future storehouses the indoor positioning techniques could make the physical distribution management more intelligent and would be an indispensable component in Internet of Things (IoT) [5] [6].

1.2 Related Works

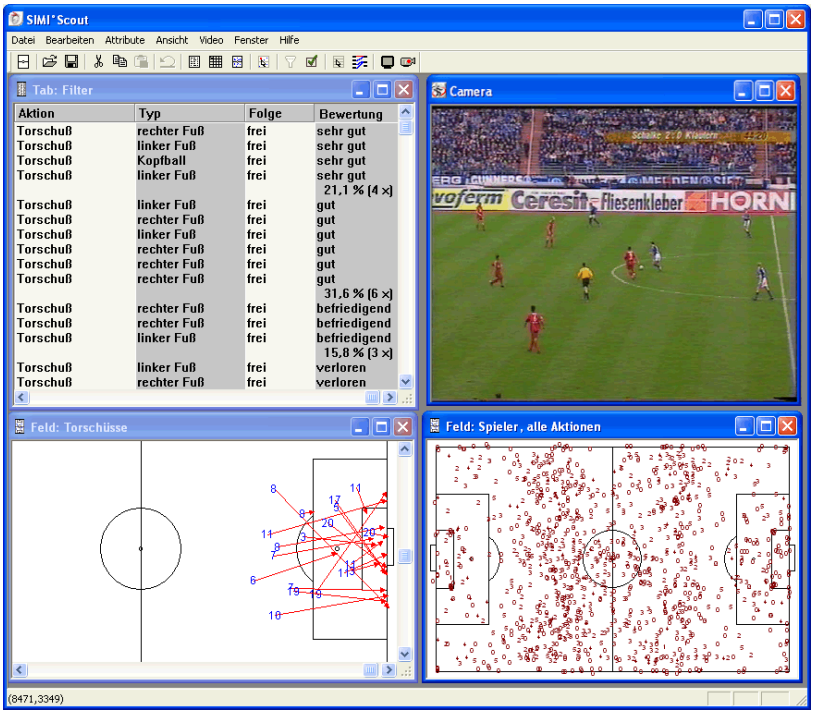

Figure 1.1: According to the real-time video, the sport assistance software SIMI Scout records the player's position as well as moving trajectory, in order to provide the reliable data support for the coach when tactics analysis and decision making. This is an instance of the vision-based positioning approach.

Concerning the GPS challenge scenarios referred to above, numerous indoor positioning techniques are implemented in the latest two decades. Vision-based systems are well-publicized choices in surveillance and could be used for position tracking [7] [8]. Because the positioning methods from

video analysis are considered accurate and real-time, they are taken advantage of in many assistance systems, especially in sport recording and statistics, as shown in Fig. 1.1 [9] [10] [11]. However, the images caught by cameras would easily be sheltered from people's bodies or other objects. Besides, some of vision-based approaches rely on the installation of beacons [12] [13] [14]. Meanwhile it has high requirements in the light intensity and the distribution of cameras. The limitations also lie in the comparative expensive equipment and sizable data amount of optical flow.

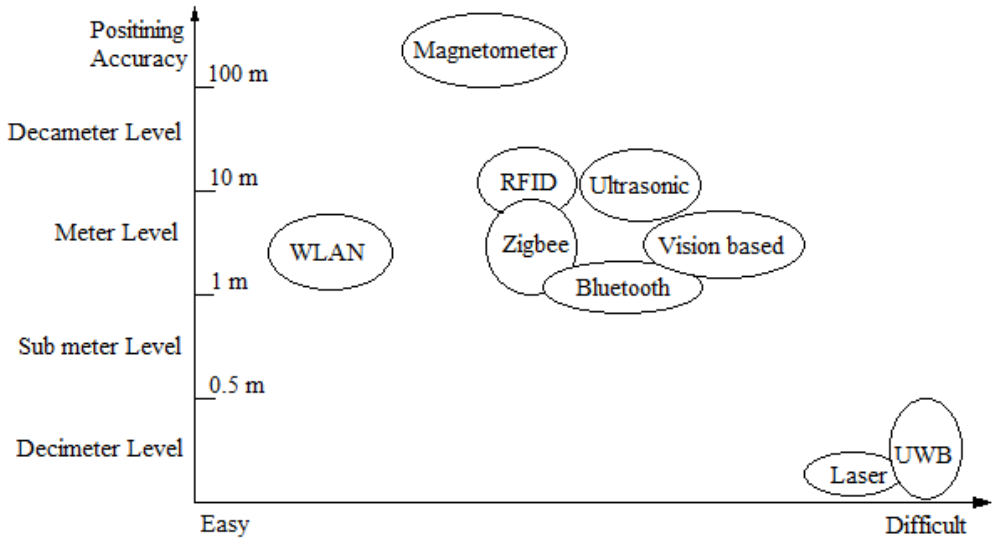

Figure 1.2: The comparison of accuracy among different positioning schemes

The similar drawbacks are found in the ultrasound and infrared method as well [15] [16]. The techniques of Radio Frequency Identification (RFID) are attempted in some experiments [17] [18], but few of them can stably achieve the required meter-level accuracy in the mentioned scenarios above. Researchers recently are more likely to employ Wireless Local Area Network (WLAN) based technologies [19] [20] [21]. The radio strength fingerprint in a certain building is analysed statistically. There are numerous literatures discussed the improvement about it [22] [23]. By means of some mathematical statistics methods, the positioning accuracy could be lower than 2 meters, which is quite satisfactory for indoor scenarios [24] [25]. But the complete Wi-Fi cover in the target building as well as the real-time interaction between the users' device and the hot spots is necessary. If there is no available Wi-Fi access point, or some access points are out of order temporarily, the WLAN based schemes will also be ineffective. Bluetooth or Zigbee based solutions are proved feasible in some experiments [26] [27]. In certain scenarios the accuracies are so satisfactory that these

Wireless Personal Area Network (WPAN) techniques are regarded as the most ideal solutions for shopping malls or exhibition halls. Basically high density equipped beacons are necessary undoubtedly. Moreover, their positioning effects are also strongly associated with the realistic environments. Even the pedestrian volume could influence the performance to a great extent. In conclusion all these schemes are compared in Fig. 1.2.

Especially in some extreme situations, such as rescue missions in a damaged architecture after an earthquake or conflagration, or archeological and scientific expeditions in a cave or underground where the navigation signals from satellite or cellular network are usually unavailable and the extra infrastructures such as WLAN are insufficient, some alternative self-contained strategies which do not rely on external signal have to be developed to continue tracking people's position.

1.3 Inertial Measurement Units

One feasible solution is taking advantage of Inertial Measurement Unit (IMU). Because of its independence, IMU has been chosen for navigation systems several decades ago [28] [29]. On account of its autonomy and interference immunity, IMU-based schemes are an ideal complementarity to current Local Positioning System (LPS) when communication signals are lacking. First and foremost, IMU needs neither passive nor positive interaction with external signals, thus it possesses superb unobtrusiveness and is invulnerable to Electromagnetic Interference (EMI). Besides, it can work all-weather and in all environments no matter outdoor or indoor, with or without shelter, in the air, underground or underwater where the satellite or WLAN based schemes are not always effective. Moreover, it cannot solely provide the location information of the devices but also some additional parameters e.g. real-time azimuth and attitude. Last but not least, compared with the schemes using communication signals, the positioning result from IMU shows better continuity, higher short-term precision and more stability. Along with the development of Micro Electro-Mechanical System (MEMS), IMU will be more portable and affordable, and would be a common component in the consumer electronics.

With respect to Inertial Navigation System (INS), a great number of methods have been discussed special for pedestrians [30] [31] [32]. Theoretically, the displacement can be calculated directly by taking the double integral of acceleration over time. There are experiments of taking inertial sensors in hand and walking through a square path whose side-length is 10 meters [33]. From Fig. 1.3, the deviation becomes larger and larger along the time (the sampling data are also filtered by several filters). Actually it must be admitted that the precision and sensitivity of IMU in usual electronics are limited due to the comparative low price. Because of serious drifts, the results from double

integrals in most situations are nothing more than rough sketches.

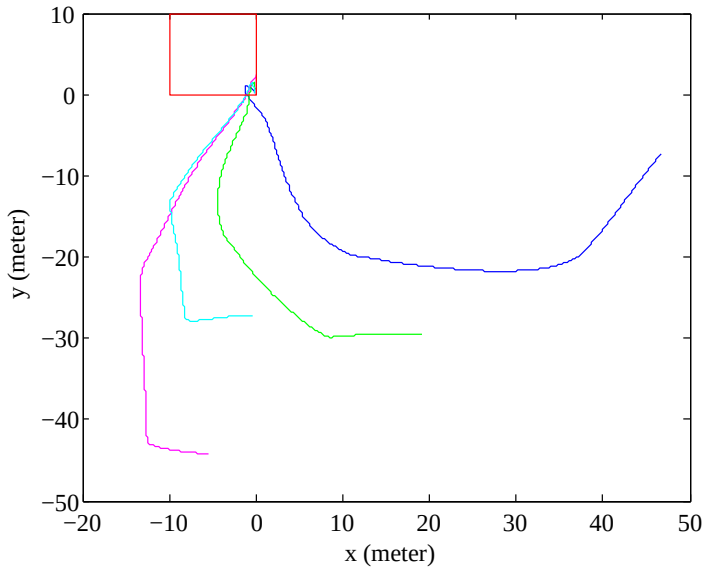

Figure 1.3: The effect of double integrals of the acceleration measured by commercial IMU. The red square is the real walking path whose side-length is 10 meters; the other 4 curves are the trajectories calculated by double integral. The drifts are rather serious.

However, the commercial IMUs with low price and limited accuracy are never useless. With these available accelerometers, gyroscopes and magnetometers in current smartphones, a wealth of brilliant apps were also developed. Many of them implemented some pretty practical functions just by capitalizing on these inexpensive sensors sensibly. Although the displacement from directly integral is invalid, from the acceleration signals generated by pedestrian's walking, a multitude of useful information could be extracted as well.

From Fig. 1.4, every step when walking can stimulate obvious discrete impulse in the acceleration signal. With these acceleration impulses not singly the steps can be count, but also the length of each step could be estimated. Besides, according to the heading direction during each step, the current position could be updated continuously. This strategy is called Pedestrian Dead Reckoning (PDR) [34] [35] which is a process of calculating one's current position by using a previously determined position, and advancing that position based upon known or estimated speeds over elapsed time and course. Inspired by the idea of PDR, an indoor positioning approach can be proposed. This approach is more likely to implement a Step and Heading System (SHS) [36] [37] which tracks the real-time position by each new step measured with IMU.

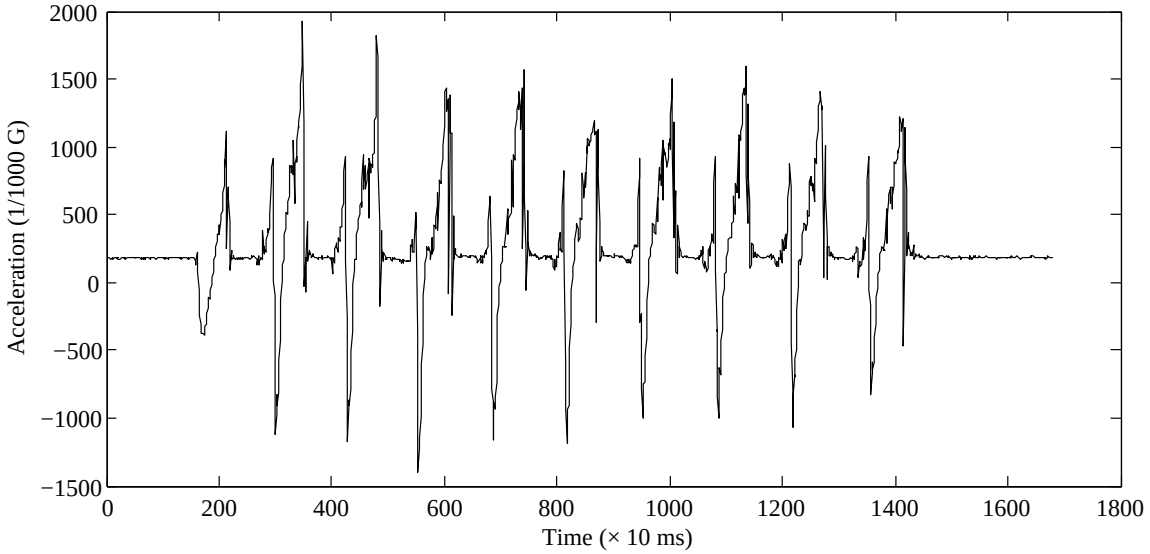

Figure 1.4: The raw acceleration recorded by IMU when pedestrian is walking. A volunteer holds the accelerometer in hand and walks for 10 steps. The plotted data is the module of the accelerations in all 3 axes. It is remarkable that each impulse is corresponding to a single step.

Therefore an indoor positioning strategy is presented in this dissertation, which lies solely on the build-in inertial sensors within the smartphones (or other portable devices). In the subsequent chapters the determination for the azimuth, the differentiation between walking and running, the recognition of climbing stairs or riding an elevator, together with the mathematical models for estimating the step length will be discussed respectively. The result from this strategy could serve as one complementary data source to improve the stabilization and accuracy of the current positioning system. Since the PDR scheme sourced from path integration, theoretically the positioning result is subject to cumulative errors and each tiny deviation would be amplified along the time. This strategy is hardly qualified for the long term positioning and navigation solely. Ideally this IMU based scheme could cooperate with other communication signals based schemes. On the one hand, other schemes could provide the initial position and calibrate the drifts and cumulative errors from the inertial sensors; on the other hand, IMU can extend navigation into areas where mainstream positioning systems are problematic. When the external navigation signal such as GPS or WLAN is temporarily unavailable or sometimes unreliable, this strategy can be adopted to maintain the performance of the whole system independently. Due to the invulnerability of IMU, more reliable result of position tracking can be achieved.

1.4 Dissertation Structure

Fundamentally this dissertation consists of 8 chapters. These chapters are organized as follows:

In Chapter 2 the framework of the positioning system is elaborated. Particularly, as the key inertial sensors, the structures of accelerometer and gyroscope are described respectively.

In Chapter 3 the pre-processing of the sampled data is introduced, including a variety of filters. Accordingly step recognition is performed.

In Chapter 4 the development of the mathematical model for step length estimation is explicated in detail.

In Chapter 5 the mathematical model special for running step length estimation is proposed as well, by which the system is compatible with multi pedestrian activities.

In Chapter 6 particle filter is employed to implement map matching. Concurrently the accuracy of positioning are further improved.

In Chapter 7 two more functions are added to the system: firstly, distinguishing between the human behaviors of walking and running; secondarily, detecting the floor number in a multi-storied scenario.

In Chapter 8 all of the research in this dissertation is summarized and a few future works are therefore discussed.

Recap

In this chapter the background of Indoor Positioning technology is introduced. Towards this subject numerous current solutions are described and compared briefly. Furthermore, the strategy based on inertial sensors is proposed. Both the advantages and disadvantages are discussed respectively. From the comprehensive elucidations, this IMU Strategy is expected to serve as one complementary method to improve the performance of the current positioning system.

Chapter 2

Design of the Positioning System

2.1 System Architecture

Primarily my work is implementing a Step and Heading System (SHS). According to the details of each step such as the length as well as the heading angle, the current position of pedestrian is supposed to be tracked. When a pedestrian is walking, some vibrations of the body would be stimulated by stepping. Basically these vibrations could be sensed by the accelerometer within the wearable devices, such as smartphone. From these vibration waves in the acceleration signals, certain feature vectors are expected to be extracted. Accordingly the step lengths could be estimated on the basis of these feature vectors. Meanwhile the heading angles are measured by the gyroscope and magnetometer. Their different properties are complementary to each other appropriately so that the most reliable azimuth parameters would result from the data fusion. On top of that, the altitude related information such as determining in which floor the user is, or whether climbing stairs or riding an elevator, are analysed from the barometer which can record the atmospheric pressure locally. With the air pressure the relative altimeter could be reckoned. Nowadays barometer is increasingly popular and can be found in a growing number of consumer electronics. Last but not least, to constrain the moving trajectory to the physical surroundings, Particle Filter (PF) is employed finally. As a supplementary solution Particle Filter can not only correct the trajectory but also deal with the instabilities by gait transition and gesture changing.

Fig. 2.1 shows the general view of this positioning system.

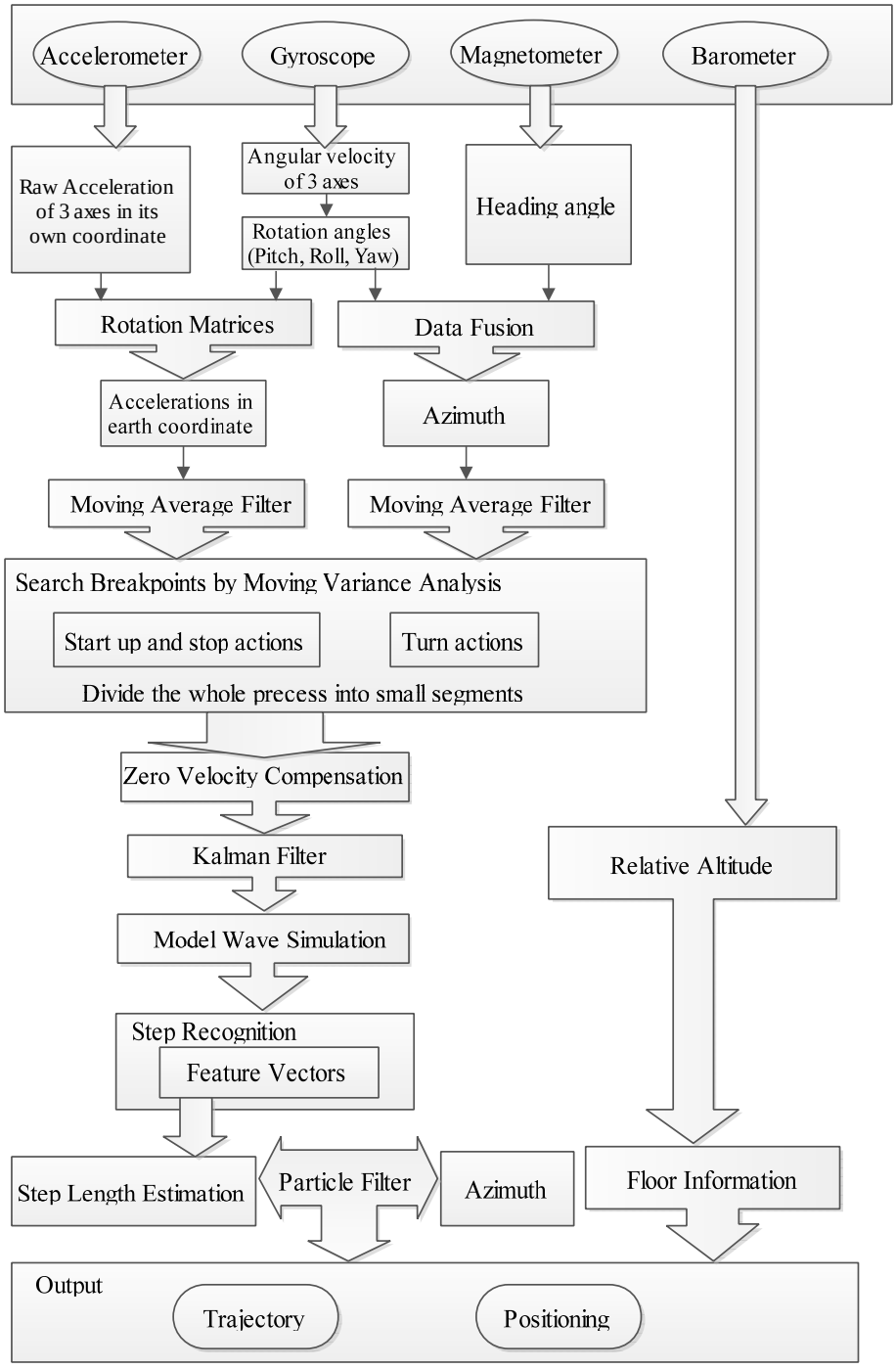

Figure 2.1: The general view of the positioning system

The whole system, from the subject determination, then to requirements analysis, eventually to the products implementation, takes more than 4 years. All the procedures as well as workflow are illustrated in Fig. 2.2, theoretically to practically.

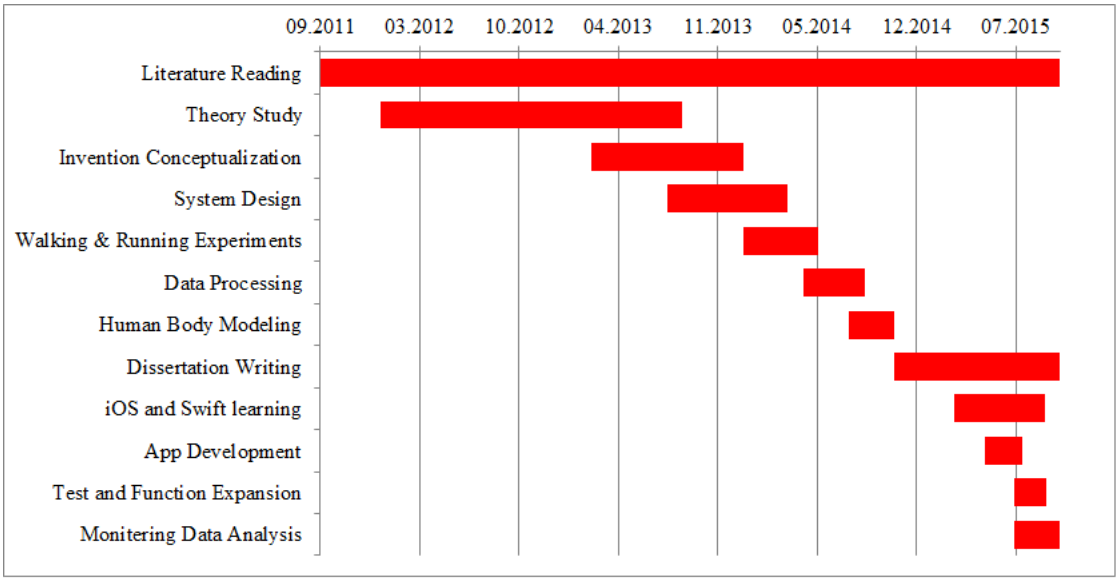

Figure 2.2: The workflow of developing the positioning system. Foremost it is the preparation stage to make acquainted with the current positioning methods and theories. The most crucial stage is developing the novel mathematical models for step length estimation so that the accuracy for positioning could be improved substantially. Lastly a set of real-time software based on smartphones is implemented as the final products.

From the progress chart shown in Fig. 2.2, the theoretical preparations take most of the time, virtually the first half of the schedule. Secondarily deducing the walking and running models for pedestrians is the part of great concern in my research, which was from the beginning of 2014 to the end of October 2014. Solely the experiments for all sorts of gaits lasted for 5 months. The achievements in these 10 months are the highlights of this dissertation, which are described in Chapter 4 and 5. Most of the theoretical works have been finished by the end of 2014. The rest time is used for implementing the real-time positioning systems which are a series of apps running on iPhone or iPad (iOS only), so that the results of my research could not merely be verified in the off-line simulations but also be tested as real products. The advantages and superiorities of the mathematical models as well as the discovered theories would be demonstrated more explicitly and convincingly.

2.2 Pre-process for Sensor data

As shown in Fig. 2.3, normally the smartphone is handled in an uncertain attitude, no matter it is taken in hand or put in pocket. Since the accelerometer can only measure the real-time tri-axial accelerations in the coordinate system of smartphone itself (red in Fig. 2.3), to draw the walking trajectory in the standard earth-fixed coordinate system (blue in Fig. 2.3), the accelerations in 3 axes must be converted to the earth coordinate. Besides, only the specific force is expected to be involved in further process. Specific force is not actually a force, but a type of acceleration. It is defined as the non-gravitational force per unit mass. This (mass-) specific force is not a coordinate-acceleration, but rather a proper acceleration, which is the acceleration relative to free-fall. Forces, specific forces, and proper accelerations are the same in all reference frames, but coordinate accelerations are frame-dependent. For free bodies, the specific force is the cause of, and a measure of, the body's proper acceleration. Therefore the gravity acceleration should be removed from the sampling data.

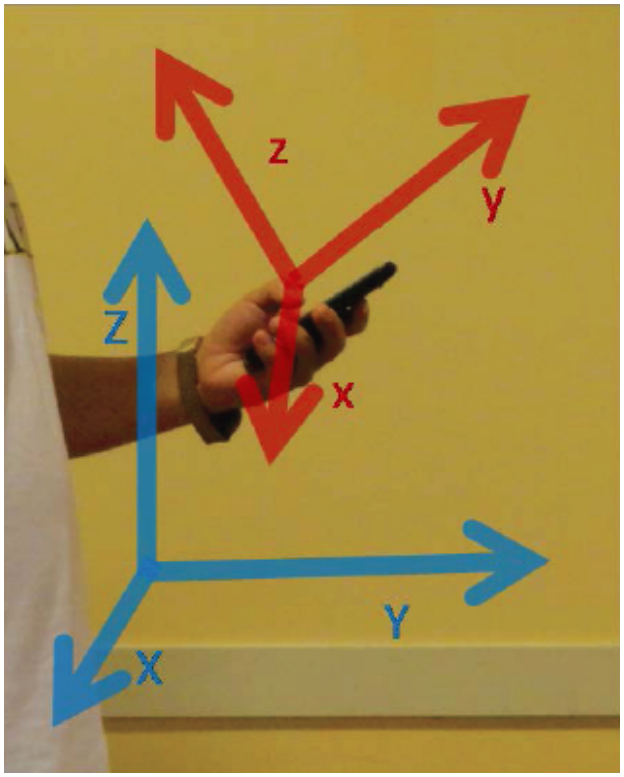

Figure 2.3: The accelerometer samples data in its own coordinate system (red). The raw data need to be transformed to the earth coordinate (blue).

As Fig. 2.4, in this dissertation, the positive directions of the 3 axes and 3 rotation angles of smartphone are also defined conventionally.

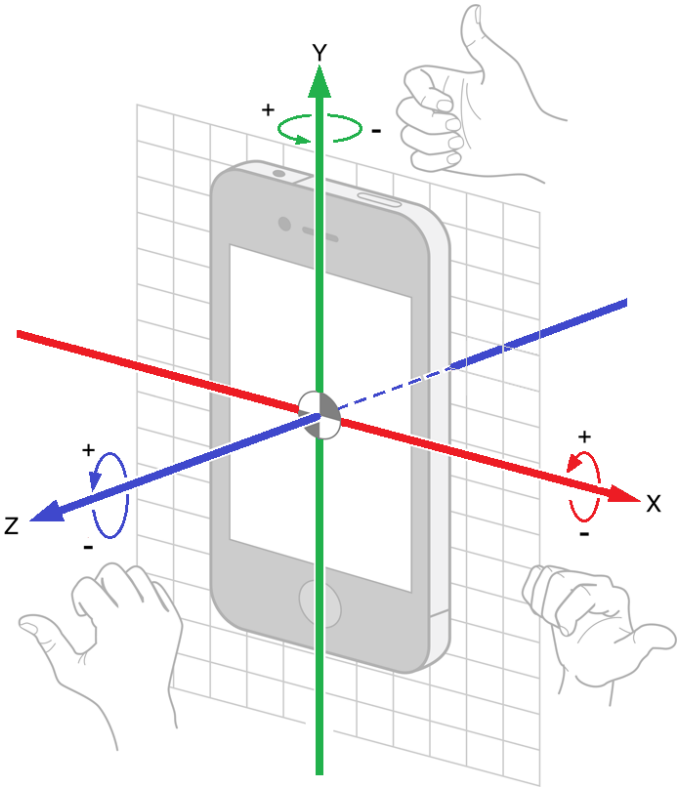

Figure 2.4: The positive directions of 3 axes of smartphone.

The positive direction of x-axis: from left to right. The positive direction of y-axis: from home button to top side. The positive direction of z-axis: from bottom to up. And the rotation directions around 3 axes follow the right hand rule.

2.2.1 Accelerometer

An accelerometer is a device that measures proper acceleration ("g-force"). Accelerometers have multiple applications in industry and science. Highly sensitive accelerometers are components of Inertial Navigation Systems (INSs) for aircraft and missiles. Accelerometers are used to detect and monitor vibration in rotating machinery. Accelerometers are used in tablet computers and digital cameras so that images on screens are always displayed upright. Along with the development of Micro Electro-Mechanical Systems (MEMSs), accelerometer becomes more inexpensive and compact.

Nowadays it is one of the most common sensors in numerous wearable devices.

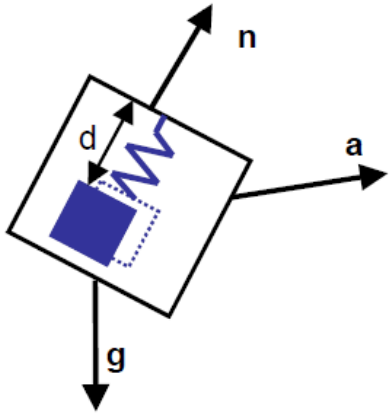

Figure 2.5: A simplified schematic diagram for a single axial mechanical accelerometer. The magnitude of acceleration in the sensitive direction can be calculated by the variation in the spring's length. The principle in the electronic accelerometer is similar.

From Fig. 2.5, theoretically an accelerometer consists of a mass, suspended by a spring. The mass is allowed to move in the sensitive direction of the accelerometer. As Hooke's Law and Newton's Second Law of Motion (described in Eq. 2.1), the distance d of the mass with respect to the sensor housing is measured and is a function of acceleration and the direction of gravity with respect to the direction of distance measurement. The unit vector n represents the sensitive axis of the sensor.

$$Hooke's\ Law: \qquad F = -kx,$$

$$Newton's\ second\ Law\ of\ Motion: \ F = ma, \tag{2.1}$$

where F denote the force; k is a constant factor characteristic of the spring, its stiffness; m indicates the mass and a the acceleration.

Concerning the multi-axial accelerometer, as Fig. 2.6, for simplification, it works with a cube-like mass inside (maybe more than one, each in every direction, or not a mass but can response to force with electrical signal). The pressure around the 6 sides can be detected when accelerating. For instance, when static, only bottom side is pressed, so an acceleration of G in the direction points to bottom (negative direction of z axis) is measured.

Because the gravity acceleration can be regarded as a Direct Current (DC) component among the

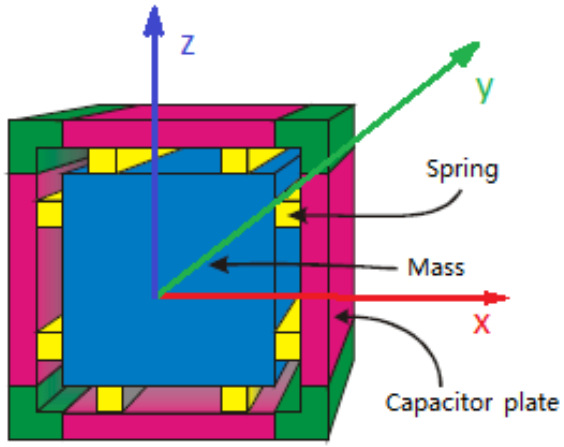

Figure 2.6: A simplified schematic diagram for a tri-axial accelerometer

sampled acceleration signals, whose value is constantly 9.8 m/s^2 and points down, theoretically it could be removed by a high pass filter. According to the methods mentioned by [38] and [39], this high pass filter can be implemented by Eq. 2.2.

$$acc_{HP\_avg} = acc_{new} \times (1 - \alpha) + acc_{HP\_avg} \times \alpha,$$

$$acc_{HP\_filtered} = acc_{new} - acc_{HP\_avg}, \tag{2.2}$$

where $acc_{HP\_filtered}$ denotes the results after high pass filter; acc_{new} and acc_{HP_avg} are the new sampled acceleration and the average value of before, respectively; α indicates the weight between new data and historical data. In experiments α is set as 0.9 empirically, which means the preceding data count more.

Obviously the high pass filter described in Eq. 2.2 is by no means meticulous. Actually it is merely an expedient if there is no gyroscope available in the system, solely the accelerometer can be relied on. In my former experiments due to the shortage of gyroscope, the attitude of device could be hardly measured, hence this method is made use of to calculate the proper accelerations with limited precision. At present a more accurate algorithm based on gyroscope is applied and the detail is elaborated in Section 2.2.3.

It is worthwhile to note that sometimes the values' directions recorded by accelerometer should be inverted. That is attributed to the principle of accelerometer [40]. When accelerating, for instance, moves to right suddenly, the acceleration should be in positive x direction (in Fig. 2.6). However, in

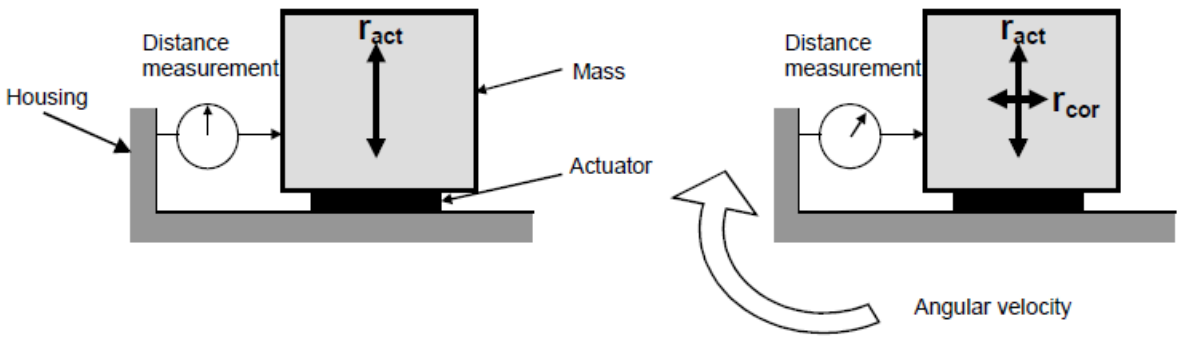

Figure 2.7: A simplified schematic diagram for a MEMS gyroscope in 2D view

this process, the left side is pressed at the beginning, therefore the acceleration detected is pointing left. This phenomenon is also verified in the experiments.

Ultimately after remove the gravitational component, the acceleration values measured in 3 axes have to be also made opposite.

2.2.2 Gyroscope

Traditionally gyroscope is a spinning wheel or disc in which the axis of rotation is free to assume any orientation. When rotating, the orientation of this axis is unaffected by tilting or rotation of the mounting, according to the conservation of angular momentum. Because of this, gyroscopes are useful for measuring or maintaining orientation.

In recent years, the gyroscopes manufactured with MEMS technology have become increasingly available. The MEMS gyroscope uses a vibrating element which reacts to the Coriolis force when rotating [41]. As illuminated in Fig. 2.7, a MEMS gyroscope consists of a mass, which is brought into vibration by an actuator in the direction given by r_{act}. When the gyroscope is rotated, the mass will not only vibrate in the actuation direction, but will also undergo a (small) additional displacement in the direction perpendicular to both the original displacement and the angular velocity vector r_{cor}. This additional displacement, also known as the Coriolis Effect, is used as a measure of angular velocity.

These are packaged similarly to other integrated circuits and may provide either analog or digital outputs. In many cases, a single part includes gyroscopic sensors for multiple axes. Like the 3D accelerometer setup, a 3D gyroscope can be assembled using three single axis gyroscopes. Ferraris [42] described a method for obtaining the gain, offset and sensitive axis of each of these gyro-

scopes with respect to the sensor housing. The output of the calibrated 3D gyroscope system is the angular velocity vector, expressed in the coordinate frame of the sensor housing. Some labs incorporate multiple gyroscopes and accelerometers (or multiple-axis gyroscopes and accelerometers), to achieve output that has six full degrees of freedom.

MEMS gyroscopes are used in automotive roll-over prevention and airbag systems, image stabilization, and have many other potential applications, especially in the flourishing intelligent wearable devices field. iPhone 4 is the first smartphone that adopts the MEMS gyroscope in consumer electronics. The newly applied gyroscopes make a great contribution to motion sensing for smartphones. Although accelerometer has been employed in all sorts of electronics for decades, the primary shortcoming lies in its incapability to measure the rotation around the axis aligns with the direction of gravity. Besides, its outputs constantly suffer from the interference of the gravitational component. The traditional solutions was using a high pass filter to eliminate the gravity acceleration as DC component firstly (such as Eq. 2.2 in last section); subsequently resorting to a low pass filter to remove the high frequency noise caused by the shaking of device. A series of filters could not only cause certain distortions in original signals but also reduce the processing efficiency. Apart from that, these weaknesses cannot be compensated by magnetometer in any way, since it takes some time to output a stable result and is vulnerable to external Electromagnetic Interference (EMI) as well. Therefore the emergence of MEMS gyroscope is considered a great breakthrough in motion sensing. It enables the device to measure the rotation related parameters in real-time and makes the precise detection of the changing in attitude possible.

As described above, the gyroscope measures the real-time angular velocities around the 3 axes (ω_x, ω_y and ω_z). The relation between the measured angular velocities and the 3 rotation angles is as follow Eq. 2.3 [43]:

$$\begin{bmatrix} \omega_x \\ \omega_y \\ \omega_z \end{bmatrix} = \begin{bmatrix} \dot{Pitch} \\ 0 \\ 0 \end{bmatrix} + R_{Pitch} \begin{bmatrix} 0 \\ \dot{Roll} \\ 0 \end{bmatrix} + R_{Pitch} R_{Roll} \begin{bmatrix} 0 \\ 0 \\ \dot{Yaw} \end{bmatrix}, \tag{2.3}$$

where *Pitch*, *Roll* and *Yaw* denote the rotation angles around *x*-, *y*- and *z*-axis separately; R_{Pitch}, R_{Roll} and R_{Yaw} are their rotation matrices:

$$R_{Pitch} = \begin{bmatrix} 1 & 0 & 0 \\ 0 & cosPitch & sinPitch \\ 0 & -sinPitch & cosPitch \end{bmatrix};$$

$$R_{Roll} = \begin{bmatrix} cosRoll & 0 & -sinRoll \\ 0 & 1 & 0 \\ sinRoll & 0 & cosRoll \end{bmatrix}; \tag{2.4}$$

$$R_{Yaw} = \begin{bmatrix} cosYaw & sinYaw & 0 \\ -sinYaw & cosYaw & 0 \\ 0 & 0 & 1 \end{bmatrix}.$$

And then,

$$\begin{cases} \dot{Pitch} = \omega_x + (\omega_y sinPitch + \omega_z cosPitch) tanRoll \\ \dot{Roll} = \omega_y cosPitch - \omega_z sinPitch \\ \dot{Yaw} = \frac{\omega_y sinPitch + \omega_z cosPitch}{cosRoll} \end{cases} \tag{2.5}$$

Eq. 2.5 can be solved in strapdown system, so that the rotation angles can be real-time updated. It is not without its drawback: when $Roll = \pm 90°$, the solutions of equations about $\dot{Pitch}$ and $\dot{Yaw}$ would be uncertain. So this method is to some degree limited. However, with respect to smartphone users, this situation is not normal and this method is still feasible.

To implement the algorithms elaborated above, an app is developed based on iOS. The app names "Meine Sensors" and can measure the accelerations, angular velocities, rotation angles, magnetic field intensities in / around all 3 axes, the air pressure of the surroundings, the relative altitude towards the initial place, the current GPS coordinates, and the azimuths between the magnetic north and the geographical north (according to GPS). It is available in App Store[1]. (also accessible via the QR code shown in Fig. 2.8 (a)). And it is universal for both iPhone and iPad.

In this app the sampling frequencies for all the inertial sensors are set as 50 Hz uniformly, while 10 Hz for displaying on screen. Because the update rate for GPS module is based on the change in location and for energy conservation the default threshold for distance filter is set as every 100 meters. The precisions can be promoted by higher refresh frequency but the power consumption would correspondingly rise. It is worthwhile to note that the build-in barometers are only available in iPhone 6 / 6 Plus and iPad Air 2 or newer devices, with operating system iOS 8.0 or newer. The roles of the barometer together with the alternative solutions are described in Chapter 7.2. In this chapter only the functions of accelerometer and gyroscope modules are involved.

[1] https://appsto.re/de/7Gek7.i or https://itunes.apple.com/de/app/meine-sensors/id992495675?l=en&mt=8

(a) (b)

Figure 2.8: The app "Meine Sensors" is used for recording the data from the sensors in iOS devices.

(a) The QR code of the link in App Store;
(b) The screenshot of the app. The 5 referred sensors are comprised of accelerometer, gyroscope, magnetometer, barometer and GPS module (among them the barometer is optional). With regard to the gyroscope module, the angular velocities around the 3 axes are measured. Accordingly the 3 rotation angles are calculated and also displayed on the right side. Other functions of this app are introduced in the following chapters of this dissertation. In addition 3 languages are supported by the interface: English, Chinese and German.

Here the function of gyroscope module is primary concerned. With the rotation angles calculated by the self-developed app shown in Fig. 2.8, both the accelerations and the attitude of the smartphone can be measured simultaneously. Subsequently the acquired accelerations in the phone's own coordinate system are able to be transformed to the standard earth-fixed coordinate system, so that

the further step recognition could be implemented subsequently.

2.2.3 Coordinate Transformation

The accelerations measured by smartphone are a vector has 3 items. Transforming the accelerations from one coordinate system to another could be regarded as rotating the vector between them. It means that 3 rotation matrices have to multiply the original vector successively so that the vector after rotation is supposed to be resulted. With respect to the order in which these 3 matrices should be multiplied, the conclusion drawn from my previous work [33] is firstly R^{-1}_{Roll}, then R^{-1}_{Pitch}, finally R^{-1}_{Yaw}.

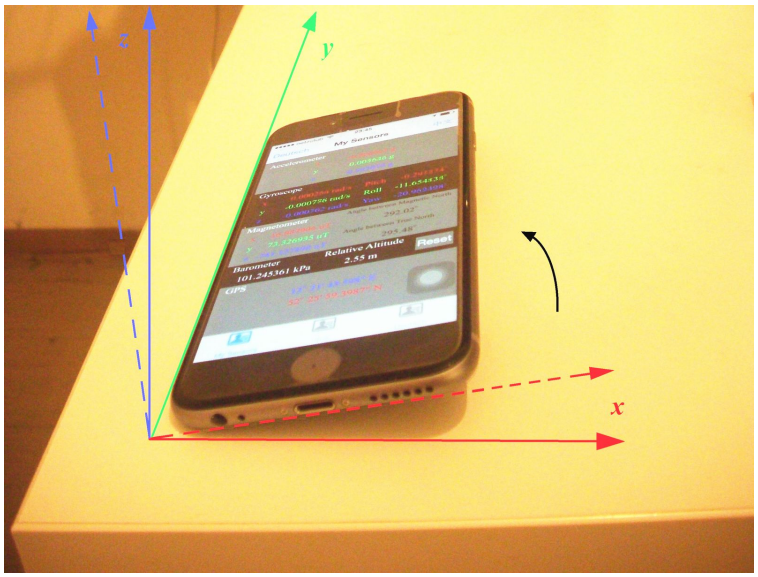

Figure 2.9: An example to illuminate what the correct rotation angles are, when smartphone tilts

Originally the 3 rotation angles were presumed to be the angle the device around their current corresponding axes. But according to some experiments, that does not turn out to be the case. As the example illustrated in Fig. 2.9, a phone tilts a little, turns around its lateral edge with a certain angle. *Pitch* was presumed to be the angle around current x axis (dashed red line), *Roll* was around current y axis (green line), and *Yaw* was around current z axis (dashed blue line). However, on the basis of observation, the correct *Yaw* is the angle the device rotates constantly around vertical direction (from down to up, original z axis, solid blue line); only the *Roll* is the angle rotates around the current y axis (green line); and the correct Pitch is the angle around the axis, which is perpendicular to the plane, in which the current y axis and original z axis lie (solid red line, in this example it is the

original x axis by coincidence).

According to the conclusion above, the correct rotating order is first around the z axis, then x axis, and finally y axis. Therefore the reasonable multiplying order should be $R_{Roll} \times R_{Pitch} \times R_{Yaw} \times vector_{earth}$. Specifically, here the rotation angles and the vector after rotated are used for calculating the original vector before rotates (accelerations in earth coordinate). Finally the multiplying order thus adopted is expressed in Eq. 2.6.

$$\begin{bmatrix} a_{earth\_x} \\ a_{earth\_y} \\ a_{earth\_z} \end{bmatrix} = R_{Yaw}^{-1} \times R_{Pitch}^{-1} \times R_{Roll}^{-1} \times \begin{bmatrix} a_{tilted\_x} \\ a_{tilted\_y} \\ a_{tilted\_z} \end{bmatrix}, \tag{2.6}$$

where the subscript "earth" means the acceleration values in the standard earth fixed coordinate system (the vector based on the earth, before tilts), while the subscript "tilted" means the values in smartphone's own tilted coordinate system. The explanations for the 3 rotation matrices are listed previously in Eq. 2.4.

After that, the gravitational component can be easily removed, just adding 1 G on each acceleration value in z direction. Last but not least, after removing the gravity acceleration, the measured values in 3 axes have to be also made opposite, due to the principle of accelerometer which is explained in Section 2.2.1. After that the proper accelerations of the smartphone in terms of the standard earth fixed coordinate system are acquired eventually.

Additional, a test app is also developed to test the effect of the coordinate transformation algorithm described above. As shown in Fig. 2.10, the real-time accelerations in 3 axes are displayed respectively. All of them are transformed and in terms of the standard earth fixed coordinate system, so that it can record the smartphone's proper accelerations more intrinsically, no matter the current attitude of the device. In order to observe the motion data more explicitly, these sampled accelerations are plotted separately as well, which is rather serviceable for the further step recognition.

Recap

In this chapter the framework of the positioning system is described. Besides, the key inertial sensors, accelerometer as well as gyroscope, are introduced respectively. Before the sampled accelerations could be used for counting steps and estimating distance, they need to be transformed, from the smartphone's own current coordinate system to the standard earth fixed coordinate system. To fulfill it, the real-time rotation angles obtained from gyroscope plays a vital role. The processes of calculating the rotation angles from angular velocities, transforming the accelerations between coordinate systems by the rotation matrices are interpreted in detail. As a part of the plan for the

future's real positioning system, some apps are also developed for evaluation.

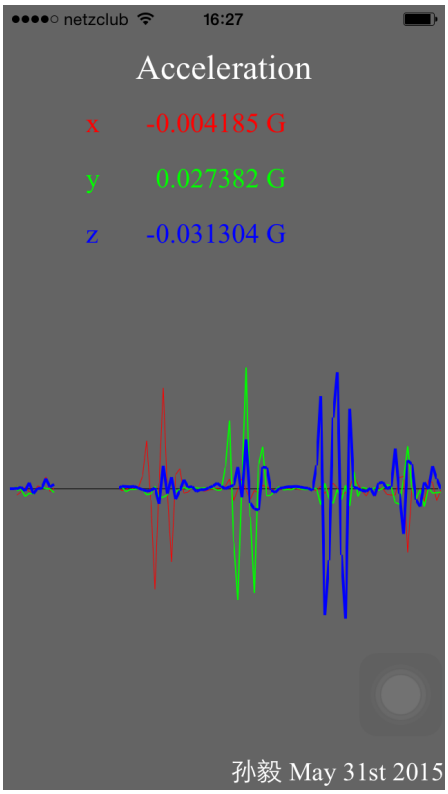

Figure 2.10: A screenshot of the test app which is used for measuring and calculating the proper accelerations of smartphone. It measures the accelerations in the device's own current coordinate system and transforms them to the standard earth-fixed coordinate system. The 3 values with 3 colors on the screen indicate the tri-axial accelerations after coordinate transform and elimination from the gravitational component. The 3 curves below are plotted from them. The directions of the 3 axes are previously explained in Fig. 2.4. During test, when the smartphone spins freely, as long as its barycenter doesn't move, the displayed accelerations' values and their curves would never vary sharply. Because the function of this test app is rather deficient, it is not publicized in App Store.

Chapter 3

Step Recognition

With the cooperation of the accelerometer and gyroscope the proper accelerations of the smartphone could be measured, which reflect the intrinsic motion of the device. Further procedure is to recognize the step according to the acceleration signals. But these proper accelerations are rather confused to be distinguished directly. A series of reforms such as a wide variety of filters have to be employed in order to ameliorate them.

3.1 Sensitive Component

Concerning the accelerations to be analyzed for step recognition, different researchers adopt different acceleration components. Some literatures utilize the module of the accelerations, such as [44] [45] [46] and [47]. More researchers tend otherwise to sole acceleration in vertical direction during their experiments [48] [39] [49] and [38].

The experiments shown in Fig. 3.1 are to investigate which component among the accelerations indicates steps most remarkably according to the different attach positions. For smartphone holding in hand or putting in pocket is more common. With reference to other wearable devices attaching on shoe is also usual.

For pedestrian, the pulses in accelerations should be conveniently differentiated. The results of the experiments above is shown in Fig. 3.2, if the sensor is taken in hand while the volunteer is walking, each pulse in vertical direction (z axis, blue) is the most remarkably to be identified among those in others 2. If the sensor is stuck on shoe, from the bottom figure, it is the component in anterior-posterior direction (y axis, green) that counts more.

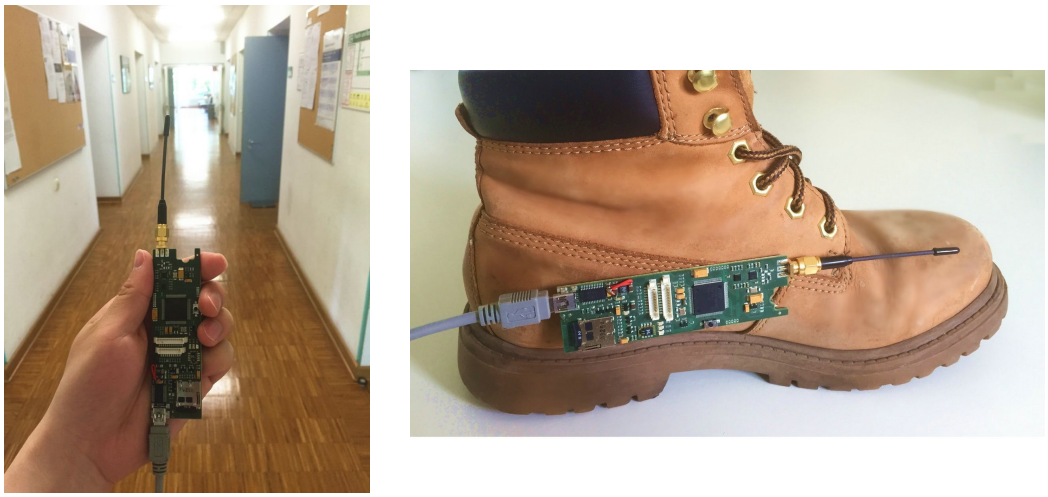

(a) Taking the sensor in hand

(b) Attaching the sensor on shoe

Figure 3.1: To determine which component of acceleration plays the most crucial role in the step recognition. A group of experiments are designed. While the volunteer is walking, the inertial sensor is held in hand and attached on shoe respectively in order to observe the different acceleration components according to the different attach positions. The results are compared in Fig. 3.2.

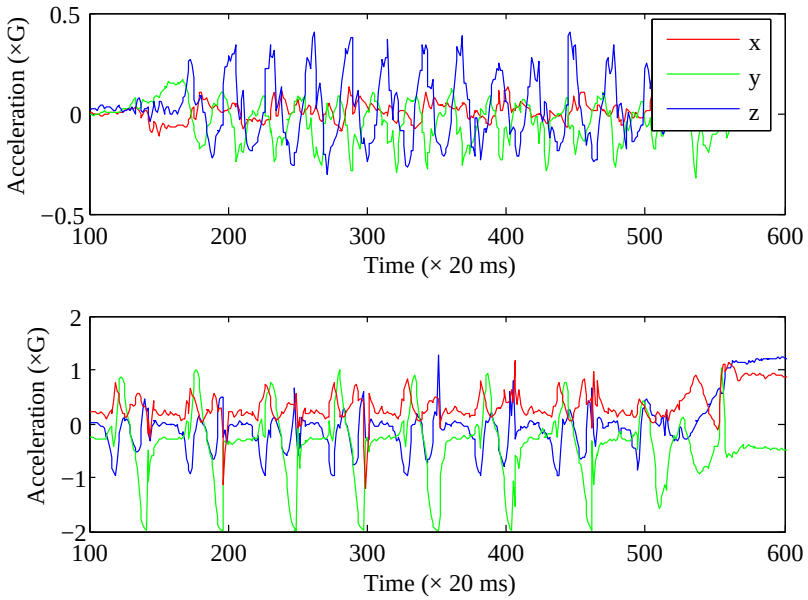

Figure 3.2: Comparison between holding inertial sensor in different positions. The upper figure is taking it in hand, from curves it is obvious that the acceleration in vertical direction (z, blue) are more remarkable; the lower figure is sticking it on shoe that the signal in anterior-posterior direction (y, green) counts more.

Some of pervious literatures argue that the module of accelerations is supposed to be utilized. But according to my experiments, only if it is without the assistance of gyroscope, the using of the module in all 3 shows a better effect. Because the attitude of the sensor is unknown, and using all of the acceleration components would be a more comprehensive solution. It is the most expedient choice in such a condition.

The experiments in this dissertation are primarily based on the platform of iOS devices. All of them are handheld devices and equipped with both the tri-axial accelerometer and gyroscope. Therefore in order to reach the optimal recognition precision, solely the acceleration signals in vertical direction (z axis) are referred to when step recognition unless otherwise indicated. The situations sticking sensors on shoe belong to other wearable devices which are beyond the works in this dissertation and would be discussed in my future research.

3.2 Zero Velocity Compensation (ZVC)

Merely with the raw accelerations in vertical direction toward the earth coordinate system is quite not enough to perform step recognition, they are usually too deviate for the further operation. Here the Zero Velocity Compensation derived from Zero Velocity Updates (ZUPTs) [50] is expected to be employed to offset this kind of deviation. It based on a premise that the object must start from stationary and after a period of motion return to a stationary state, so that according to the difference between the calculated terminal velocity and the actual terminal velocity (virtually 0), the progressive deviation could be compensated theoretically. On the basis of this principle, before starting up and after the last step finished, the actual velocities of device together with the holder could be regarded as approximately 0. The calculated velocity at the end of walking can be drawn on to eliminate the distortion.

$$a'_n(t) = a_n(t) - \frac{v_n(t_2) - v_n(t_1)}{t_2 - t_1} \cdot \frac{1}{T_s} \tag{3.1}$$

where $a_n(t)$ and $a'_n(t)$ denote the raw acceleration value and the value after ZVC; t_1, t_2 are the starting and end time of the segment of walking; $v_n(t_1)$ and $v_n(t_2)$ are the calculated instantaneous velocity at t_1 and t_2; T_s is the sampling duration. Fig. 3.3 is a demonstration how to calculate $a'_n(t)$ from $a_n(t)$.

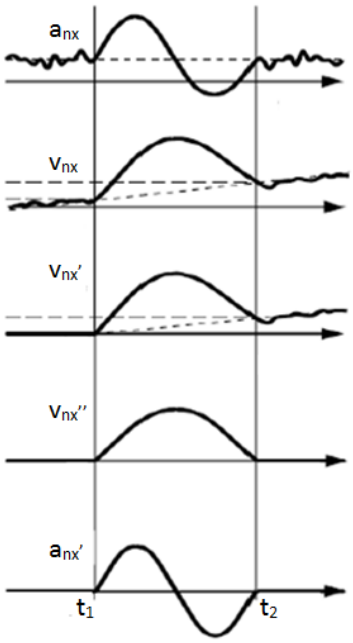

$$a_n(t)$$

$$v_n(t) = \sum_{j=t_1+1}^{t} \frac{a_n(j) - a_n(j-1)}{2} \cdot T_s$$

$$v_n'(t) = \begin{cases} 0 & ,t \le t_1 \\ v_n(t) - v_n(t_1) & ,t > t_1 \end{cases}$$

$$v_n''(t) = \begin{cases} 0 & ,t \le t_1 \\ v_n'(t) - v_n'(t_2)\dfrac{t - t_1}{t_2 - t_1} & ,t_1 < t \le t_2 \\ 0 & ,t > t_2 \end{cases}$$

$$a_n'(t) = \begin{cases} 0 & ,t \le t_1 \\ a_n(t) - \dfrac{v_n'(t_2)}{t_2 - t_1} \cdot \dfrac{1}{T_s} & ,t_1 < t \le t_2 \\ 0 & t > t_2 \end{cases}$$

Figure 3.3: The operation of Zero Velocity Compensation (ZVC)

In the Equations in Fig. 3.3, the velocities are integrated of acceleration over time. Practically, as the accelerations measured are discrete, the integration is done on the basis of Eq. 3.2.

$$\begin{aligned} v_n &= v_0 + \sum_{i=0}^{n-1} \frac{a_i + a_{i+1}}{2} \cdot T_s \\ &= v_0 + \frac{1}{2}a_0 T_s + \sum_{i=1}^{n-1} a_i T_s + \frac{1}{2}a_n T_s, \end{aligned} \tag{3.2}$$

where normally v_0 is regarded as 0.

In view of the fact that the commencing and ending velocities are both required to be approximately 0, the ZVC method is more suitable for the off-line situation, that a set of acceleration data for the whole walking segment are operated after stop which the initial and final state of the smartphone could be considered stationary. However, my positioning system is expected to be an intelligent real-time system which must implement a series of operation at the same time as pedestrian walking. Performing ZVC afterwards cannot in any way be acceptable. Nevertheless, a procedure of calibration is proposed at the very beginning to deal with this weakness. While it is calibrating, the pedestrians are required to hold their devices as still as possible for certain time, without any

movement or vibration. The corresponding operations toward ZVC can be performed during this time, and the acquired parameters in terms of accelerations' drift could be used to compensate the deviation in all the following walking time.

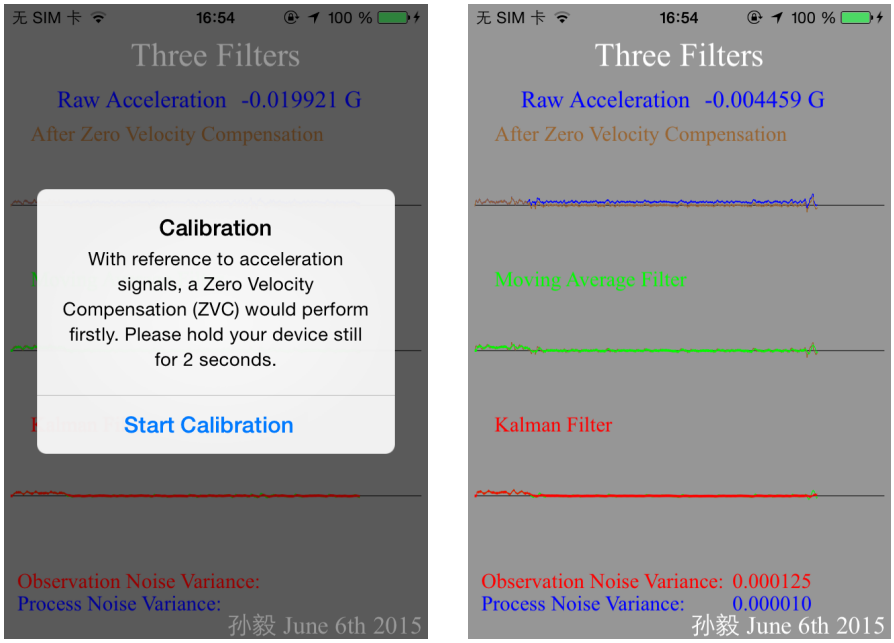

(a) (b)

Figure 3.4: The screenshot of the test app for 3 filters

This test app is to implement the 3 filters for the vertical acceleration. Here the effect of Zero Velocity Compensation (ZVC) is displayed. Because a premise for ZVC is at the beginning and end the object must be stationary. A procedure of self-calibration is designed to provide this stationary phase. During the calibrating time, the parameters about the distortion caused by the inherent deviation in accelerometer are measured by ZVC algorithm. Accordingly the deviation can be abated and the subsequent data can be ameliorated continually.

(a) A dialog box is popped up when this app is newly booted, in order to inform users that before walking a 2 seconds' calibration for ZVC is required and during this time the smartphone should be held as stable as possible;

(b) The effect of ZVC is obvious. In the upper figure, before, the raw acceleration (blue) and the treated data (brown) deviate from the zero base line; afterwards the data is corrected and conformed to the base line.

Other functions of this test app will be introduced in the following sections. Because the functions of this app are rather monotonous, it is not publicized in App Store. But they are involved in the final system.

As shown in Fig. 3.4 (a), the self-calibration is performed at the very beginning, before user starts walking. When a user firstly opens the app, a dialog box appears in order to remind the user that after presses the "Start Calibration" button, s/he should hold the device still for 2 second. After the calibration finished, then s/he is allowed to walk. The effect of the calibration for ZVC is shown in Fig. 3.4 (b). The raw data of vertical accelerations are plotted in blue color, while the result after ZVC is in brown. It can be seen that during the initial calibrating time, the acceleration data is above the zero base line. That is because of an inherent deviation in the output of the accelerometer. After calibration the ZVC takes effect. The operated data is separated from raw data and goes along the zero line (at this moment the device is still not moving).

Because the inherent deviations in the accelerometers of new iPhone 6 / 6 Plus are quite low, in order to demonstrate a more obvious effect for the ZVC algorithm, an old iPhone 4 is adopted to test here. Therefore the screenshots shown in Fig. 3.4 are taken from an iPhone 4 whose built-in inertial sensors are old and not so precise.

3.3 Moving Average Filter

After the inherent deviations in acceleration signals are reduced, there are a great deal of noises have to be further rejected. These noises derived from both inertial units and measuring process cause a multitude of jitters in the acceleration signals. Because to some extent these jitters could be regarded as kinds of high frequency components in original signal, certain low pass filter has to be employed to eliminate these high frequency jitters.

The Moving Average Filter is employed as a low pass filter to deal with these random jitters. According to Eq. 3.3, for each data in the acceleration sequence, the value is replaced by the average value among the adjacent several sampling points within a moving window with certain size. Because of the checks and balances among the neighborhood, the accidental jitters can be in a certain probability smoothed away.

$$a_{movAvg}[i] = \frac{1}{M} \cdot \sum_{j=-\frac{M-1}{2}}^{\frac{M-1}{2}} a_{raw}[i+j] \tag{3.3}$$

where $a_{raw}[]$ is the input signal which is after ZVC; $a_{movAvg}[]$ is the output signal after Moving Average Filter; M is the fixed size of the moving window. In my experiments the value of M is set

as 5, which is empirically determined through the signal analysis.

In view of the fact that the data to be processed should be at the center of the current moving window, with respect to the few data near the two end points, some different calculating methods is supposed to be applied. Actually the expressions for different data segments are as Eq. 3.4.

$$a_{movAvg}[i] = \begin{cases} \frac{1}{\frac{M}{2}+i+1} \sum_{j=0}^{\frac{M}{2}+i+1} a_{raw}[j] & (0 \leqslant i < \frac{M}{2}) \\ \frac{1}{M} \sum_{j=i-\frac{M}{2}}^{i+\frac{M}{2}} a_{raw}[j] & (\frac{M}{2} \leqslant i < n - \frac{M}{2}) \\ \frac{1}{\frac{M}{2}+n-i} \sum_{j=i-\frac{M}{2}}^{n} a_{raw}[j] & (n - \frac{M}{2} \leqslant i < n) \end{cases} \tag{3.4}$$

where i denote the index of data sequence; n indicates the data size of the whole segment to be processed; j is the index within in each window.

An experiment is designed to verify the function of the Moving Average Filter: a volunteer holds the sensor and walks for 9 steps. The vertical accelerations are measured and smoothed by the Moving Average Filter. The result of the off-line simulation is shown in Fig. 3.5. Most of noises in the raw accelerations are reduced.

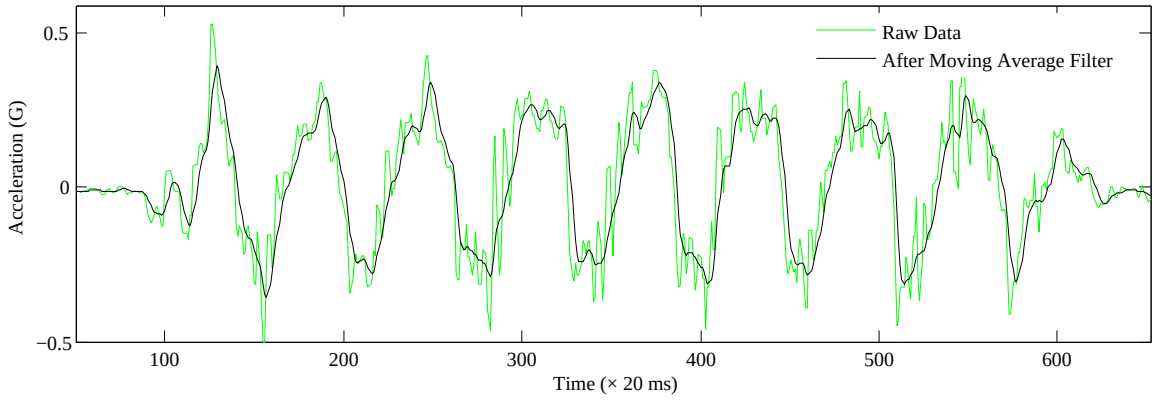

Figure 3.5: The effect of the Moving Average Filter in off-line simulation. The vertical accelerations while pedestrian is walking are recorded. With the Moving Average Filter the jitters in raw data have been eliminated to some extent.

On top of that, the test app shown in Fig. 3.4 also has the function of Moving Average Filter. The effect in real-time is demonstrated in Fig. 3.6. The subfigure (a) is the screenshot from iPhone 4 while (b) is that from iPhone 6. It is a comparison between the oldest and latest available iOS devices. In both figures, the brown lines denote the acceleration signals before processed by the Moving Average Filter, while the green lines indicate the signals after filtered. From both test platforms, it can be observed that the jitters on brown lines are rejected by the filter to a great extent.

Nevertheless, the intrinsic waveforms and useful features are reserved.

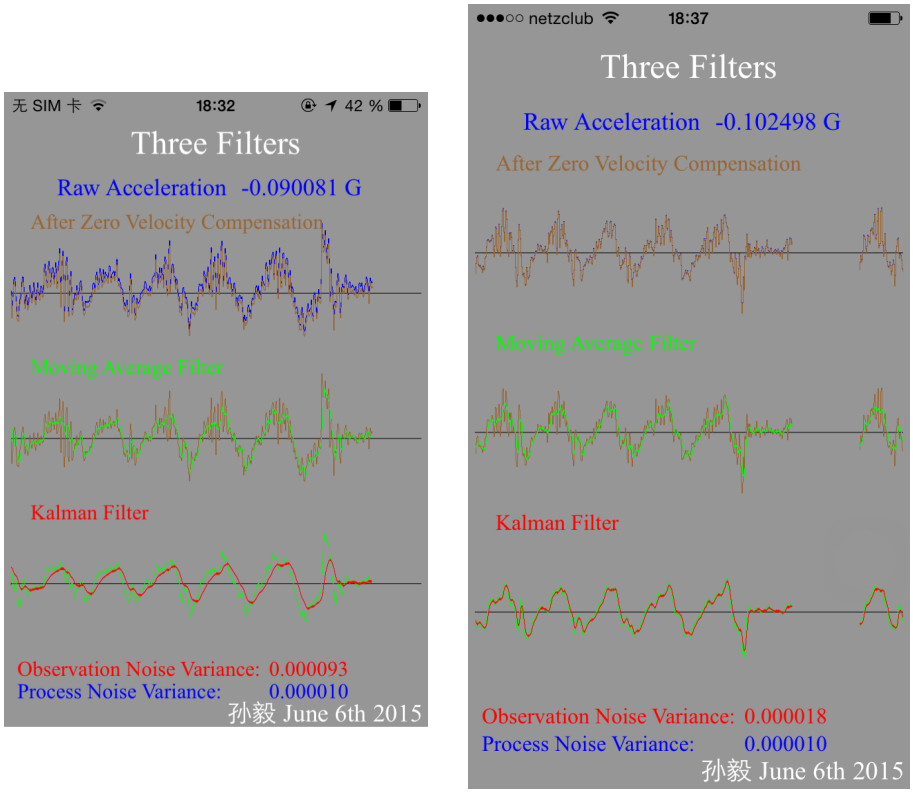

(a) Test with iPhone 4 (b) Test with iPhone 6

Figure 3.6: The effects of Moving Average Filter

Incidentally, it can be found that in the subfigure(b), the data before and after ZVC are no different (the brown line and blue line on the top, but the blue line is virtually overlapped by the brown). That is the reason why an old iPhone 4 is chosen for test in Fig. 3.4. In new devices with precise sensors, the inherent deviation is so tiny that the effect of ZVC is inconspicuous for demonstration.

This Moving Average Filter is also utilized in the pre-process of the azimuth data which is described in Section 3.4.2.

3.4 Divide and Conquer

After filtered, the vertical accelerations are adequate for step detection. To recognize each step according to acceleration waves, there are several features are supposed to be extracted and analyzed.

With respect to a segment of stable and constant wave, all of these numerous physical features could be captured easily. Nevertheless, if the wave is generated when pedestrian is changing the gait, the recorded waveform would be too chaotic to recognize and analyze. Normally this kind of disorder could not be handled by most mathematical filters, including the ZVC and Moving Average Filter introduced in Section 3.2 and 3.3.

Actually the steady stepping is just a part in all of the walking behaviors. If the abnormal or transitional activities such as jerk, halt, turn, wander, push or pull a door are all involved, the step detection would be rather complicated. The data gathered when gait changes are too instable and intricate to be tackled. For simplification, for a steady output of step recognition and further distance estimation, an innovative strategy is introduced in this section. Because it divides the whole into small parts and processes them separately in order to reduce the complexity, its idea is similar with an algorithm named Divide and Conquer. First and foremost the whole walking process is divided into separate segments by several breakpoints such as turning, stop or starting up. So, simply straight walking is involved in each segment, no transition state at all. As a result the specified parameters for respective segment would improve the filtering effect and the recognition rate as well. Furthermore, unlike others' works such as that solely vertical acceleration [49] or the module of 3 axes accelerations [44] is drawn on, in my experiments both vertical and anterior-posterior data are analyzed respectively, so that the activities like stepping backwards, marking time (stepping but makes no progress) or lateral shift can be distinguished from the normal walking.

3.4.1 Recognition for Start-up and Stop Actions

As discussed above the accelerations collected when unconscious shaking during turning or standing are misleading to step recognition, the data while stably walking are hence supposed to be separated from them. Determining the breakpoints among the valid walking waves and invalid fluctuations is so necessary that the confusion jamming could be ignored accordingly. One kind of the breakpoints is the time when pedestrian starts up and intermittently stops. In this section the Moving Variance Analysis is employed for the accelerations in both vertical and anterior-posterior directions to identify this kind of breakpoints.

As shown in Fig. 3.7, the variance of a set of data indicates how far these values are spread out. And the variance of the successive accelerations is regarded as an index how severe the device oscillates currently. When pedestrian walks or even runs, the variance at the moment is definitely larger than that when s/he unconsciously shakes. Around the transforming points there are certainly some jumps on the variances. According to these varied variances, the breakpoints derived from the start-up and stop actions could be determined distinctly.

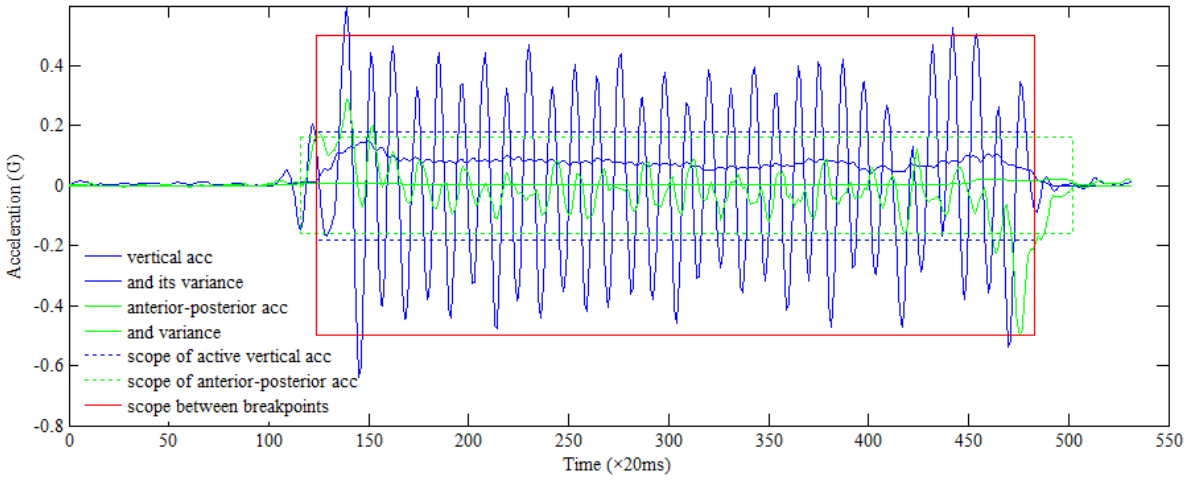

Figure 3.7: Searching the breakpoints by Moving Variance Analysis. The active domains for vertical (blue) and anterior-posterior (green) accelerations are calculated by the variance analysis respectively. Then the valid phase for pure walking is determined by their intersection set. Therefore not only the disordered data when walking pattern transforms can be eliminated, but also the abnormal gaits such as marking time and lateral shift could be differentiated from normal walking because their accelerations in both directions are not coincide.

In my experiences the active domain for vertical and anterior-posterior data are searched separately, and then the boundaries of their intersection set are adopted as the breakpoints for the corresponding walking segment. Though that the normal walking and marking time can be distinguished, because if stepping but makes no progress, the active domains of the accelerations in vertical and anterior-posterior directions would not be coincident.

The method simply bases on a fixed threshold of variance is attempted but the performance is barely satisfactory due to the great diversity among volunteers. In my experiments the variance thresholds for breakpoints searching are set as dynamic values. In vertical direction, the threshold is set as 50 times the variance during the stationary calibration at the very beginning (about the calibration, see Section 3.2); while in anterior-posterior direction the threshold is empirically 12 times the static variance. From observations, if the window size for variance analysis is set between one to two cycles of the wave, the most remarkable effect towards the variance curve is achieved. Normally the step frequencies are between 1 step per second and 4 steps per second, and according to the experiment performed in Section 3.1 one step makes up one wave cycle. Here the sampling rate for accelerometer is 50 Hz. Therefore the window size for variance analysis is set as 50 sampling points. As the instance shown in Fig. 3.7, the 2 intervals determined by 2 pairs of breakpoints

represent the active domains in 2 directions respectively and the final valid walking phase is reckoned from the intersection set between them. As a result the confused perturbations when starting up and stop can be rejected previously.

The test experiments as well as the evaluation for this solution are in Section 3.4.3, together with the method searching for the turn action related breakpoints.

3.4.2 Recognition for Turn Actions

The searching algorithm for the first category of breakpoints is illuminated in the last section. While another category caused by pedestrian's turn actions is discussed here. Detecting the turn actions, along with measuring the turning direction in real-time is more significant for a positioning system, because the heading angle is a crucial element for PDR scheme. Comparing with the misrecognition for a few steps, the inaccuracy of azimuth may lead to more serious deviation in the final positioning result.

a) Data Fusion of Gyroscope and Magnetometer Data

The purpose for this section is to determine the turning points in the whole walking process. Gyroscope is widely used for measuring the rotation angles with high sensitivity. Besides, magnetometer can provide the absolute heading direction and already becomes a common instrument for all sorts of outdoor applications such as electronic compass. The characteristics of both sensors are contrasted in Table 3.1 [51].

Table 3.1: Comparison between Gyroscope and Magnetometer

	Advantage	**Disadvantage**
Gyroscope	No external disturbance	Drift along time
	Short term accuracy	
Magnetometer	Absolute heading	Unpredictable external disturbances
	Long term stable accuracy	

The emerging of gyroscope enhances the smartphones' capability in motion sensing greatly. Precise and sensitive rotation related data can be returned in real-time. But similar to other inertial sensors, the results from gyroscope would also suffer from drift. What worse, the longer gyroscope works the more serious drift it would be. Fortunately this diverging drift could be corrected by magnetometer whose long term stability is satisfactory. However, it takes magnetometer an uncertain time to provide a steady output. In other words the real-time reading from magnetometer could be considered reliable if and only if the motion state of device has not varied for a while. In addition

the accuracy of magnetometer is rather limited and it is vulnerable to EMI as well. Especially in an indoor scenario, for example in an exhibition hall or a library where is fully equipped with electrical cables as well as metal surroundings. All of them play the part of the potential interference sources toward magnetometer. In contrast the sensitivity and interference immunity of gyroscope could serve well in these conditions regardless of external disturbances. Therefore an optimal and reliable system might be expected to combine the data from both gyroscope and magnetometer. In the data fusion scheme, the magnetometer can provide the initial orientation of smartphone and correct the drift of the gyroscope's output regularly or irregularly, while the gyroscope would work independently in some extreme environments such as too severe magnetic interferences occur [45].

The optimal heading angle is estimated as follow:

$$\hat{h} = (1 - w_M)h_G + w_M h_M, \tag{3.5}$$

where $\hat{h}$ denote the estimated heading; h_G and h_M indicate the results from gyroscope and magnetometer, respectively; w_M are the weight for magnetometer.

The variance of estimated heading is

$$\sigma^2 = (1 - w_M)^2\sigma_G^2 + w_M^2\sigma_M^2, \tag{3.6}$$

where σ_G^2 and σ_M^2 denote the variances from the gyroscope and magnetometer's measurements. The more precise the sensors, the less the variances would be.

To minimize the variance σ^2, the optimal magnetometer's weight is

$$w_M = \frac{\sigma_G^2}{\sigma_G^2 + \sigma_M^2} \tag{3.7}$$

With this optimal weight value, the heading angle is finally estimated as Eq. 3.8, whose variance is lowest.

$$\begin{aligned}\hat{h}_t &= (1 - \frac{\sigma_G^2}{\sigma_G^2 + \sigma_M^2})h_G + \frac{\sigma_G^2}{\sigma_G^2 + \sigma_M^2}h_M \\ &= \frac{h_G\sigma_M^2 + h_M\sigma_G^2}{\sigma_G^2 + \sigma_M^2}\end{aligned} \tag{3.8}$$

Concurrently the variance of the estimated heading angle is

$$\sigma^2 = (1 - \frac{\sigma_G^2}{\sigma_G^2 + \sigma_M^2})^2\sigma_G^2 + (\frac{\sigma_G^2}{\sigma_G^2 + \sigma_M^2})^2\sigma_M^2$$

$$= \frac{\sigma_G^2 \sigma_M^2}{\sigma_G^2 + \sigma_M^2}. \tag{3.9}$$

The test of the sensors fusion is implemented as following: volunteers are required to take smartphone in hand and walk along a square path in within a building. In Fig. 3.8 the effect is demonstrated. Here the geographical north regards as 0; the heading angle regards as the angle between the heading direction and the geographical north, clockwise, from $-\pi$ to π (rad).

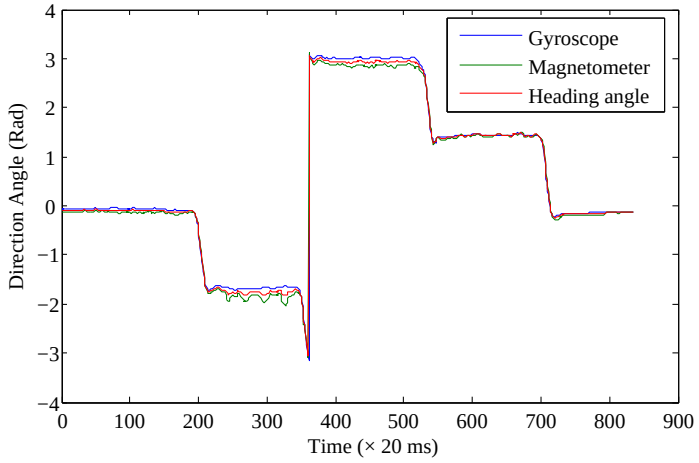

Figure 3.8: The effect of Sensors Fusion in terms of heading angle

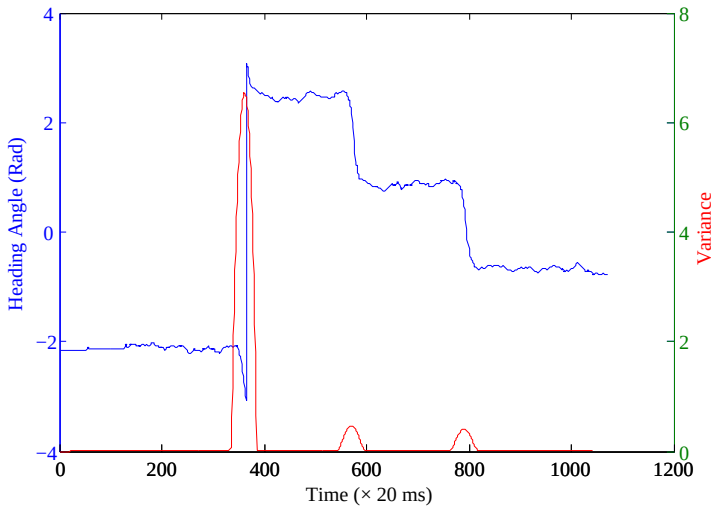

Figure 3.9: Identifying the turning points by Moving Variance Analysis

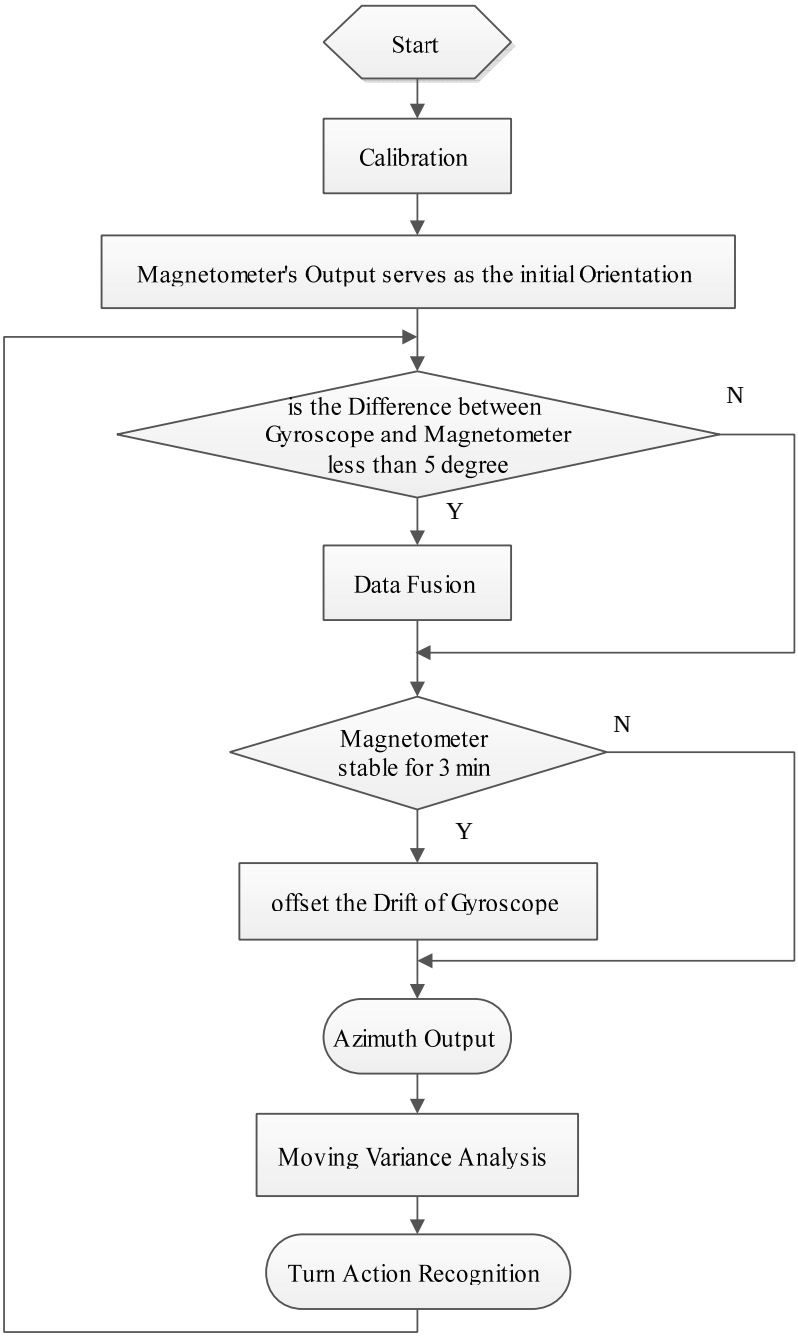

Figure 3.10: The flow chart for azimuth measurement and turn action recognition. Usually the azimuth results from the data fusion of gyroscope and magnetometer. If the EMI is too severe, gyroscope would support the azimuth system independently. When magnetometer is stable, the output can provide an initial orientation and offset the drift of gyroscope timely.

b) Turning Detection

Subsequently, the turning time is determined by the heading data. The method is also Moving Variance Analysis. Likewise, the window size for calculating the variance is set as 50 (1 second). As shown in Fig. 3.9, according to the sampled data from Fig. 3.8, the effect of searching for the turning points is remarkable.

When the pedestrian is walking at an indoor scenario, the electromagnetic interference is unknown and the disturbance sources changes unpredictably, which would degrade the performance of the azimuth estimation seriously. This kind of degradation can be reduced by assessing the disturbance. If the difference between the outputs from magnetometer and gyroscope is larger than a given threshold, some uncertain disturbance is considered existent and the magnetometer measurement is therefore ignored temporarily.

The whole operating process for the turn action recognition is demonstrated by the workflow chart in Fig. 3.10.

In this section, the turning points are searched as the breakpoints which are merely for dividing the whole walking phase into segments. With regard to each step, the heading is addressed respectively, rather than using a single average orientation for all of steps in the same segment. The heading for each step is calculated from the average heading angle during that step.

3.4.3 Evaluation

Spirited by the idea of Divide and Conquer, the whole walking phase would be divided into a series of segments and the further filters, recognitions and estimations are supposed to be implemented respectively. On one hand, using separate parameters for different segments could improve the accuracy in recognition as well as estimation; on the other hand, the instable and complicated acceleration waveforms when gait transforms are avoided.

A group of experiments are designed to test the effect of searching the breakpoints. Among them a combine instance is presented here, which takes place in the corridor of our institute as Fig. 3.11. In this test experiment the volunteers are required to hold the smartphone and walk through the corridor in the same floor. Several temporary halt and turning actions are included in the walking experiment. According to the data recorded by the built-in accelerometer, gyroscope and magnetometer, these breakpoints in the walking phase are searched. In this realistic scenario it is full of metal and cables which are potential EMI source for magnetometer.

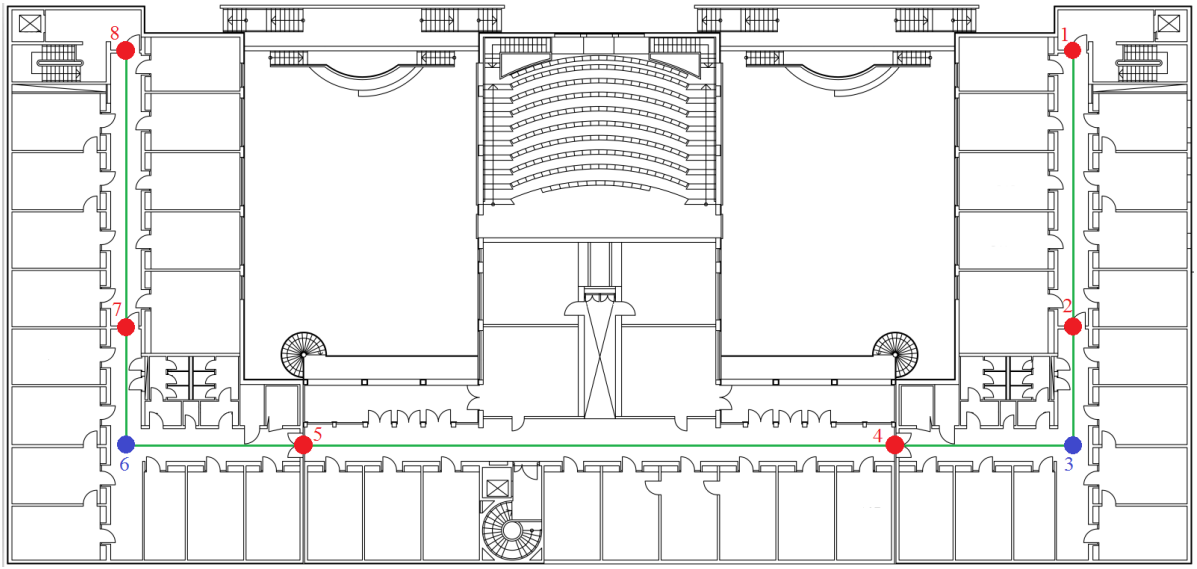

Figure 3.11: The map of the corridor in our institute. A pedestrian walks along the green line, from the door at up-right corner (Point 1) through the corridor to the door at up-left corner (Point 8). In this 136 meters long distance, totally 8 breakpoints are involved: 6 stop points with red sign (including start and end points) and 2 turning points with blue sign.

The outputs from the magnetometer and the gyroscope are demonstrated in Fig. 3.12. With reference to the magnetic heading angle, the values on the longitudinal axis of the upper figure in Fig. 3.12 denote the angle between the orientation of device and the magnetic north, in clockwise direction. They are interpreted in Table 3.2 in detail.

Table 3.2: The Interpretation of the Magnetic Heading Angles

Magnetic Heading Angle	**Direction**
0°	Magnetic North
90°	Magnetic East
180°	Magnetic South
270°	Magnetic West
<0°	Invalid Value

From the heading angles measured by magnetometer, it is obvious that the unpredictable EMI in surroundings influence the magnetometer severely.

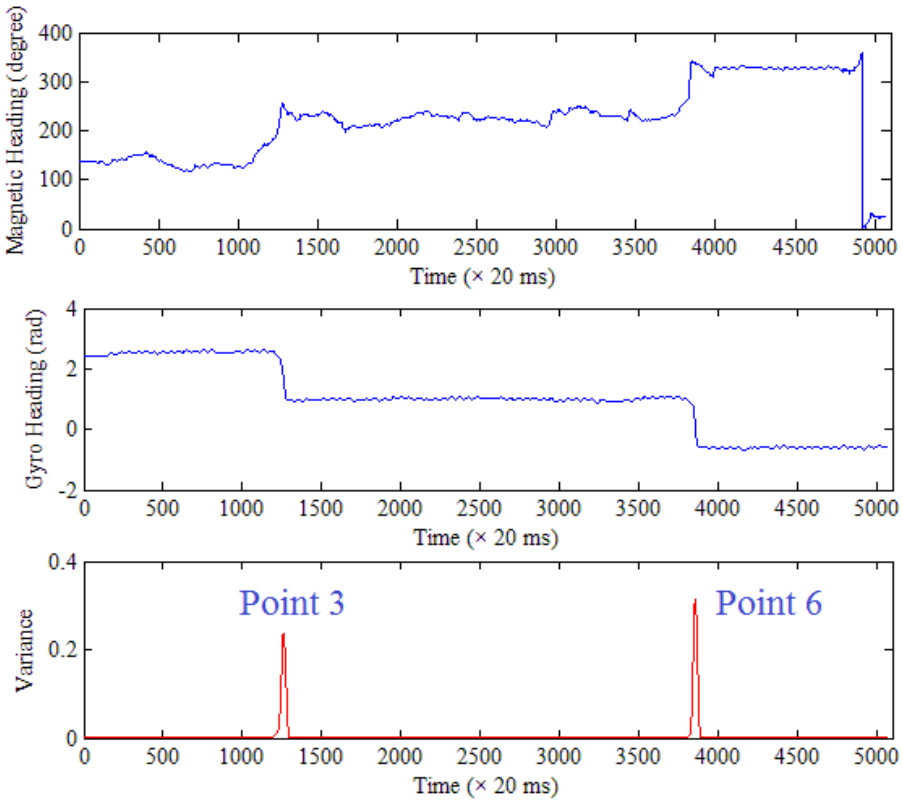

Figure 3.12: By mean of the data measured by the magnetometer and the gyroscope, the breakpoints results from turn actions are searched (as Point 3 and 6 in Fig. 3.11) according to Moving Variance Analysis.

In the walking experiment demonstrated in Fig. 3.11 and 3.12, the volunteer turns twice (around the corners at Point 3 and Point 6). The whole process takes 136 meters and lasts for more than 100 seconds. In this not so long a time, the drift of gyroscope is not serious, its output is hence not corrected by magnetometer. In contrast, due to the instabilities caused by IMF, the data from the magnetometer are temporary ignored several times.

This walking experiment takes the volunteer nearly 200 steps. From Fig. 3.13, these steps generate the waves in acceleration signals pretty distinctly. Since the changing in the variance curve is so conspicuous, these halt points are determined precisely by the Moving Variance Analysis. The 4 breakpoints derive from occasional stop are sharply indicated in the figure. The coincidence toward the active domains in both anterior-posterior and vertical directions verifies these breakpoints as well. To demonstrate the effect briefly, only the accelerations after filters are displayed in Fig. 3.13 rather than the raw data.

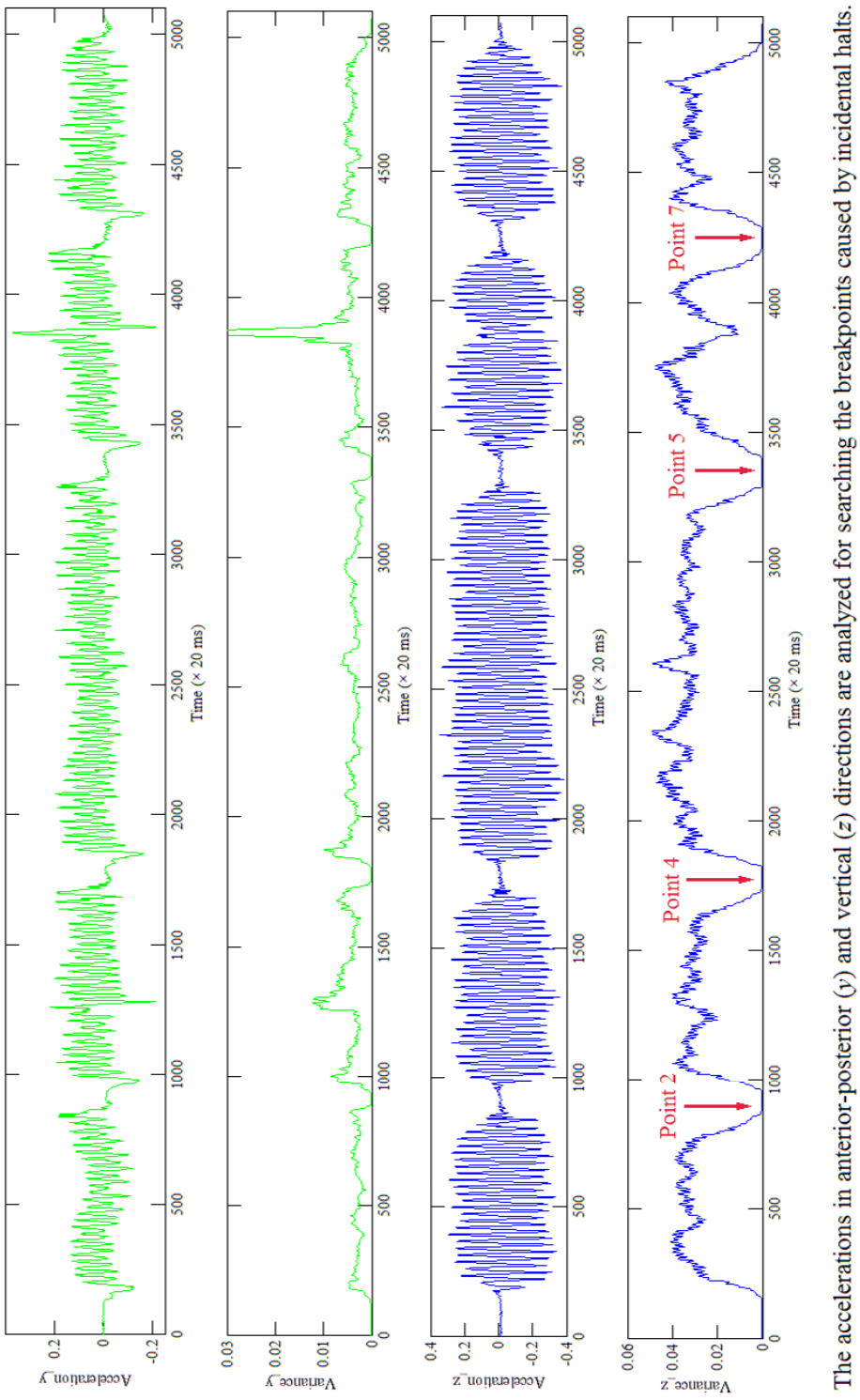

The accelerations in anterior-posterior (y) and vertical (z) directions are analyzed for searching the breakpoints caused by incidental halts.

Figure 3.13: The effect of the breakpoints searching

After divide the whole walking process into separate segments, the approaches and algorithms introduced in the following sections are expected to "conquer" these data subsequently. Within each small walking segment, the state as well as the gait is comparative monotone and the corresponding recognition and estimation would be less complicated and more precise.

3.5 Kalman Filter

After several procedures, the step recognition is ready. According to the vertical acceleration wave the step features are supposed to be extracted. As shown in Fig. 3.14, how the acceleration wave is generated during a step is illuminated in simplification. As described, there are 1 peak and 1 trough related to a step (half stride). The harsher the feet strike the ground, the larger the amplitude of vibration are resulted.

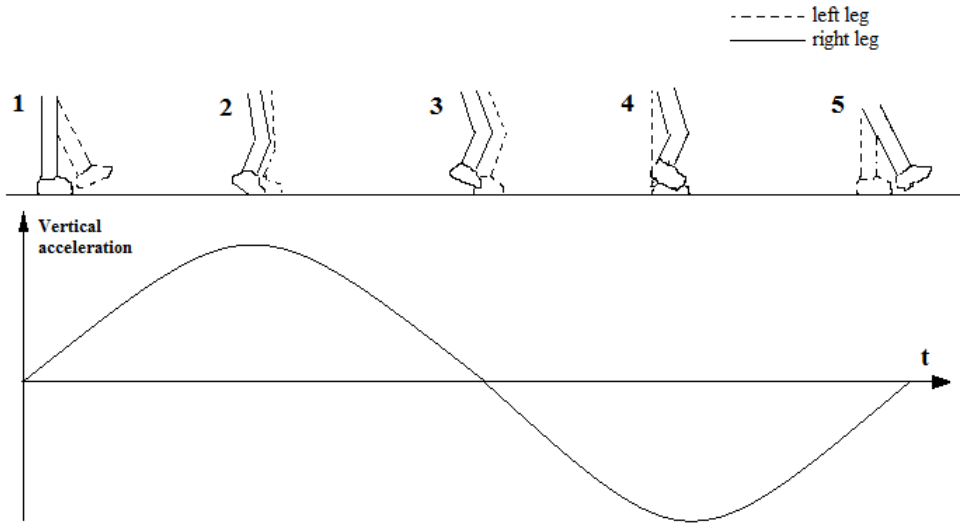

Figure 3.14: The oscillation in the vertical acceleration is generated by walking. Each step corresponds to a cycle of wave. When one foot strikes the ground with the most force, the wave reaches its peak; a trough is detected when a foot swings over the contralateral leg.

While a pedestrian is walking, the reciprocating actions of legs drive the oscillations of the body in vertical direction, and these oscillations are recorded by accelerometer.

Timestamp 1: the right leg (icon in solid line) is standing straightly and the left leg (dashed icon) swings in front of the right leg. In this moment the barycenter is at normal height and on the right leg side;

Timestamp 2: the left foot just touches the ground, both the legs bend tinily, the barycenter falls to its lowest point and are transferring to the left leg side, the vertical acceleration caused by the feet pressing reaches its peak value;

Timestamp 3: the right leg is going to leave the ground and the barycenter rises;

Timestamp 4: the right leg swings over the left leg. The barycenter reaches its highest point, the acceleration reaches the minimum (with the positive direction: up);

Timestamp 5: the right leg is going to touch the ground, and the barycenter is transferring to the right leg side.

Both the legs move iteratively and the oscillation in the acceleration wave is driven continually. The essential work for the step recognition is to detect all the valid peaks and troughs, so that the corresponding step length could be estimated successively.

However, in certain extreme conditions, for example when the smartphone is shaken very severely, although a series of filters are already employed to reject jitters as well as noise, some peaks and troughs are still rather ambiguous to be distinguished. As the treated accelerations shown in Fig. 3.15, the current filters are remains inefficacious in some cases. In order to extract the step features more accurately, several additional operations are requisite.

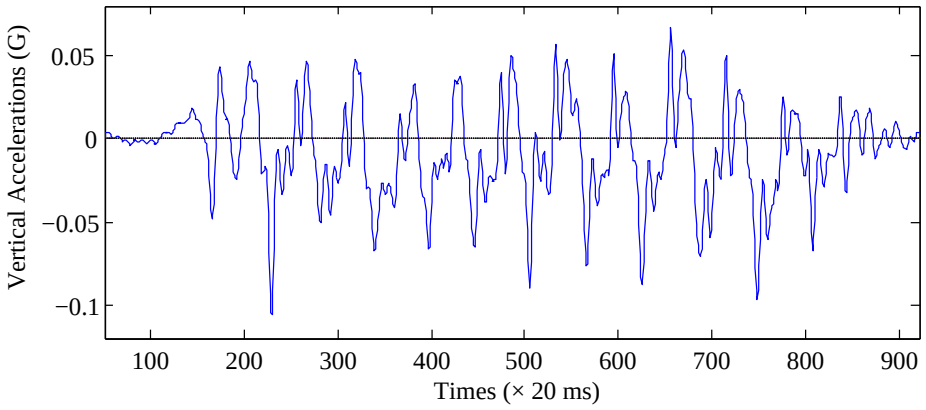

Figure 3.15: An instance of acceleration data after prophase filters. It is still rather difficult to recognize every single step accurately. Certain further processes are still necessary.

Because within each divided waking segment, only straight walking is included, no stop, no turning, and even no transitional activity, the random process noise as well as observation noise are considered following the normal distribution. Kalman Filter can be taken advantage of to further reduce Gaussian noise.

Kalman filtering, also known as Linear Quadratic Estimation (LQE), is an algorithm that uses

a series of measurements observed over time, containing statistical noise and other inaccuracies, and produces estimates of unknown variables that tend to be more precise than those based on a single measurement alone [52] [53]. The filter is named after Rudolf E. Kalman, one of the primary developers of its theory.

The Kalman filter has numerous applications in technology. A common application is for guidance, navigation and control of vehicles, particularly aircraft and spacecraft. Furthermore, the Kalman filter is a widely applied concept in time series analysis used in fields such as signal processing and econometrics. Kalman filters also are one of the main topics in the field of robotic motion planning and control, and they are sometimes included in trajectory optimization. The multi-fractional order estimator is a simple and practical alternative to the Kalman filter for tracking targets.

The algorithm works in a two-step process. In the prediction step, the Kalman filter produces estimates of the current state variables, along with their uncertainties. Once the outcome of the next measurement (necessarily corrupted with some amount of error, including random noise) is observed, these estimates are updated using a weighted average, with more weight being given to estimates with higher certainty. The algorithm is recursive. It can run in real time, using only the present input measurements and the previously calculated state and its uncertainty matrix; no additional past information is required.

In order to use the Kalman filter to estimate the internal state of a process given only a sequence of noisy observations, one must model the process in accordance with the framework of the Kalman filter. This means specifying the following matrices: $\mathbf{A}_k$, the state-transition model; $\mathbf{H}_k$, the observation model; $\mathbf{Q}_k$, the covariance of the process noise; $\mathbf{R}_k$, the covariance of the observation noise; and sometimes $\mathbf{B}_k$, the control-input model, for each time-step, k, as described below.

The Kalman filter model assumes the true state at time k is evolved from the state at k-1 according to

$$\mathbf{x}_k = \mathbf{A}_k\mathbf{x}_{k-1} + \mathbf{B}_k\mathbf{u}_k + \mathbf{w}_k, \tag{3.10}$$

where $\mathbf{A}_k$ is the state transition model which is applied to the previous state $\mathbf{x}_{k-1}$; $\mathbf{B}_k$ is the control-input model which is applied to the control vector $\mathbf{u}_k$; $\mathbf{w}_k$ is the process noise which is assumed to be drawn from a zero mean multivariate normal distribution with covariance $\mathbf{Q}_k$.

$$\mathbf{w}_k \sim \mathbf{N}(0,\ \mathbf{Q}_k). \tag{3.11}$$

At time k an observation (or measurement) $\mathbf{z}_k$ of the true state $\mathbf{x}_k$ is made according to

$$\mathbf{z}_k = \mathbf{H}_k\mathbf{x}_k + \mathbf{v}_k, \tag{3.12}$$

where $\mathbf{H}_k$ is the observation model which maps the true state space into the observed space and $\mathbf{v}_k$ is the observation noise which is assumed to be zero mean Gaussian white noise with covariance $\mathbf{R}_k$.

$$\mathbf{v}_k \sim \mathbf{N}(0,\ \mathbf{R}_k). \tag{3.13}$$

The initial state, and the noise vectors at each step $\{\mathbf{x}_0, \mathbf{w}_1, \ldots, \mathbf{w}_k, \mathbf{v}_1, \ldots, \mathbf{v}_k\}$ are all assumed to be mutually independent.

The data flow of Kalman Filter is illuminated briefly in Fig. 3.16.

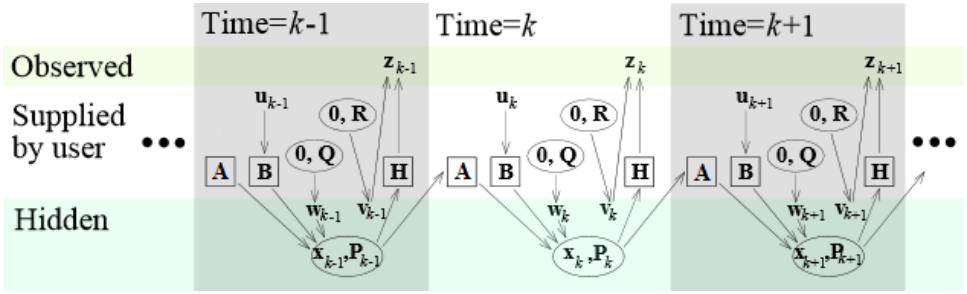

Figure 3.16: The schematic diagram for Kalman Filter The squares represent matrices. The ellipses represent multivariate normal distributions (with the mean and covariance matrix enclosed). The unenclosed values are vectors.

Simplified, the purpose of the Kalman Filter is: with the observation $\mathbf{z}_k$, to calculate the optimal estimation for the true state $\hat{\mathbf{x}}_k$, in order to minimize the covariance of the (*a posteriori*) state estimate's error $(\mathbf{x}_k - \hat{\mathbf{x}}_k)$.

The process of the Kalman Filter is explicated as follow:

Step 1: according to the (*a posteriori*) state estimate at time $k-1$, $\hat{\mathbf{x}}_{k-1}$, to predict the (*a priori*) state estimate at time k, $\hat{\mathbf{x}}_{\bar{k}}$:

$$\hat{\mathbf{x}}_{\bar{k}} = \mathbf{A}\hat{\mathbf{x}}_{k-1} + \mathbf{B}\mathbf{u}_{k-1}, \tag{3.14}$$

where the descriptions for the vectors $\mathbf{A}$, $\mathbf{B}$ and $\mathbf{u}$ are the same with those in Eq. 3.10.

Besides, the (*a priori*) estimate covariance is:

$$\hat{\mathbf{P}}_{\bar{k}} = \mathbf{A}\hat{\mathbf{P}}_{k-1}\mathbf{A}^T + \mathbf{Q}; \tag{3.15}$$

Step 2: according to the (*a priori*) estimate $\hat{\mathbf{x}}_{\bar{k}}$, to predict the observation:

$$\hat{\mathbf{z}}_{\bar{k}} = \mathbf{H}\hat{\mathbf{x}}_{\bar{k}}; \tag{3.16}$$

Step 3: to calculate the difference between the measurement $\mathbf{z}_k$ and the estimation $\hat{\mathbf{z}}_{\bar{k}}$ in order to update $\hat{\mathbf{x}}_{\bar{k}}$ to $\hat{\mathbf{x}}_k$:

$$\hat{\mathbf{x}}_k = \hat{\mathbf{x}}_{\bar{k}} + Kg(\mathbf{z}_k - \hat{\mathbf{z}}_{\bar{k}}). \tag{3.17}$$

With the Eq. 3.16,

$$\hat{\mathbf{x}}_k = \hat{\mathbf{x}}_{\bar{k}} + Kg(\mathbf{z}_k - \mathbf{H}\hat{\mathbf{x}}_{\bar{k}}), \tag{3.18}$$

where $\mathbf{z}_k - \mathbf{H}\hat{\mathbf{x}}_{\bar{k}}$ is the residual, Kg denotes the weight between the estimation and the residual, and also called as Kalman Gain.

Step 4: the covariance of the (*a posteriori*) state estimate's error:

$$\hat{\mathbf{P}}_k = cov(\mathbf{x}_k - \hat{\mathbf{x}}_k). \tag{3.19}$$

With Eq. 3.18 and 3.12,

$$\hat{\mathbf{P}}_k = cov[(\mathbf{I} - Kg\mathbf{H})(\mathbf{x}_k - \hat{\mathbf{x}}_{\bar{k}}) - Kg\mathbf{v}_k], \tag{3.20}$$

Step 5: to differentiate Eq. 3.20, and to make the derivative equal to 0. As a result, the optimal Kalman Gain is:

$$Kg = \frac{\hat{\mathbf{P}}_{\bar{k}}\mathbf{H}^T}{\mathbf{H}\hat{\mathbf{P}}_{\bar{k}}\mathbf{H}^T + \mathbf{R}}. \tag{3.21}$$

The $Kg \in [0,\ 1/\mathbf{H}]$, which means if Kg is approaching to 0, the result totally depends on the (*a priori*) state estimate and the measurement is wholly ignored; if Kg is approaching to $1/\mathbf{H}$, the result totally depends on the measurement and estimation is wholly ignored.

Moreover, the minimum of $\hat{\mathbf{P}}_k$ is:

$$\hat{\mathbf{P}}_k = (\mathbf{I} - Kg\mathbf{H})\hat{\mathbf{P}}_{\bar{k}}. \tag{3.22}$$

The 5 equations Eq. 3.14, 3.15, 3.18, 3.21, 3.22 are the key ingredients of the Kalman Filter. The update process is demonstrated in Fig. 3.17 as well.

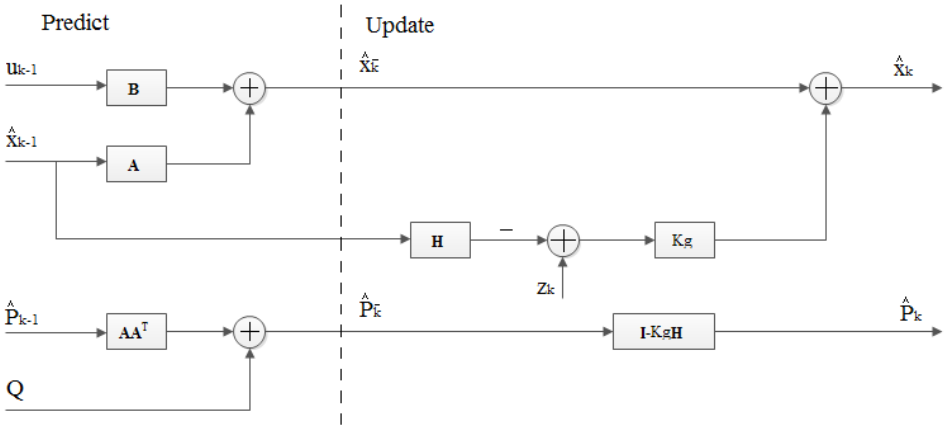

Figure 3.17: The flow chart of the Kalman Filter

In this dissertation, the variance of observation noise R is set as the variance of the vertical accelerations when the device is considered static. That "static" period is regarded as the stationary calibration phase which is described in the Section 3.2. Besides, with respect to the variance of the process noise Q, according to the datasheets of accelerometer and gyroscope from several mainstream inertial sensor corporations, this value is set as 0.00001 constantly.

The algorithm for the Kalman Filter is as follow:

Algorithm: Kalman Filter

Input: $input[]$ with size N;
R, Q;
Output: $predicted[]$ with size N;

```
1 begin
2   p[] with size N, whose first item is 1 and the rest are 0;
3   while i < N − 1 do
4     p_temp ← p[i] + Q;
5     Kg ← p_temp / (p_temp + R);
6     predicted[i + 1] ← predicted[i] + Kg × (input[i] − predicted[i]);
7     p[i + 1] ← (1 − Kg[i]) × p[i];
8     i ← i + 1;
9 end
```

where Kg denotes the Kalman Gain.

The effect of the Kalman Filter in the off-line simulation is shown in Fig. 3.18. From the treated data after the Kalman Filter, the jitters and noise are eliminated to a great extent.

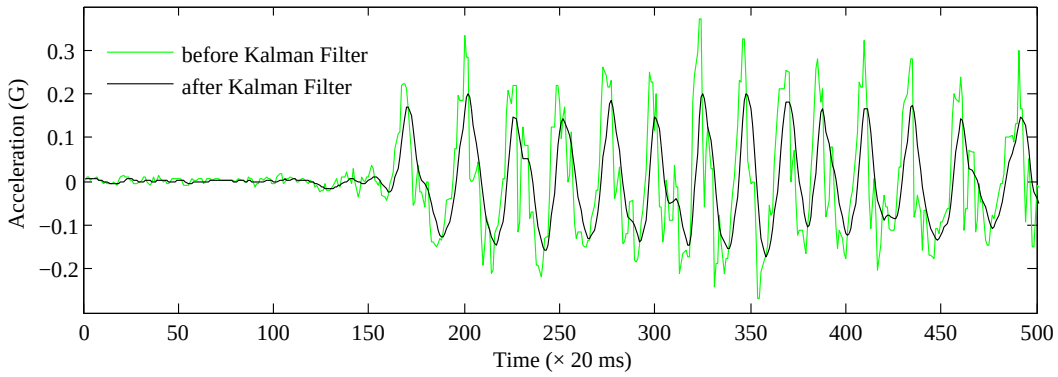

Figure 3.18: A segment of acceleration signals are processed by the Kalman Filter. The input signal is after the Moving Average Filter, while the output is after the Kalman Filter

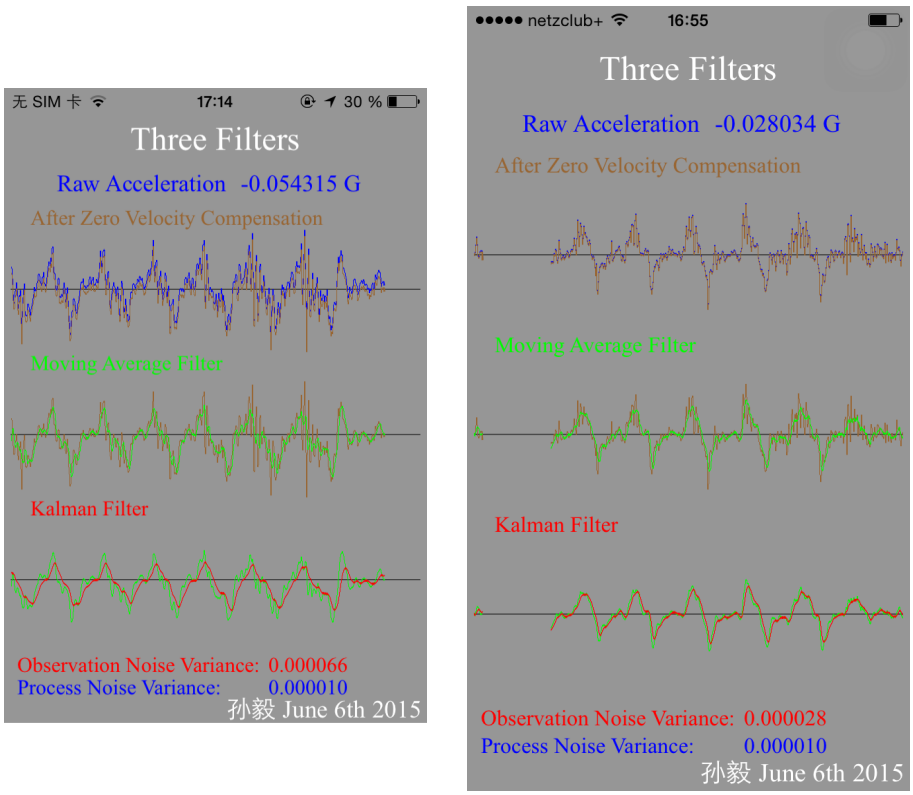

(a) Test with iPhone 4 (b) Test with iPhone 6

Figure 3.19: The effects of Moving Average Filter

On top of that, the test app shown in Fig. 3.4 also has the function of Kalman Filter. The effect in real-time is demonstrated in Fig. 3.19. In the experiments, the pedestrian's hand trembles a bit to simulate severer noise so that the role of Kalman Filter would be more impressive.

In Fig. 3.19 (a) is the screenshot from iPhone 4 while (b) is that from iPhone 6, which is a comparison between the oldest and latest available iOS devices. In this test experiment, the volunteer is required to hold the smartphones with a trembled hand in order to highlight the effect of the Kalman Filter. In both figures, the green lines denote the acceleration signals before processed by the Kalman Filter, while the red lines indicate the signals after filtered. From both test platforms, it can be observed that the jitters on the green lines are rejected by the filter to the great extent. Nevertheless, the intrinsic waveforms and useful features are reserved.

3.6 Step Recognition

3.6.1 Related Works

a) Zero Cross Detection

A step is recognized when a pair of valid peak and trough is detected within a segment of vertical acceleration signal. A convenient way to use the cyclic property is to monitor the accelerations for zero crossings [54]. This is a popular choice for pedometers or activity monitors due to its simplicity. However, sometimes (just like the situation in Fig. 3.15) this scheme would result in several mistakes. In other words, merely with zero cross detection the effectiveness of step recognition will be unquestionably disappointing. For a satisfactory stabilization in the future positioning application, a number of additional schemes are supposed to be employed to cope with all the latent unsteadiness, just like those listed in zero cross detection above. Naturally these extreme situations are seldom but difficult to handle.

b) Flat Zone Detection

This scheme caters to the situation that placing the sensors on shoes [48] or shanks [55] [56]. With reference to shoes, between foot-strike and toe-off there is a "flat" pause in the acceleration signal. Concerning the shank-worn sensors, the shank vertical event can be detected by gyroscope. These flat zones can be used to mark the borders between steps and therefore the recognition is implemented. But in this paper the platform for the positioning system is smartphone, the possible position for sensors is in hand or pocket, this scheme is thus inappropriate.

Both the methods above are adopted in numerous personal fitness applications or Wearable Health Monitoring Systems (WHMS). The pedometer module uses various schemes for recognizing steps. The zero cross detection is easy to implement but it is vulnerable to the latent disturbances which

degrades the stabilization of the system greatly. In my preliminary experiments, when pedestrian is slowly wandering that the measured acceleration signal fluctuates around the 0 axis slightly, the zero cross points are rather confused to be identified. With regard to the flat zone detection, as introduced above this scheme is primarily for the systems which place the sensors on humans' lower limbs. In this dissertation my positioning system is concerning the platform of smartphone, this scheme is therefore not under my consideration.

3.6.2 Peaks and Troughs Detection

The step recognition approach eventually employed in my system is peaks and troughs detection, which detects a series of valid peak-trough pairs in the acceleration signal and accordingly extracts the useful features for step classification and length estimation.

The technique details lie in the following 3 aspects:

a) Dynamic Thresholds

In most current pedometer or similar applications, a step is detected when the acceleration exceeds a preselected fixed threshold. This method is simple but also with limited precision. Different pedestrians with various gaits in manifold shoes all lead to totally diverse acceleration waveforms. If the system is simply for roughly daily activities monitoring, it is barely adequate. However, with respect to the indoor positioning system whose requirement in accuracy is comparatively high, this fixed threshold method is quite incapable. In order to detect these peaks and troughs more precisely, a dynamic relative threshold scheme is presented by [32] [39].

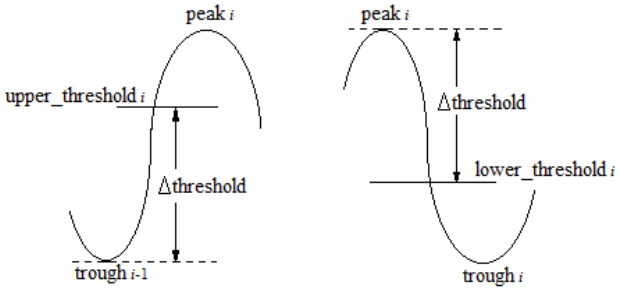

Figure 3.20: The peak and trough of the ith step are identified by the dynamic thresholds

A series of dynamic thresholds are set to identify the successive peaks and troughs. The threshold for a peak was determined by the value of the last trough, while the threshold for a trough was calculated from the amplitude of the last peak. As Fig. 3.20, the threshold for the *i*th peak $peak_i$, $upper\_threshold_i$, is the value of the last trough $trough_{i-1}$ plus a relative parameter $\Delta threshold$.

Similarly the threshold for the ith trough $trough_i$, $lower\_threshold_i$, is the value of the last peak $peak_i$ subtracts a relative parameter $\Delta threshold$. Because of the correlation among the adjacent steps, to some degree, this scheme is invulnerable to gait change that the amplitude of the acceleration may vary gradually. During my experiments this relative $\Delta threshold$ is set as $0.2\ G$ empirically.

b) Level Crossing Algorithm

Normally a peak is defined as the point whose value is larger than the adjacent points on both sides, while likewise a trough is less than its neighbors. A simple way for peak trough detection is searching all these points with above characteristics. Nevertheless, occasionally there are more than one peaks or troughs could be found in one single wave cycle (as Fig. 3.18, near point 425, there are still 2 troughs detected in a single wave cycle). With regard to these stubborn jitters directly using the maxima and minima will definitely mislead the further steps length estimation. As a result an advisable scheme is introduced in this section to deal with these intractable jitters so that more reliable peak-trough pair could be identified for every wave cycle.

A Level Crossing Algorithm is utilized to search the unique peak and trough in a single wave cycle [57] [58]. Suppose the series of acceleration values up to now are $a_0, a_1, \ldots, a_n$, where a_n is the most recent. a_n is mapped as a beacon on the basis of

$$sign(a_n) = \begin{cases} 1, & if \ \ a_n > \mu_n + \sigma_n \\ 0, & if \ \ a_n < \mu_n + \sigma_n \\ \wedge, & otherwise \end{cases} \tag{3.23}$$

where μ_n denotes the average of the series, σ_n is the standard deviation, and $\wedge$ indicates an undefined state. Two thresholds $\mu_n + \sigma_n$ and $\mu_n - \sigma_n$ are the two levels for characterizing "up" and "down" respectively. Both μ_n and σ_n can be updated incrementally based on the new incoming signal. This mapping yields a sequence of beacons. Then the consecutive 1-beacons are merged into a single bit 1, 0-beacons into 0, and $\wedge$s into $\wedge$. A pattern "10" or "$1 \wedge 0$" is considered a valid peak. The 2 temporary thresholds $\mu_n + \sigma_n$ and $\mu_n - \sigma_n$ can be adjusted for better performance. Similarly, the trough items can also be identified by the patterns "01" or "$1 \wedge 0$".

Rather than the simple maxima or minima, the operative peaks and troughs could be targeted with higher accuracy by the Level Crossing Algorithm.

c) Double Peaks (Troughs) Merging Algorithm

The filters, approaches, algorithms employed above can to a great extent reject the jitter in the acceleration waveform, but sometimes after those there are still successive double peaks or troughs in a single wave cycle left (although not common). In this case, the 2 successive peaks or troughs

need to be further combined. Consequently an algorithm is developed specially for this residual problem after all of the foregone processes.

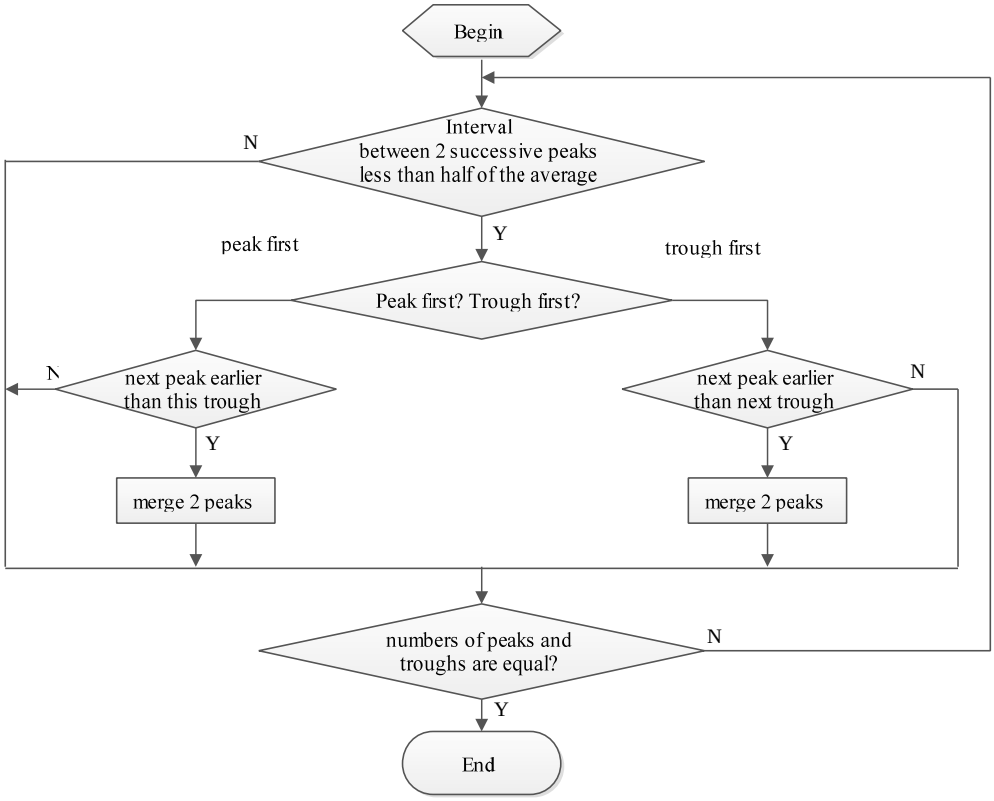

Figure 3.21: The flow chart of the algorithm for removing potential double peaks within a single step wave cycle; for troughs is similar.

In Fig. 3.21, the algorithm for removing the residual jitters toward peaks is demonstrated. After the previous approaches, there is an array for peaks, in which all of the indexes (time points) for each peak are stored, while for troughs also. Initially, every 2 successive peaks' time interval is calculated. If any 2 peaks are too close (their interval is less than half of the average interval of a whole walking segment), a case of double peaks may occurs. Subsequently, according to different situations (peak first, or trough first), different processes are implemented to verify whether successive double peaks are recorded accidently or not.

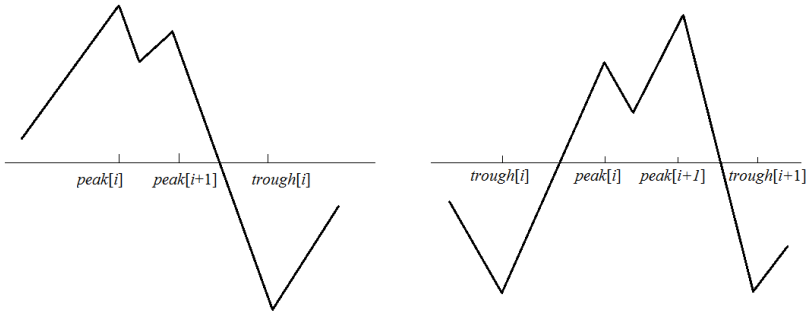

(a) The situation, peak first then trough (b) The situation, trough first then peak

Figure 3.22: When a jitter happens, double peaks may be recorded within a single wave cycle. The arrays *peak*[] and *trough*[] store the indexes of every peak and trough detected. (a) is for the situation, peak first, then trough; while (b) is for trough first and then peak.

As shown in Fig. 3.22, normally the peaks and troughs recorded should take place by turn. In other words, the indexes which are stored, should be $\ldots < peak[i] < trough[i] < peak[i+1] < trough[i+1] < \ldots$ (if peak first), or $\ldots < trough[i] < peak[i] < trough[i+1] < peak[i+1] < \ldots$ (if trough first). But when successive double peaks occur, $peak[i+1]$ would smaller than $trough[i]$ (the next peak would earlier than the trough in the current step); or $peak[i+1]$ would smaller than $trough[i+1]$ (the next peak would earlier than the trough in the next step). Once these happen, the 2 successive peaks would be merged, that means only the larger acceleration value's index would remain and the smaller one's index would be deleted from the array *peak*[].

Likewise, the potential successive double troughs can also be removed by this algorithm. The corresponding flow chart as well as the similar procedure is not described repeatedly here.

After this algorithm takes effect, the faults could be tolerated in a great measure. Although therotically it can never guarantee that all of jitters would be removed unconditionally, practically according to my multitudinous experiments, none of this kind of accident happens again. A possible reason is that after a mixed variety of filters plus algorithms, and the instability during gait transition are excluded also, the extreme situations are already few and far between.

A demonstration app is developed and shown in Fig. 3.23, which integrates all the filters and algorithms discussed in this chapter to perform the function of step recognition. The ZVC, Moving Average Filter, Divide and Conquer Strategy, Kalman Filter are utilized to meliorate the sampled acceleration waveform. Moreover, the Dynamic Threshold, Level Cross Algorithm and Double Peaks (Troughs) Merging Algorithm presented in this section are for peak-trough pairs detection.

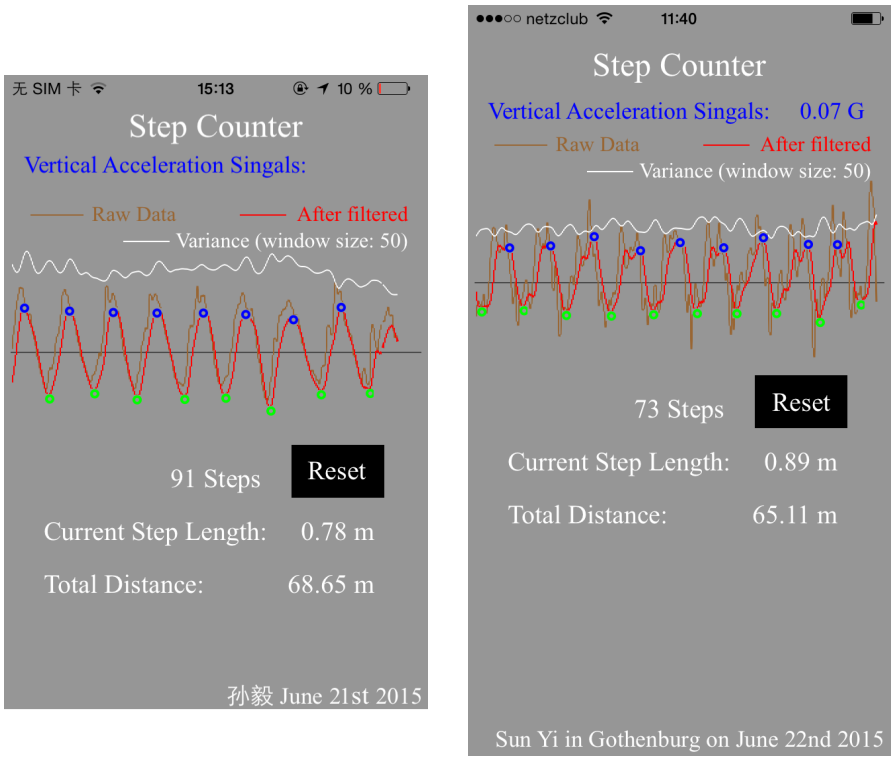

(a) Demo on iPhone 4 (b) Demo on iPhone 6

Figure 3.23: The screenshot of the demo app for step recognition

The brown lines denote the raw accelerations and the red lines indicate the data after multiply filtered. The white lines are the variance of the filtered data, which is used for activating the step recognition (determining the active walking phase discussed in Section 3.4). All the valid peaks are highlighted with blue signs and troughs with green. According to these alternate peaks and troughs, each step is counted successively.

This demo app is running on different iOS devices and tested by diverse volunteers. From the experiments the accuracy of step recognition is completely satisfactory. Particularly in the (b) figure, although several intractable jitters remain on the treated waveform, the identification for peaks and troughs is still precise.

As other test apps shown in this chapter, this “Step Counter” is also not submitted to App Store, because a more comprehensive app which includes more functions is already available in App Store and will be introduced in the next chapter (Fig. 4.16).

3.7 Alternative Scheme

3.7.1 Model Wave Simulation

As discussed before a series of filters and algorithms can reduce all kinds of noises to the minimum. Their serviceability is proved by all range of off-line experiments as well as the real-time app. However, so much prophase processes before walking distance estimation are a great challenge for certain smartphone platforms. In my dissertation most of the experiments are based on iOS devices whose hardware capability is superior among the similar products. Once a less advanced terminal device is referred to, probably the computation cost towards these multiple filters and algorithms is rather large and furthermore the performance of the final positioning system may be subject to this disadvantage.

To develop a universal system which could be spread to a wide variety of portable devices with various processing capacities, an alternative approach is proposed in this section. In contrast, the bias towards the step recognition is also acceptable but its computation cost is relative low.

In this section a simulation algorithm is introduced. With the inspiration of template matching, a set of standard sine waves are created to simulate the original data. These artificial model waves should fit the features in original signal as much as possible. From this model wave all of the feature vectors for step length estimation are extracted instead, so that the potential instabilities caused by the distortion in acceleration signals are eliminated thoroughly.

First of all, the active domain for Model Wave needs to be determined as usual. These boundaries are delimited by the moving variance analysis for the acceleration data (as Section 3.4). Because both the boundaries for the anterior-posterior and vertical data are searched respectively and the intersection set of those is defined as the active walking phase, the perturbations when nonconventional activities (marking time or unconscious shaking, etc.) and state transforming are supposed to be excluded. As Section 3.4.1 the window sizes for the moving variance analysis in both the directions are set as 50 sampling points.

As discussed before every peak-trough pair represents a wave cycle which relates to a single step. These waves can be considered as sine-like waves. Every wave cycle has its unique upper amplitude, lower amplitude and a frequency. In order to make the created model waves fit the original signals as coincident as possible, for every wave cycle within an active walking interval, the optimal upper / lower amplitudes and frequency are searched. These “optimal” parameters mean that the sum of the differences between each point on the simulated wave and its corresponding point on original signal is expected to be made to the minimum.

The algorithm of the Model Wave Simulation is described as follow:

Algorithm: Model Wave Simulating

Input: $Wave_O[]$; //Original Wave between breakpoints

Output: $Wave_M[]$; //Simulated Model Wave

```
1 begin
2 for ith step
3  for upper_amplitude[i] ⇐ 0.1 to 0.5
4   for lower_amplitude[i] ⇐ 0.1 to 0.5
5    for frequency[i] ⇐ 1.0 to 4.0
6     find min Σ_{j∈movWindow[i]} |Wave_M[j] − Wave_O[j]|;
7     save the fittest amplitudes and frequency for this step;
8 Create sine waves by saved parameters of each step;
9 end
```

The moving window size is set as 3 steps in my experiments. In other words, the parameters of each step are depended on its previous step and following step. Because of the shaking when walking, the vibrations of other body parts are also recorded by smartphone. Especially when pedestrian changes gait or speed up suddenly, the disordered data around these transition points are rather complicated and difficult to handle. With the new model wave the disorders are smoothed away but useful features are kept. This Model Wave Simulation Algorithm can simplify the process of step recognition and shows better operability on the embedded platform, especially on certain less advanced smartphones.

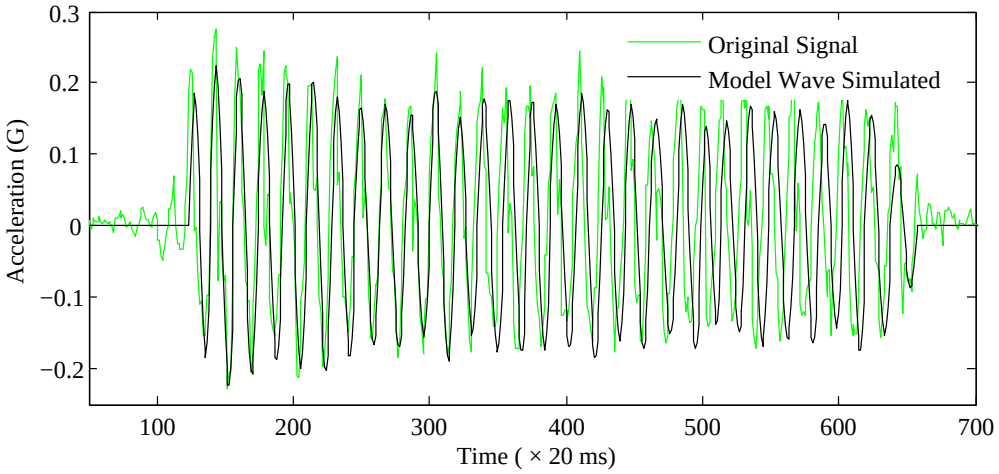

Figure 3.24: The effect of Model Wave Simulation Algorithm

3.7.2 Evaluation

The effect of the Model Wave Simulation Algorithm is demonstrated in Fig. 3.24. In the figure the new created model waveforms are perfectly conformable with the original waveforms. After that the feature vectors for step length estimation can be copied but the ambiguous distortions are therefore ignored.

Progressing to the comparison between this algorithm and previous schemes, in view of the fact that the results from the model wave simulated are often not exactly the points of peaks and troughs, there is no comparability in precision between previous analytic schemes and this simulation algorithm. Nevertheless with respect to the reject rate and the misrecognition rate, this algorithm is flawless. Although the error rate of previous schemes is quite low, they cannot provide absolute reassurance. Once a couple of peaks or troughs are missing, misrecognized or disordered, this imperfect input could cause a series of meaningless results in further step length estimation, and for the whole positioning system is a potential factor of instability. Hence this is also a unique advantage of the Model Wave Simulation Algorithm and it is reasonable to employ this algorithm in the realistic system especially when the hardware condition is limited.

Recap

In this chapter with the sampled data form the IMUs, the prophase processes for the step length estimation are explicated. They consist of using ZVC and Moving Average Filter to ameliorate the acceleration signal; dividing the whole walking phase into small segments to abate the complexity; applying Kalman Filter to further reject the noises; then with the treated acceleration signal, the Dynamic Threshold, Level Cross Algorithm and Double Peaks (Troughs) Merging Algorithm are employed successively to recognize and count the steps. Taking the computation cost into consideration, an alternative scheme named Model Wave Simulation is proposed lastly to adapt to the less advanced devices with relative low processing capability. Although the filters and algorithms introduced in this chapter are not the key ingredients in the final indoor positioning system, they lay an indispensable foundation to the crucial procedure of step length estimation.

Chapter 4

Walking Step Length Estimation Model

Based on the meliorated acceleration waveform the approaches of step recognition and counting for pedestrian are explicated in the last chapter. In this chapter the key procedure for positioning is introduced, which is to estimate the step length according to the walking acceleration features. On the basis of the system architecture stated in Section 2.1, it is also the core of a Step and Heading System (SHS).

4.1 Related Works

As discussed in the last chapter, the stepping of pedestrian can generate discrete impulses in the acceleration signals. According to a few physical features of these special waveforms, the horizontal moving distance of the body barycenter could be reckoned statistically. The wearable IMUs are widely utilized in numerous sports training and personal fitness systems for recognizing and analyzing humans' daily activities. In terms of the step length estimation, comprehensively there are 9 mathematical models concluded from the previous literatures [59].

4.1.1 Static Models

1) Constant Step Length

Some applications employ this method. The users have to measure their average step lengths by theirselves (walk with a certain amount of steps and measure the distance), or use the recommended value by default.

2) Determined by height

The step length for male is regarded as 0.415 times his height, while for female is 0.413 her

height [60]. This is a convenient method in a few pedometers based apps which counts the steps by the acceleration impulses and simply cumulates the step length and energy expenditure within a period.

4.1.2 Dynamic Models

Obviously the 2 static models above are rather rough and solely capable in certain imprecise applications. For more scenarios which have higher requirement in accuracy, a series of dynamic mathematical models based on a variety of physical items of acceleration were developed by previous researchers.

3) Weinberg Model [61]

$$step\_length = k \cdot \sqrt[4]{a_{max} - a_{min}}\,, \tag{4.1}$$

where a_{max} and a_{min} denote the peak and trough value of the vertical accelerations in that step; k represents the user specified parameter. This classical model was proposed by Weinberg in 2002, which uses the difference between the peak and trough values for reckoning the step length. The larger the drop between maximum and minimum is measured, the longer the corresponding step is supposed to be taken by the pedestrian. The customized parameter is adopted to cater to exacting users.

4) Kim Model [45]

$$step\_length = k \cdot \sqrt[3]{\frac{\sum_{i=1}^{N} |a_i|}{N}}. \tag{4.2}$$

There are N sampling points in the step and a_i is the vertical acceleration of the ith sampling point; k indicates also the user parameter. In this model, the magnitude of the acceleration (the expression in the cubic radical sign) is drawn upon, which is regarded as an index for describing the intensity level of the physical vibration. It is reasonable to consider that the more intense vertical vibrations of the body lead to the bigger strides.

5) Scarlett Model [62]

$$step\_length = k \cdot \frac{\frac{\sum_{i=1}^{N} |a_i|}{N} - a_{min}}{a_{max} - a_{min}}. \tag{4.3}$$

The explanations for the parameters are the same as the equations above. The peak and trough values, their difference as well as the magnitude are utilized.

6) Xu Model [46]

$$step\_length = k \cdot [(a_{max} - a_{min}) + \sqrt[4]{a_{max} - a_{min}}]. \tag{4.4}$$

This model was patented. Similar to Weinberg Model, merely the difference between the peak and trough value is made use of. But the expression of Xu Model is a bit more complicated.

7) Frequency Related Models

A number of researchers also maintain that there is a linear relation between the step length and the step frequency [21] [63] [64]. They harbor the idea that the pedestrian with a higher walking frequency is more likely to make a longer step length, because it is universally acknowledged that when a pedestrian walks faster, s/he tends to raise the step length and the frequency at the same time. Fig. 4.1 is a typical experiment result from [44].

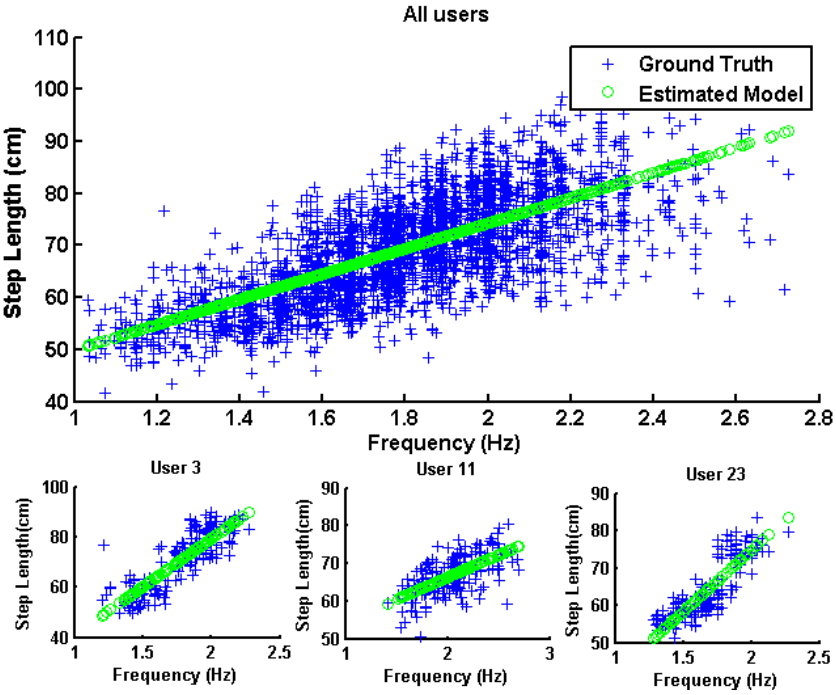

Figure 4.1: The relation between step length and frequency. According to the experiment results from [44], the step length is proportional to the step frequency, which can be applied to estimate the step length.

Other literatures also draw the similar conclusion. Although the concrete mathematical expressions are various, the basic models are like this:

$$step\_length = af + b, \tag{4.5}$$

where f denotes the step frequency, while a, b indicate the customized coefficients which are non-

negative. This model is abstracted from the proportional relation between the step length and the frequency.

Furthermore, more precise nonlinear model is presented by other researcher as well [65]. Rather than using the direct step length and frequency, their rates are referred to instead. Besides, the relation is nonlinear:

$$\begin{cases} k_d = 1.5k_f^2 - 1.8475k_f + 1.3468 \\ k_l = l/l_n \\ k_f = f/f_n \end{cases} \tag{4.6}$$

where k_l denotes the step length rate; while k_f indicates the frequency rate. l and f represent the step length and frequency. l_n and f_n are the step length and frequency when pedestrians walk with their most normal gait (or their average values), which are considered constant.

On one hand, these frequency related models above show better operability and higher fault tolerance ability than the peak-trough pair based models introduced before, in view of the fact that if a couple of peaks or troughs are misrecognized, the unfavorable influence over the measured step frequency is comparative low, but towards the peak-trough schemes it would lead to a meaningless result in that step. On the other hand, the real-time performance in the peak-trough based models is more satisfactory, for the reason that once a pair of peak and trough is recognized, the step length can be calculated immediately, but the measurement for the step frequency could not be implemented instantaneously in any way. Practically the step frequency is a physical quantity with regard to a period of time. In other words, for a single step to precisely measure its frequency is rather intricate. Solely with a handheld device to determine the exact starting and end time of one step is excessively intractable. More feasible solution towards a system based on smartphone is to calculate the average step frequency within a short period of the preceding time. However, the real-time performance of the system is undoubtedly influenced by this inevitable delay. For a health monitor application whose requirement for the timely data is relative low, this short delay is still acceptable, but as an indoor positioning system it is an obtrusive disadvantage. In conclusion, both sorts of the current models have their superiorities and deficiencies. The evaluations toward the accuracy are not the topic here and will be discussed in Section 4.3 exclusively.

Moreover, according to my experiments, there is a fact that, all of linear and nonlinear models above are based on an assumption, or a premise: all of volunteers are required to walk with their normal or comfortable gaits. It can be therefore rationally explained that, why the larger frequency the pedestrian walks with, the longer step length s/he makes. Consequently, the utilization of these

models is limited. They are only suitable for the most normal gaits. Small steps with high frequency and large paces but low frequency are naturally never referred to.

8) Shin Model [54]

$$step\_length = af + bv + c. \tag{4.7}$$

In this model, not only the step frequency (f) but also the variance (v) during that step is involved. As a result it is more delicate than the frequency singly related models listed before because to a certain extent it takes the fact into account that solely a high frequency could not definitely result in a large step.

9) Bylemans Model [38]

$$step\_length = \sqrt[2.7]{\frac{\sum_{i=1}^{N}|a_i|}{N} \cdot \sqrt{\frac{k}{\sqrt{\Delta t \cdot (a_{max} - a_{min})}}}} \cdot 0.1, \tag{4.8}$$

where Δt denotes the duration of the step (in ms), the meanings of the rest of the parameters are similar to those of the models before. In Eq. 4.8, the magnitude of the accelerations, the frequency and the peak-trough difference are all included. Thus the advantages of the peak-trough pair based models, the magnitude involved models and the frequency related models are all incorporated in this model. Contrary to Weinberg Model and Xu Model, it argues that the step length decreases with the increasing of the peak-trough difference. The reason for this contradiction is investigated in my experiments and will be analyzed in the following section. After all, Bylemans model is up to now the most meticulous and comprehensive step length estimation model and was employed in my previous works [33] [66] as well.

4.2 Walking Step Length Estimation Model

Although some of the current models already show their conveniences, most of them are only suitable for the most common gait for human (step length: 0.65 to 0.75 meters, frequency: 90 to 120 steps per minute). When it comes to more varied and abundant gaits, the effect is less than satisfactory. For higher precision of the step length estimation as well as positioning, a novel mathematical model is investigated in this section. This new model is supposed to be general for all sorts of gaits, because the pedestrian activities may also include wander and roam. For the application scenarios of museum or exhibition hall, a lower walking speed is more preferred, while a higher speed is geared towards the walking race.

This estimation model is expected to be one or a set of mathematical expressions that the step

length could be deduced from other physical items measured by inertial sensors. Due to the diversity of the human bodies, theoretically modeling for individuals' physical structures is extremely complicated. For that reason an exact analytic model which is universal to all kinds of the human gaits does not appeal to most of the researchers. It is widely shared that the statistical models are more feasible. All of the previous investigations listed in the last section also focused on the statistical relations among the step length and other acceleration related physical items such as the magnitude of accelerations, the peak value, the trough value, the variance and the frequency of that step. In order to discover more substantive relations among the step length and those physical items, a multitude of experiments are designed and implemented in my research.

The experiments are based on the built-in IMUs of smartphone. The sampling rate is set to 50 Hz. All the acceleration related data are measured in G, which denotes 1 unit of gravity acceleration (c.a. 9.8 m/s^2). The coordinate transformation and filtering for the accelerations comply with the approaches explicated in Chapter 2 and 3. The step length is set from 0.4 to 0.9 m, every 0.05 m a group, and 11 groups in all; while the frequency varies from 60 to 180 spm, every 5 spm a group, and 25 groups in all, where spm represents steps per minute. For every step length group, and every frequency group: the magnitude, the average peak value, the average trough value, and the variance for the acceleration data in both the anterior-posterior direction (y-axis), the vertical direction (z-axis) and their module (m) are recorded (12 items in total). The definition of the magnitude is the same as that in Eq. 4.2, 4.3 and 4.8). Although it has been discussed in Section 3.1 that solely the accelerations in vertical direction are the most sensitive to stepping, here in order to discover more potential relations among the step length and other physical items as comprehensive as possible, the quantities in the y-axis and their module ($\sqrt{y^2 + z^2}$) are also recorded for analysis. Each combine group contains a certain step length and a certain frequency, so there are 275 combine groups altogether. In order to reduce the random errors, all of these experiments are implemented by just one volunteer, and every combine group with the same gait is performed at least 10 times. All these experiments were performed in the corridor of our institute (as Fig. 4.2). A treadmill is not adopted due to the potential influence of conveyer belt in the y-accelerations. The walking distance for 1 time is between 20 and 30 meters (20 to 50 steps). As a result the whole walking distance for this volunteer is more than 50 km. The first stage for the experiments lasted for 3 weeks (The following stages are for running, putting smartphone in pocket and climbing stairs).

As shown in Fig. 4.2, to adjust the volunteer's steps to a preselected frequency, a metronome app for musical instrument is utilized. To make the volunteer's steps coincide with a certain length, a measuring tape is laid on the floor and all of the foot striking points are marked with color tags (Fig. 4.3).

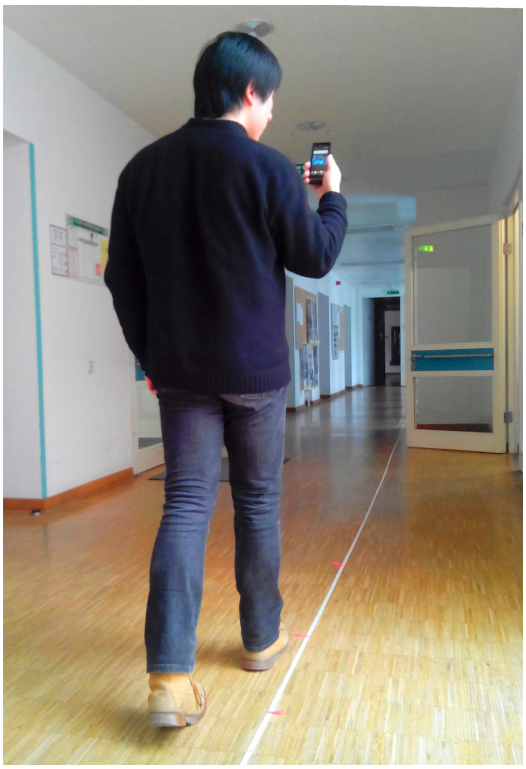

Figure 4.2: To develop the step length model, a large number of experiments are implemented by volunteer. The step length and frequency are calibrated by measuring tape and metronome. The acceleration data are collected by smartphone.

Figure 4.3: The step lengths are adjusted by the tags on the measuring tape.

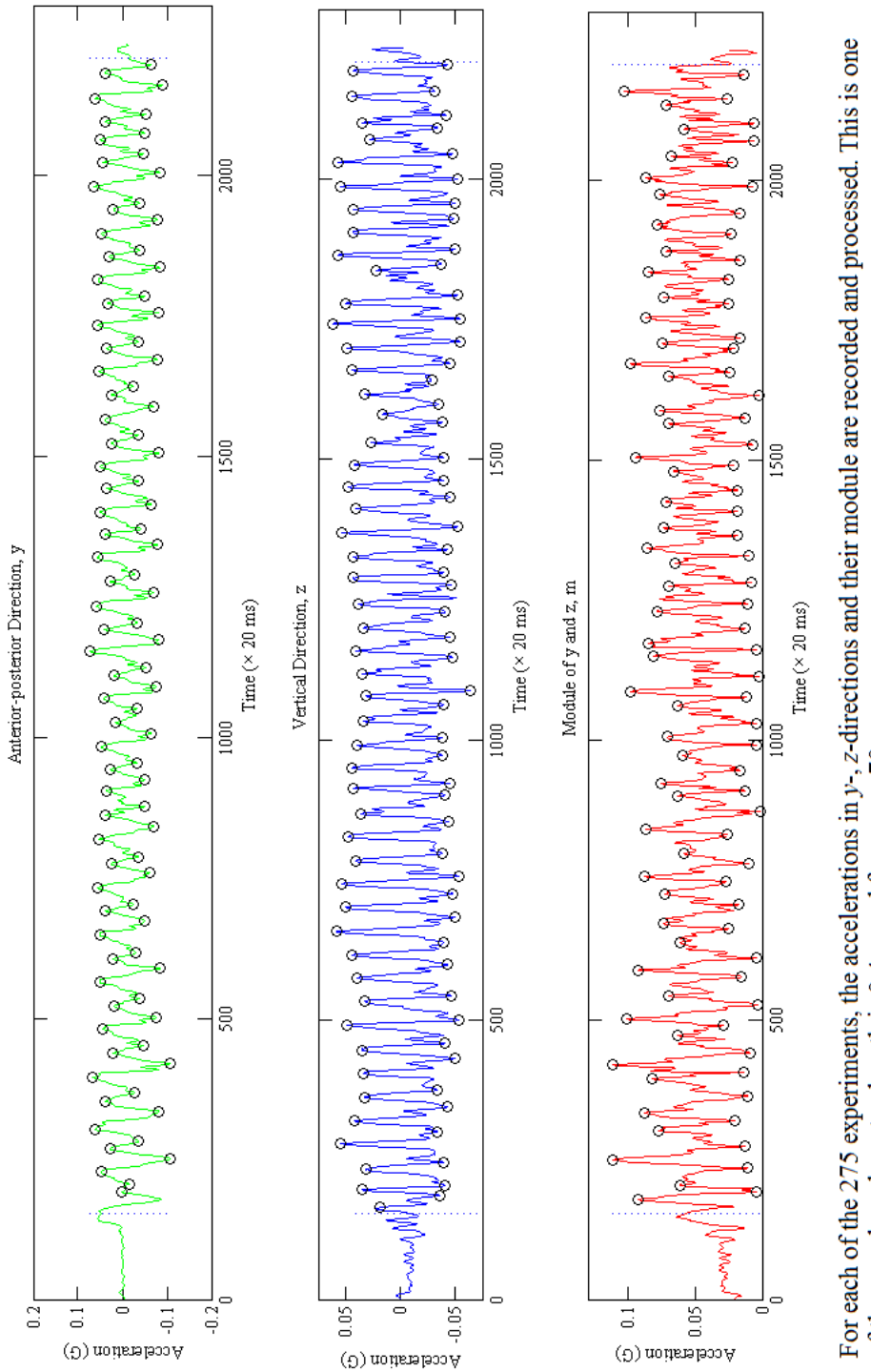

For each of the 275 experiments, the accelerations in *y*-, *z*-directions and their module are recorded and processed. This is one of the samples when step length is 0.4 *m* and frequency 70 *spm*.

Figure 4.4: The sampled data during the experiments

After 3 weeks of the walking experiments, a considerable quantity of data are acquired. An assumption has to be accepted that the variation in the volunteer's weight could not impact the collected data greatly.

As an instance, Fig. 4.4 shown a set of acceleration data collected from one walking experiment. In this group the volunteer is required to walk for 50 steps, with each step length 0.4 *m* and frequency 70 *spm*. The walking distance is 20 *m*. The acceleration signals displayed in Fig. 4.4 are filtered. According to the Divide and Conquer Algorithm introduced in Section 3.4, the starting and end points of the valid walking phase are indicated by dashed lines. On the basis of the step recognition algorithms illustrated in Section 3.6.2, all of the peaks and troughs on the 3 waves are extracted and marked. The values and the timestamps of these peaks and troughs would play a crucial role in the discovery of the decisive feature vectors.

Furthermore, in order to compare the influence of the given physical items, the relations between these items and the frequency are demonstrated from Fig. 4.5 to 4.10. The sources of these 6 figures are the data recorded when the step length = 0.4, 0.5, 0.6, 0.7, 0.8 and 0.9 *m*. Particularly, instead of the peak and trough values separately, their differences are plotted here.

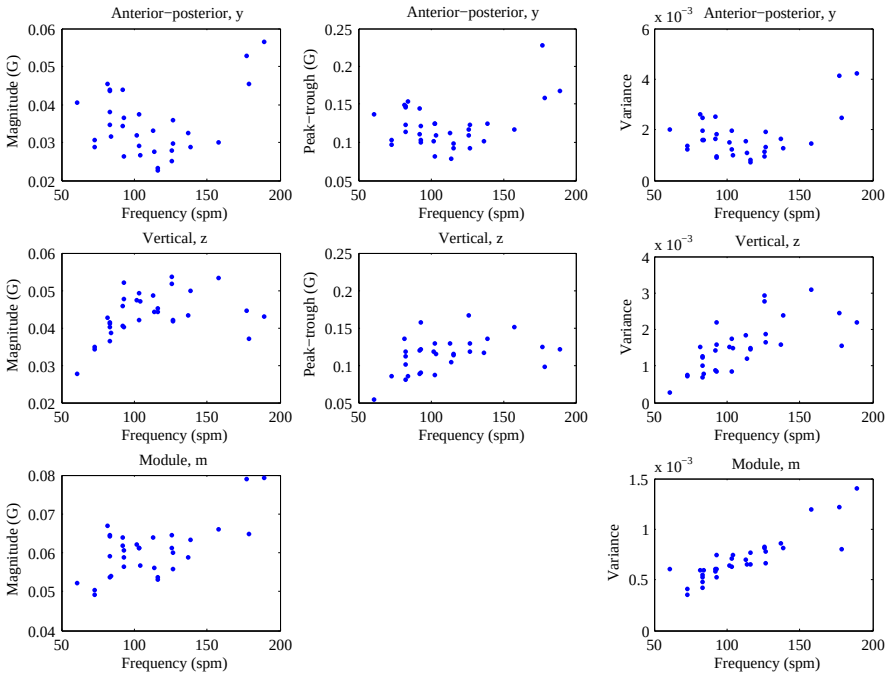

Figure 4.5: With the step length 0.4 *m*, the 8 items vary with the different frequencies

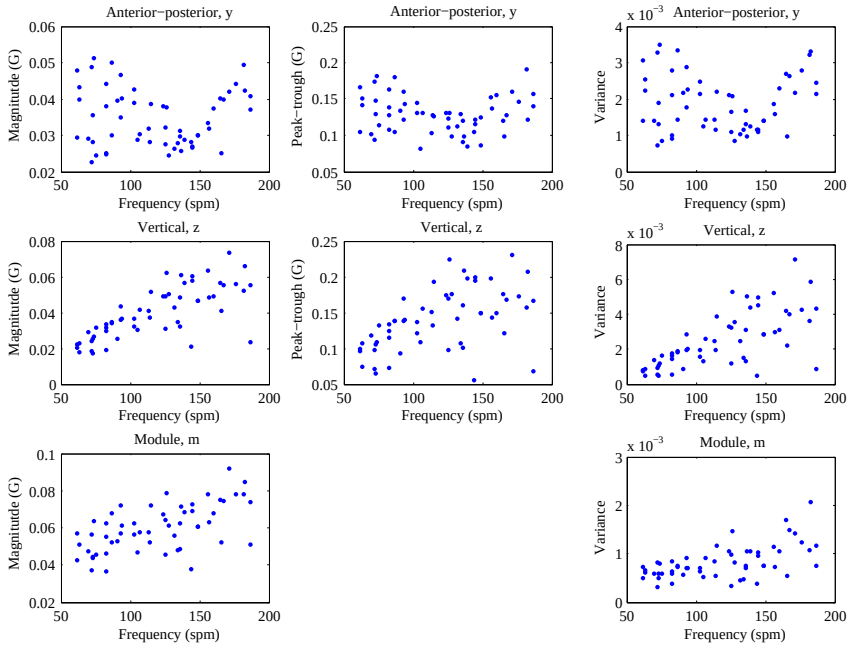

Figure 4.6: With the step length 0.5 *m*, the 8 items vary with the different frequencies

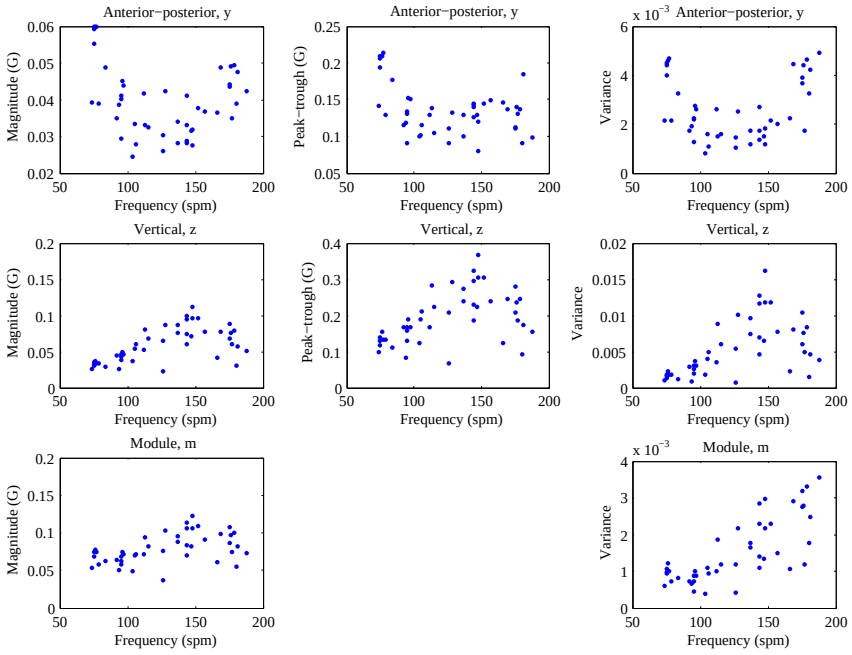

Figure 4.7: With the step length 0.6 *m*, the 8 items vary with the different frequencies

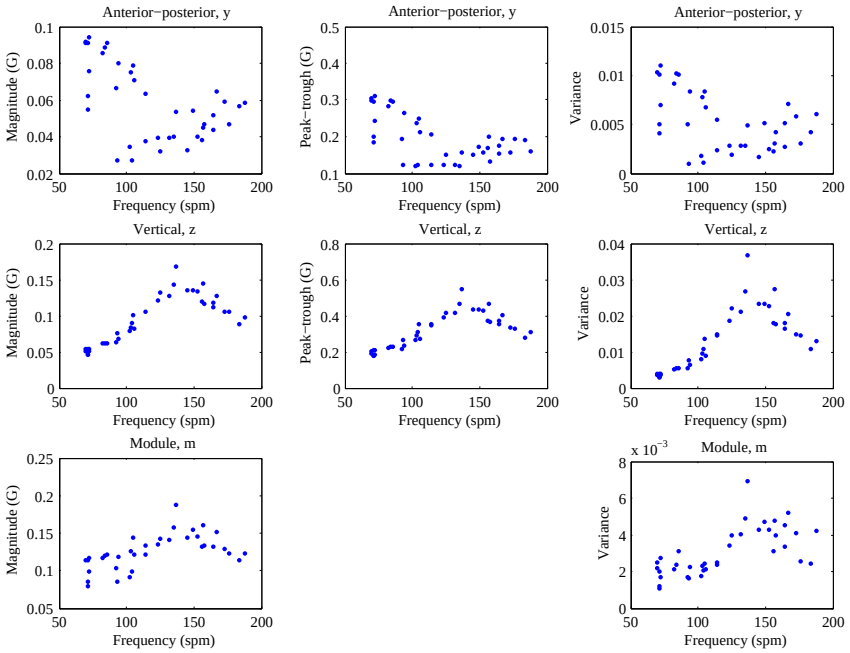

Figure 4.8: With the step length 0.7 *m*, the 8 items vary with the different frequencies

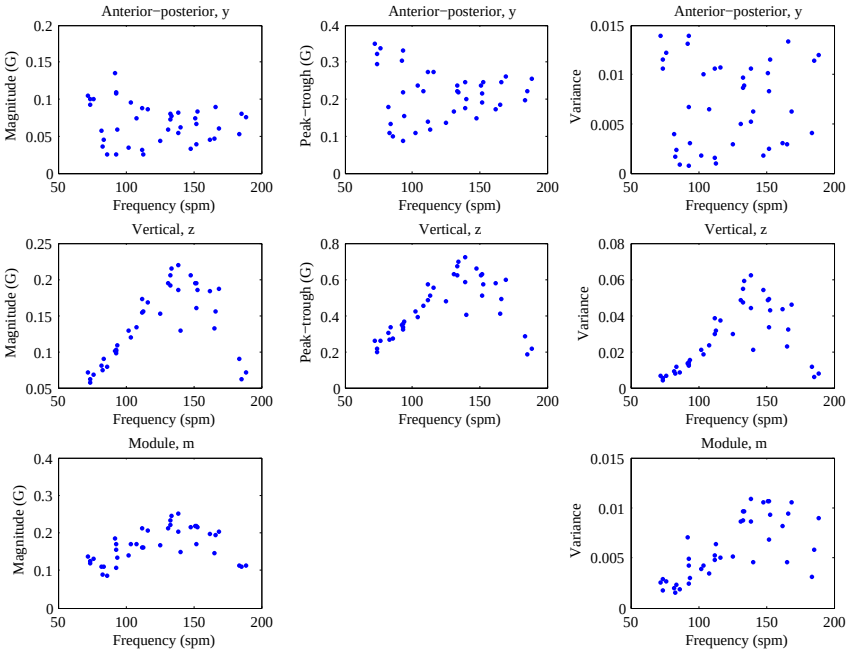

Figure 4.9: With the step length 0.8 *m*, the 8 items vary with the different frequencies

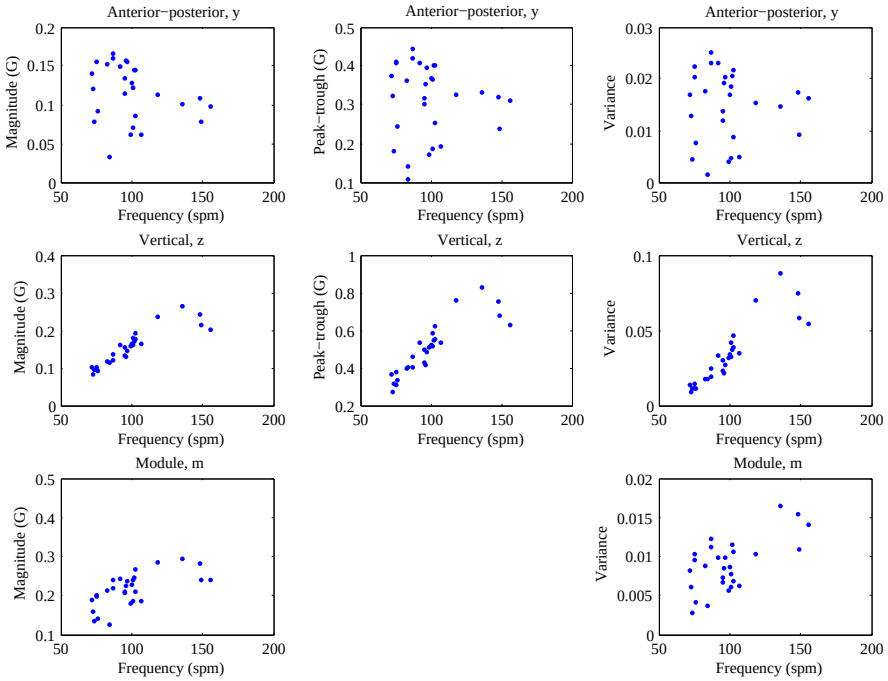

Figure 4.10: With the step length 0.9 *m*, the 8 items vary with the different frequencies

In these 6 figures, from top to bottom they are the physical items in *y*-axis (the anterior-posterior direction), *z*-axis (the vertical direction) and their module (*m*) respectively. From left to right they are the magnitude, the difference between the peak and trough, and the variance of the accelerations successively. Because there is too much confusion in the item towards the peak-trough difference of the module values, the figures for this item are not displayed.

From these 6 figures, it could be noticed that, the relations regarding the *y* data show less regularity than those about the *z* data. Even the longer the step length is, the more confused points are obtained. In order to find out the reason, several raw data are contrasted and analyzed specially. In reality, the waveforms in the *y* direction are not constantly the same. As an instance, in Fig. 4.11, 3 acceleration waveforms in the *y* direction are compared. All of these signals are sampled with the same step length (0.8 *m*) and the same frequency (130 *spm*). Initially, every peak in the upper figure is quite distinct. Subsequently in the middle figure a few troughs rise. And beside the "rising" trough, the 2 peaks draw closer. As a result in the bottom figure, the 2 adjacent peaks almost merge and it is difficult to distinguish them. In other words, every 2 steps make up 1 wave cycle finally. The phenomenon is common in all of the *y*-axis accelerations. At first every step is differentiable. After several times in the same experiment group with the identical gait, the adjacent steps draw closer,

just like the situation in a walking race: in the anterior-posterior direction, weaker impulses would be made, and the body is more likely to make a uniform motion. This phenomenon leads to the distortion in the y signals, and along with the growth of the walking speed, the confusion in the y signals becomes increasingly severe. In contrast, the peaks in the z signals are invariably distinct, without merging tendency. That is why the z data in the 6 figures above show more regularity while the y data not. Since the module comprises both the y and z data, the confusions exist also in its items. In conclusion, solely the z data related items would be involved in my model. This decision is consistent with the conclusion of Section 3.1 as well.

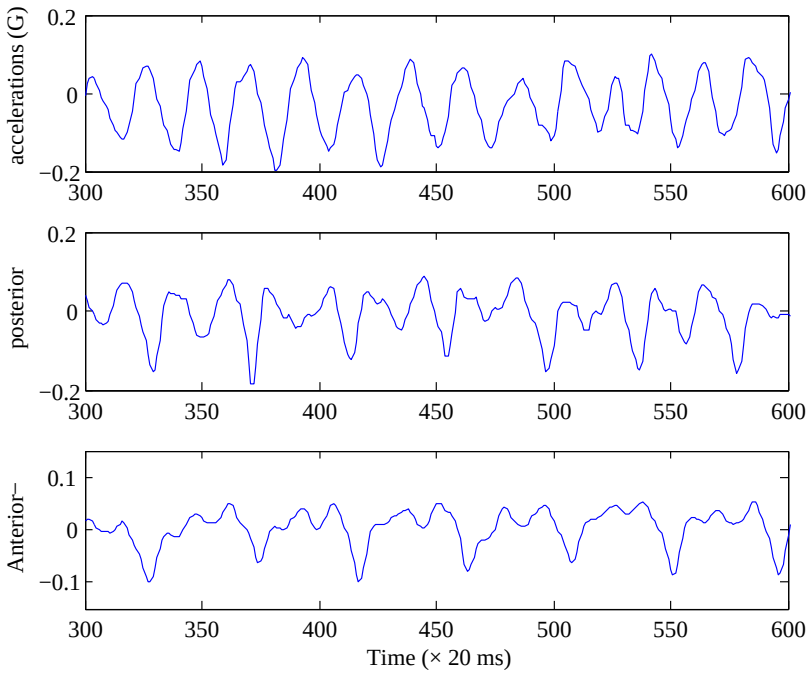

Figure 4.11: Even with the identical gait (the same step length and frequency, the waveforms in the anterior-posterior direction change uncertainly. There is an obvious tendency that 2 adjacent peaks are merging gradually.

The aim of this chapter is to discover a relation that the *step length* can be expressed by the measured physical items. Fig. 4.12 shows in different $frequencies$, the variation relations between the 3 items and *step length*s. Due to the instability in the y data, merely the items regarding the z data are referred to. Here 11 frequency ranges are adopted rather than 11 certain frequency values because during the realistic experiences it is too intractable for a volunteer to adjust his or her steps to a definite frequency precisely for dozens of steps. There are unavoidable deviations in the

frequencies measured afterwards.

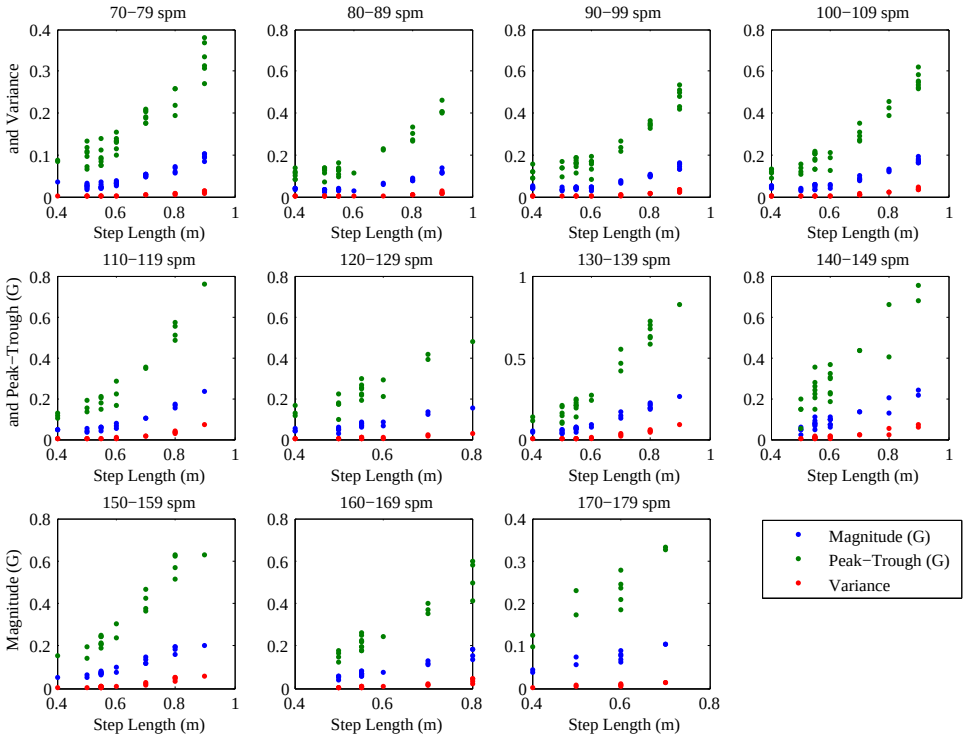

Figure 4.12: The relations between *magnitude*, *peak − trough dif ference*, *variance* and *step length* are demonstrated according to different *frequency* groups.

Table 4.1: The fitting equations of *magnitude* (m) to *step length* (s) in terms of the different *frequency* ranges

Step Frequency Range (*spm*)	**Equations** m **to** s
70-79	$m = 0.25985s^2 - 0.18975s + 0.054113$
80-89	$m = 0.57327s^2 - 0.58185s + 0.18041$
90-99	$m = 0.66367s^2 - 0.65849s + 0.20161$
100-109	$m = 0.63265s^2 - 0.55973s + 0.16571$
110-119	$m = 0.92774s^2 - 0.81974s + 0.22392$
120-129	$m = 0.50208s^2 - 0.31359s + 0.090053$
130-139	$m = 0.78336s^2 - 0.52417s + 0.11824$
140-149	$m = 0.31979s^2 - 0.024486s - 0.01065$
150-159	$m = 0.38369s^2 - 0.12163s + 0.025127$
160-169	$m = 0.33562s^2 - 0.064275s + 0.00059466$
170-180	$m = 0.28869s^2 - 0.1197s + 0.045024$

From Fig. 4.12, it is evident that in all of the 11 frequency ranges, there are obvious quadratic relations between these 3 items and *step length*. By defining just one of these 3 quadratic relations, the step length model could be accordingly developed.

For each of the 11 frequency groups, there would be a corresponding quadratic relation between the 3 items and *steplength*s. Consequently there are theoretically 33 quadratic relations in total. All of these 33 relations are fitted and their equations are listed in Table 4.1, 4.2 and 4.3.

Table 4.2: The fitting equations of $peak - trough\ difference$ (d) to $step\ length$ (s) in terms of the different $frequency$ ranges

Step Frequency Range (spm)	**Equations** d **to** s
70-79	$d = 0.82686s^2 - 0.57518s + 0.17609$
80-89	$d = 1.0236s^2 - 0.76574s + 0.24469$
90-99	$d = 1.4939s^2 - 1.2416s + 0.379$
100-109	$d = 1.3399s^2 - 0.85151s + 0.23725$
110-119	$d = 2.409s^2 - 1.8603s + 0.47695$
120-129	$d = 1.09s^2 - 0.40694s + 0.12914$
130-139	$d = 2.167^2 - 1.2163s + 0.23003$
140-149	$d = 0.9095s^2 + 0.051136s - 0.072082$
150-159	$d = 1.004s^2 - 0.087144s - 0.024795$
160-169	$d = 0.95522s^2 - 0.044558s - 0.056652$
170-180	$d = 0.63705s^2 - 0.031979s + 0.031102$

Table 4.3: The fitting equations of $variance$ (v) to $step\ length$ (s) in terms of the different $frequency$ ranges

Step Frequency Range (spm)	**Equations** v **to** s
70-79	$v = 0.06528s^2 - 0.064894s + 0.016909$
80-89	$v = 0.10454s^2 - 0.1025s + 0.02598$
90-99	$v = 0.15669s^2 - 0.15557s + 0.039663$
100-109	$v = 0.2008s^2 - 0.19112s + 0.046707$
110-119	$v = 0.36055s^2 - 0.34934s + 0.085233$
120-129	$v = 0.17212s^2 - 0.1344s + 0.028213$
130-139	$v = 0.43013s^2 - 0.39086s + 0.090263$
140-149	$v = 0.30767s^2 - 0.27938s + 0.067228$
150-159	$v = 0.23666s^2 - 0.18803s + 0.038631$
160-169	$v = 0.30128s^2 - 0.2862s + 0.071869$
170-180	$v = 0.10899s^2 - 0.081083s + 0.017486$

In addition, the fitting curves for these 33 relations are compared in Fig. 4.13 as well.

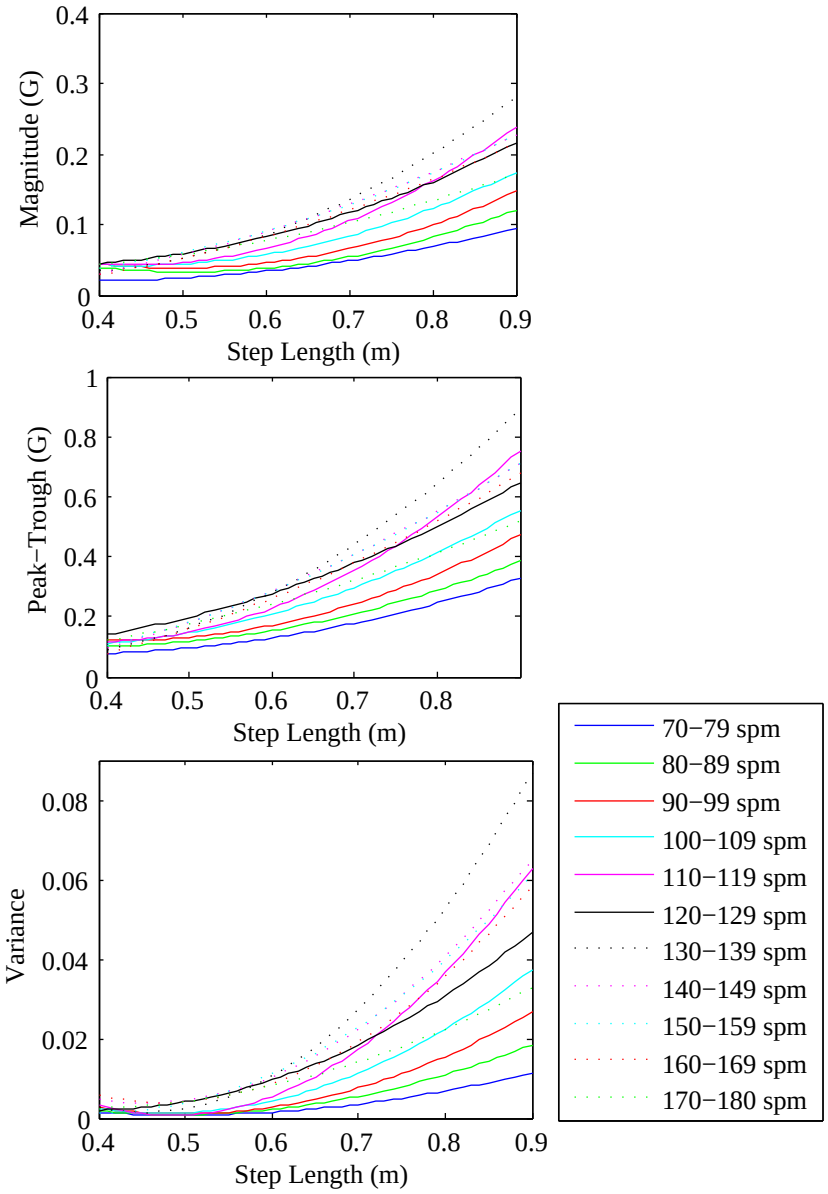

Figure 4.13: The fitting curves of *magnitude*, *peak − trough dif ference*, *variance* to *step length* are illustrated with different *f requency* ranges.

As a result the item *variance* is chosen as the independent variable in the prospective model for the step length estimation. Because from Fig. 4.13, the curves in the bottom figure vary most sharply. Among these 3 items, *variance* shows the most remarkable relation with *step length*. Consequently the objective model is expected to be in the form that *step length* is a function of *variance* and

frequency.

According to Fig. 4.13, it is assumed that the relation between *variance* (v) and *step length* (s) is quadratic:

$$v = as^2 + bs + c, \tag{4.9}$$

where a, b, c are the coefficients to be determined. These coefficients are also the functions of *frequency*. In order to determine these coefficients, the relations between *frequency* and *variance* under certain *step length* are necessary. These relations can be obtained from the data displayed in Fig. 4.5 to Fig. 4.10. As Fig. 4.14, this example is an $f - v$ figure when *step length* is 0.7 m. This figure is already shown as a part in Fig. 4.8.

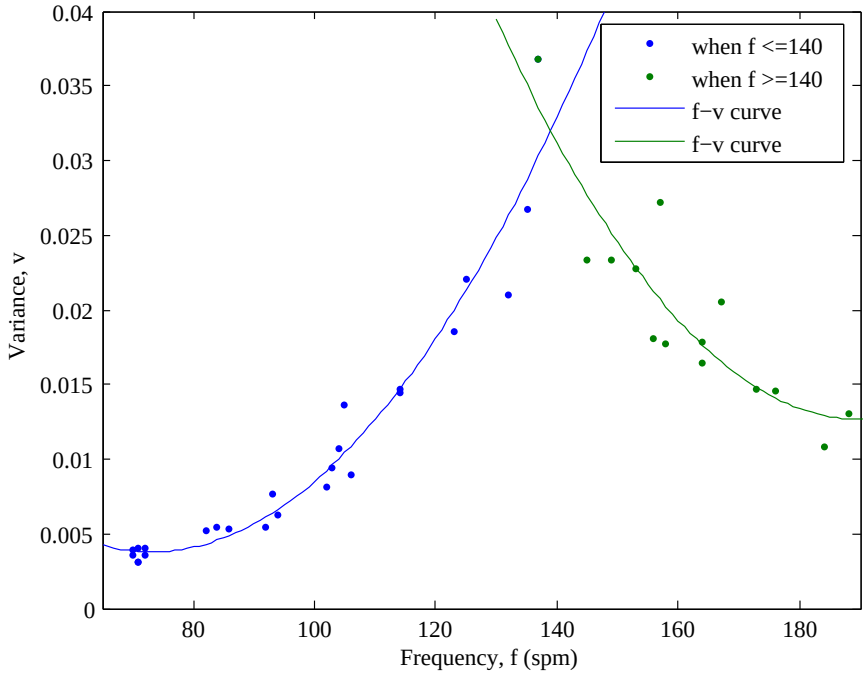

Figure 4.14: When step length is 0.7 m, the relation between *frequency* and *variance* is demonstrated. Two quadratic functions can be fitted accordingly.

When *step length* is 0.7 m, the relation between *frequency* and *variance* is expressed by a piecewise function:

$$\begin{cases} v = 0.00000650f^2 - 0.000951f + 0.0386 \ (f < 140) \\ v = 0.00000750f^2 - 0.00285f + 0.283 \quad (f \geqslant 140) \end{cases} \tag{4.10}$$

Along with the growing *frequency*, at first the motion in vertical direction would be increasingly

intense, and then becomes calmer and calmer. As analyzed before, when the step frequency is high, the pedestrian tends to adopt a gait just like that in a walking race. The acceleration impulse related to each step is less distinct and the body is prone to make a uniform motion.

Similarly, the relations between $frequency$ and $variance$ at other $step\ length$s (part of) are listed in Table 4.4.

Table 4.4: The $frequency - variance$ relations at different $step\ length$s

Step Length (m)	**Frequency-Variance relations**
0.4	$v = 1.61 \times 10^{-8} f^2 + 0.0000203f - 0.000768$ (f <140) $v = 0.00000214f^2 - 0.000776f + 0.0722$ ($f \geqslant 140$)
0.5	$v = 1.52 \times 10^{-8} f^2 + 0.0000344f - 0.00141$ (f <140) $v = 0.00000483f^2 - 0.000924f + 0.0779$ ($f \geqslant 140$)
0.6	$v = 0.00000221f^2 + 0.000293f - 0.0113$ (f <140) $v = 3.075 \times 10^{-7} f^2 - 0.000155f + 0.0256$ ($f \geqslant 140$)
0.7	$v = 0.00000650f^2 - 0.000951f + 0.0386$ (f <140) $v = 0.00000750f^2 - 0.00285f + 0.283$ ($f \geqslant 140$)
0.8	$v = 0.00000826f^2 - 0.000888f + 0.0287$ (f <140) $v = -0.000719f + 0.147$ ($f \geqslant 140$)
0.9	$v = 0.0000128f^2 - 0.00131f + 0.0407$ (f <140) $v = -0.00135f + 0.263$ ($f \geqslant 140$)

With the 6 pairs of equations in Table 4.4, the coefficients a, b, c are calculated by the least square method:

$$\begin{bmatrix} c \\ b \\ a \end{bmatrix} = \begin{bmatrix} 6 & \sum_{i=1}^{6} s_i & \sum_{i=1}^{6} s_i^2 \\ \sum_{i=1}^{6} s_i & \sum_{i=1}^{6} s_i^2 & \sum_{i=1}^{6} s_i^3 \\ \sum_{i=1}^{6} s_i^2 & \sum_{i=1}^{6} s_i^3 & \sum_{i=1}^{6} s_i^4 \end{bmatrix}^{-1} \begin{bmatrix} \sum_{i=1}^{6} v_i \\ \sum_{i=1}^{6} s_i v_i \\ \sum_{i=1}^{6} s_i^2 v_i \end{bmatrix} \tag{4.11}$$

where s_i are [0.4 0.5 0.6 0.7 0.8 0.9]; v_i are the equations in Table 4.4. Therefore, when f <140 spm:

$$\begin{bmatrix} a \\ b \\ c \end{bmatrix} = \begin{bmatrix} 0.0000545f^2 - 0.00501f + 0.15495 \\ -0.0000461f^2 + 0.00404f - 0.130 \\ 0.0000102f^2 - 0.000913f + 0.0336 \end{bmatrix}; \tag{4.12}$$

when $f \geqslant$140 spm:

$$\begin{bmatrix} a \\ b \\ c \end{bmatrix} = \begin{bmatrix} 0.000178f^2 - 0.0613f + 5.381 \\ -0.000177f^2 + 0.0607f - 5.272 \\ 0.0000423f^2 - 0.0145f + 1.248 \end{bmatrix}. \tag{4.13}$$

From Eq. 4.9,

$$s = k \cdot \frac{-b + \sqrt{b^2 - 4a(c - v)}}{2a}. \tag{4.14}$$

The Eq. 4.12, 4.13 together with 4.14 constitutes the main ingredients of the mathematical model for step length estimation. The step length is ultimately a nonlinear function of $frequency$ and $variance$.

However, all of the sampling data are sourced from 1 volunteer. Hence theoretically the equations above are solely suitable for that specified volunteer. If a pedestrian prefer to walk calmly, with the same step length a comparative lower variance would be measured, or if the feet strike ground harshly a higher variance is apt to be resulted. Even the gesture or position taking smartphone can also influence the variance greatly. In order to generalize the model, a customized parameter k is proposed to adapt to various individuals.

One or more test walking could be performed for the parameter calibration. The distance could be estimated with the initial $k = 1$, and compared with the real distance measured by user. Eq. 4.15 is used to calculate the user specified parameter.

$$k = \frac{d_{real}}{d_{estimated}}, \tag{4.15}$$

where $d_{estimated}$ denotes the distances estimated with the initial parameter $k = 1$, while d_{real} indicates the real distance during the test walking.

Adding with Eq. 4.15, the model is completed for step length estimation.

4.3 Evaluation for the Model

In order to test the accuracy of the achieved mathematical model for step length estimation, 10 different volunteers (male and female, height from 1.60 m to 1.80 m, weight from 60 kg to 75 kg) are required to walk a distance at least 30 meters with smartphone held in different gestures (except swinging or changing between gestures). The real length and estimated length for every step are recorded.

Afterwards, the accuracies of the estimation results from all of the available models are counted

and compared in Table 4.5 and Table 4.6. The accuracy is measured by 2 indexes: the Root Mean Squared Error (RMSE) and the Average Deviation Rate.

Table 4.5: The comparison of RMSE among all available models

Step length domains (m)	**0.50-0.59**	**0.60-0.69**	**0.70-0.79**	**0.80-0.89**	**0.90-0.99**	**1.00-1.09**	**All**
Weinberg Model	0.16951	0.10327	0.07335	0.06191	0.07402	0.11029	0.10089
Kim Model	0.17543	0.08457	0.08985	0.09550	0.10316	0.10242	0.10655
Scarlett Model	0.34873	0.19269	0.10021	0.01141	0.09738	0.19708	0.17335
Xu Model	0.10489	0.07248	0.09493	0.12298	0.17271	0.15061	0.11661
Frequency related Model	0.37316	0.32566	0.26572	0.18114	0.13944	0.24883	0.26419
Shin Model	0.33404	0.28898	0.23151	0.16262	0.13738	0.21270	0.23997
Bylemans Model	0.17029	0.08246	0.08512	0.09099	0.10198	0.15163	0.10835
My Model	**0.13880**	**0.00685**	**0.05675**	**0.05212**	**0.08716**	**0.05060**	**0.07681**

The RMSE is defined as

$$RMSE = \sqrt{\frac{\sum (s_{estimated} - s_{real})^2}{n}}. \tag{4.16}$$

The RMSE of the estimation results from all of the available models are compared by the bar chart demonstrated in Fig. 4.15.

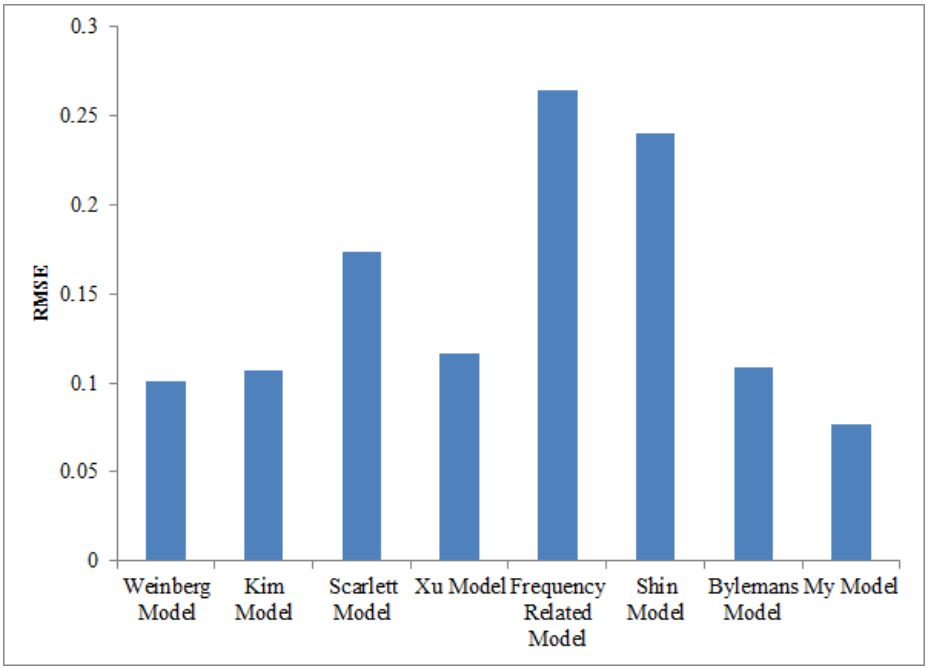

Figure 4.15: The comparison of RMSE among all of the available models

In terms of the different step length groups, the RMSE of all of the available models are compared in Fig. 4.16.

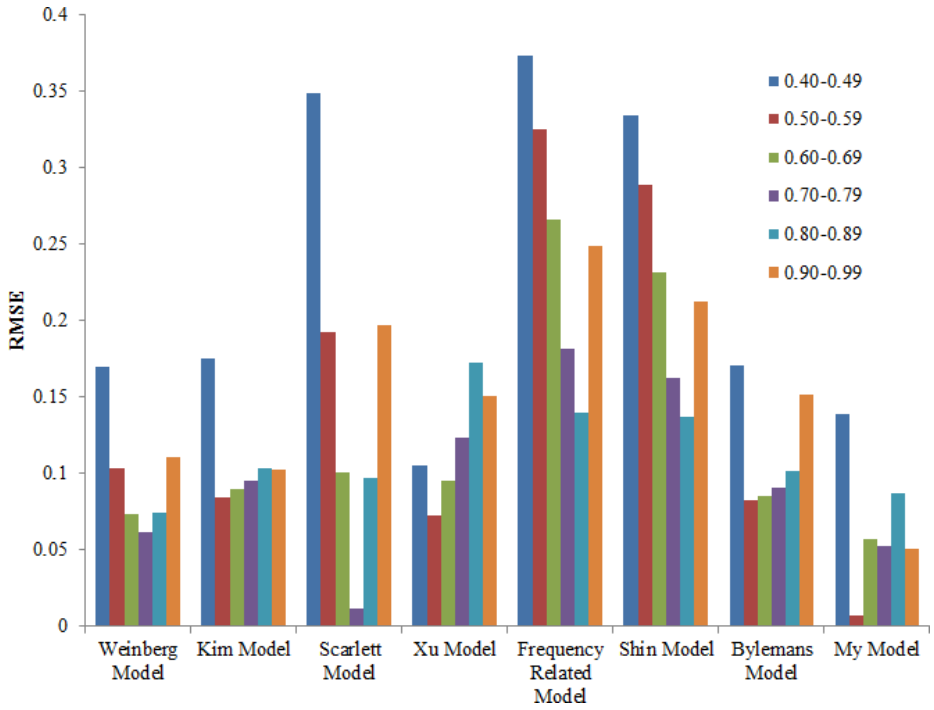

Figure 4.16: The comparison of RMSE in different step lengths among all of the available models

The Average Deviation Rates of all models with reference to the different step lengths are listed in Table 4.6.

Table 4.6: The comparison of Average Deviation Rates among all available models

Step length domains (m)	**0.50-0.59**	**0.60-0.69**	**0.70-0.79**	**0.80-0.89**	**0.90-0.99**	**1.00-1.09**	**All**
Weinberg Model	41.61%	18.55%	10.14%	7.58%	8.26%	9.84%	15.79%
Kim Model	43.37%	14.14%	12.85%	12.01%	12.14%	8.66%	16.34%
Scarlett Model	86.95%	38.34%	16.36%	1.37%	12.25%	21.98%	28.11%
Xu Model	24.36%	12.03%	12.67%	14.65%	18.85%	13.15%	15.24%
Frequency related Model	87.40%	57.01%	35.75%	20.98%	15.58%	26.44%	40.71%
Shin Model	76.99%	48.62%	30.56%	19.58%	15.03%	22.36%	35.99%
Bylemans Model	42.57%	13.69%	12.73%	11.47%	11.27%	14.17%	16.16%
My Model	**33.17%**	**13.68%**	**7.24%**	**5.88%**	**8.78%**	**4.73%**	**10.90%**

The deviation rate is calculated by

$$deviation\_rate = |\frac{s_{estimated} - s_{real}}{s_{real}}| \times 100\%, \tag{4.17}$$

where $s_{estimated}$ denotes the estimated step length, while s_{real} is the real observed value.

Due to the cumulative errors toward the Dead Reckoning approach, the average deviation rate is a more appropriate index for the accuracy than RMSE. For example, if a pedestrian walks with the step length of 0.4 m and another with 0.8 m, both have a deviation of 0.04 m per step, both RMSEs are 0.04 but naturally the model for the second one shows higher accuracy.

The Average Deviation Rates of the estimation results from all of the available models are compared in Fig. 4.17 as well.

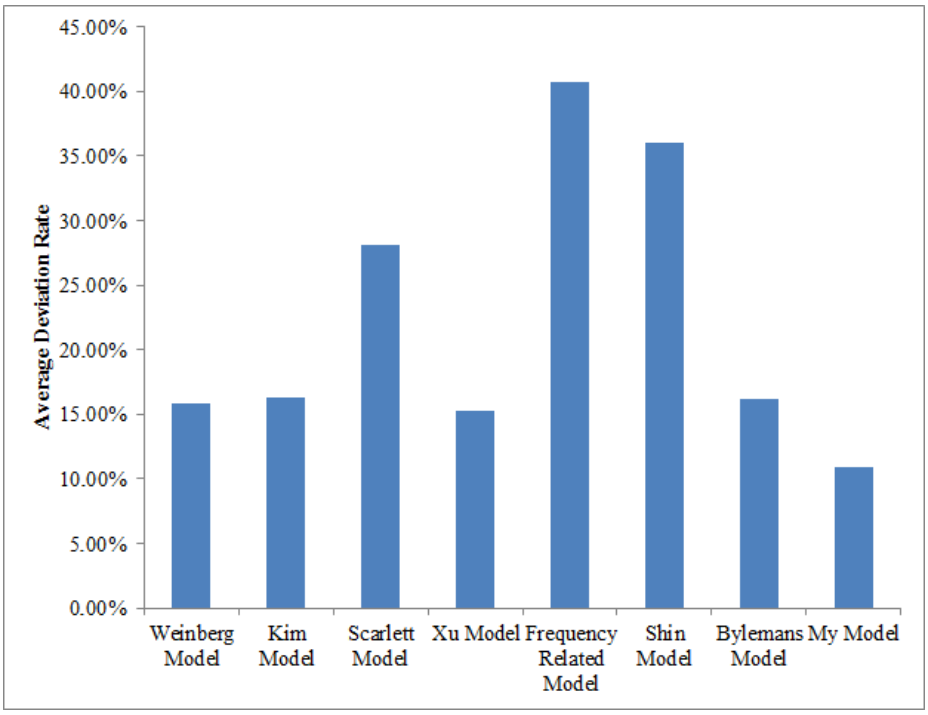

Figure 4.17: The comparison of the Average Deviation Rates among all of the available models

In terms of the different step length groups, the Average Deviation Rates of all of the available models are compared in Fig. 4.18.

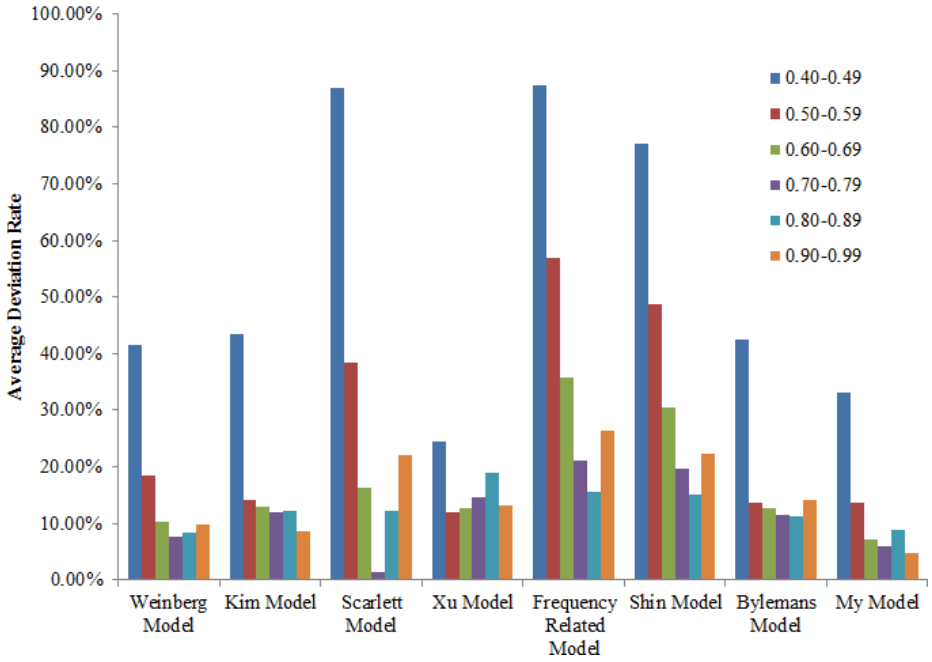

Figure 4.18: The comparison of the Average Deviation Rates in different step lengths among all of the available models

From the results demonstrated in Tables and Figures above, Weinberg and Xu Models are both based on the peak-trough difference. Their accuracies are on a similar level. Xu Model has comparative constant accuracies toward different step lengths but Weinberg Model performs better in 0.7 to 0.9 m length domains in which pedestrians usually walk. The Frequency Related Models show lower accuracies in the experiments. The reason has been analyzed before: they are principally suitable for the most common gaits (step length 0.65-0.75 m and frequency 90-120 spm), but here the abnormal gaits are involved. The diversity in gaits leads to the degradation in their estimation accuracies. Shin Model refers to the variance additionally, for that reason its performance is better than the solely frequency based models. My model is the most accurate model of all. The average deviation rate for each step is 10.90%. This is merely an average accuracy. In terms of those more general step length domains, the deviations are even lower.

4.4 Implementation of the Application

In order to popularize my walking step length estimation model, an app is developed on iOS. This app names “Walk Recorder” and the screenshots are demonstrated in Fig. 4.19.

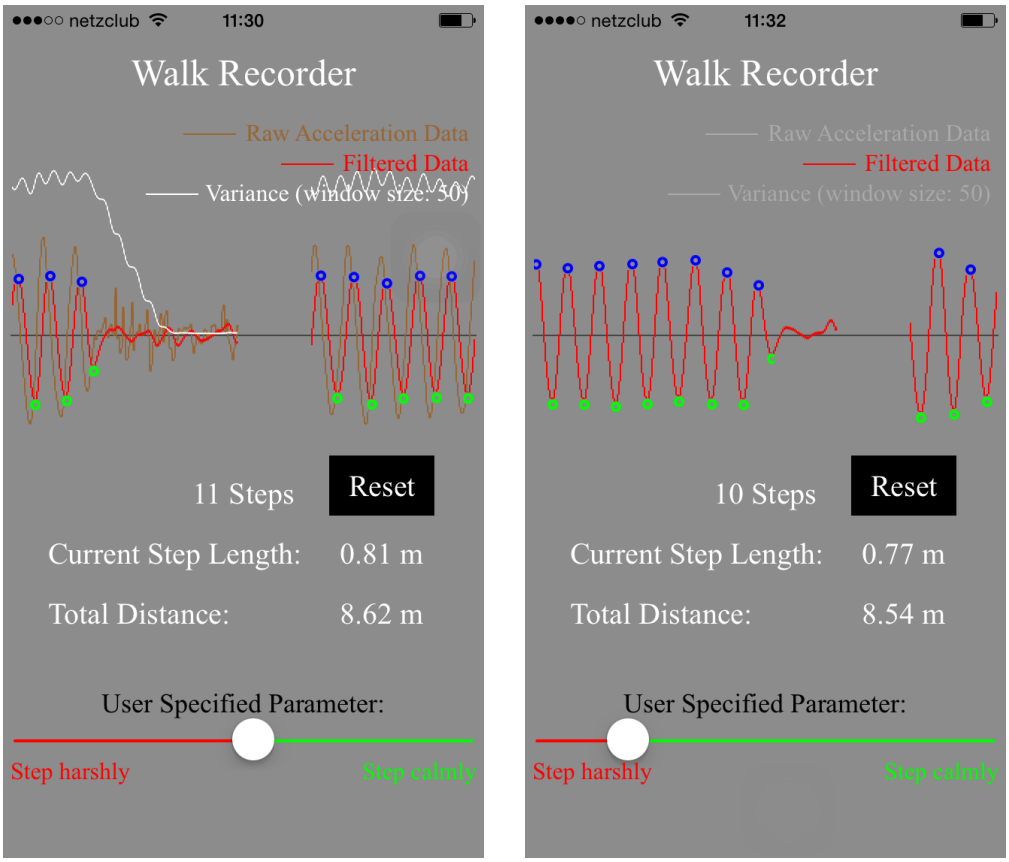

(a) (b)

Figure 4.19: The screenshot of the app "Walk Recorder". According to the mathematical model developed in this chapter, the length of each step is estimated and the whole walking distance is therefore calculated. Pedestrians can use the slider at the bottom to adjust their specified parameter. For the concision of the interface, the curves of the raw data (brown line) and the variance (white) could be hidden temporarily as the right figure.

"Walk Recorder" records the steps for pedestrian and estimates the step lengths as well as the whole walking distance. On the basis of the algorithms presented in Chapter 3, each valid step is recognized and marked by the blue peak and green trough. Besides, by clicking the label "Raw Acceleration Data" or "Variance" the brown or white curve would be hidden temporarily for conciseness. When the app is newly booted, a calibration for 2 seconds is also required as the previous test app demonstrated in Fig. 3.4. When using, the information of the step number, current step length and total distance are displayed in real-time. In view of the fact that even with the same step length, the acceleration signals generated would be varied from individuals, the slider placed at the

bottom is used for adjusting the customized parameter: the harsher steps a pedestrian walks with, the more left the slider is supposed to be set; the calmer s/he steps, the more right it should be (for more details about the user specified parameter please see the end of Section 4.2). The users can adjust this parameter according to their own walking habits in order to reach the most accurate result.

It is available in App Store[1] (also accessible via the QR code shown in Fig. 4.20). And it is universal for both iPhone and iPad as well.

(a) (b)

Figure 4.20: The QR code and the launch image of the app "Walk Recorder"

[1]access link: https://appsto.re/de/N0Q_8.i or https://itunes.apple.com/de/app/walk-recorder/id1023323431?l=en&mt=8

Recap

In this chapter the development of a novel mathematical model for step length estimation is introduced. It is the core content and the major contribution in this dissertation. In the model the relations among the step length, frequency and the variance of the accelerations is revealed systematically. Compared with the previous models, the accuracy of the step length estimation is improved substantially. Furthermore this model is implemented by an available app so that my research could serve the public better.

Chapter 5

Running Step Length Estimation Model

The history of self-tracking using wearable sensors in combination with wearable computing and wireless communication already exists for several decades. In 2007 Gary Wolf and Kevin Kelly first proposed the term "Quantified Self (QS)" and spread this concept at TED in 2010 [67]. Literally the QS is a movement to incorporate technology into data acquisition on aspects of a person's daily life in terms of inputs (e.g. food consumed, quality of surrounding air), states (e.g. mood, arousal, blood oxygen levels), and performance (mental and physical) [68]. Such self-monitoring and self-sensing, which combines wearable sensors (IMU, ECG, thermometer, piezometer, etc.) and wearable computing, is also known as life logging. In short, QS is self-knowledge through self-tracking with technology. The advancement of QS allows individuals to quantify biometrics that they never knew existed, as well as make data collection cheaper and more convenient [69].

A typical application of QS is in the health and wellness improvement field. As Fig. 5.1, in a well-liked sports training and personal fitness system, various self-tracking techniques are adopted to monitor people's physical activities, caloric intakes, postures, sleep qualities, and other factors involved in personal well-being. By "quantifying" a person's daily activities, the QS system is able to draw up the customized training plan and help users achieve their exercise goals. As a sport assistance system, the data-driven QS application analyzes individuals' progresses around their endeavors and assesses their exercise levels, provides personalized consultations intelligently such as which is beneficial while which need to change, and eventually improves humans' physical fitness as well as quality of life.

Figure 5.1: All sorts of fitness tracker devices enable people to quantify their exercises.

5.1 Related Works

Along with the booming wearable techniques recent years, the Wearable Health Monitoring Systems (WHMS) are sprouting up in our life [70]. Among the fitness and sports applications, the most basis function is step tracking and exercise statistics. When a person is jogging, not only the duration and distance of running is expected to be logged but also the energy expenditure and moving trajectory in real-time are preferred.

With regard to this kind of applications, currently there are several off-the-shelf commercial products available, either hardware or software. For instance, Nike+Running and Runtastic (Fig. 5.2) are popular sports apps based on smartphone, which use successive GPS signals to update the running displacement and draw the moving trajectory. However, as discussed in Section 1.1: when the

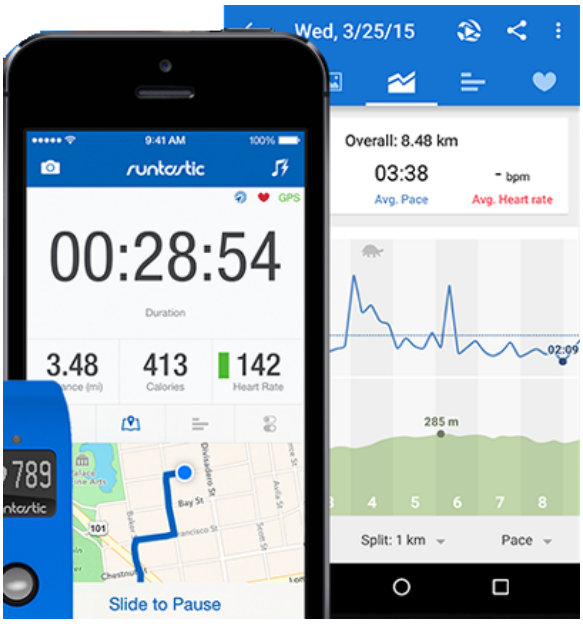

Figure 5.2: A popular fitness app names Runtastic. It tracks runner by GPS.

GPS-challenged environments are referred to, the effect of this sort of apps would be limited, such as racing in an indoor gymnasium that the players could not be tracked precisely as usual. Besides, if a player runs on a rugged mountain road where consists of quite a few ups and downs, the calculated distance would be imprecise due to the 2D localization coordinates from the GPS. Moreover, because of the poor continuity of satellite signals, the running velocity estimated could never be considered to be instantaneous but a reference average value.

The advent of Apple Watch in April 2015 has opened up a whole new frontier in the area of the wearable techniques. Actually the electronic products in the same category have already served the public for a few years. As shown in Fig. 5.3, a wide variety of smart bracelets as well as watches sample the manifold biometrical data in real-time, including the blood pressure, respiration status, pulse rate, blood oxygen saturation, surface temperature and hydration level all the time. With multifarious micro sensors equipped in and on these bracelets, the human's activity intensity, sleep quality and health condition are able to be monitored unobtrusively.

Despite these smart bracelets show their superb capabilities to sense the users' biometrical data, for a practical fitness and sports system only with these healthcare related parameters is far from comprehensive. One of their advantages lies in the fact that with the sensors next to the skin, they are able to sample the biometrical data more seamlessly and precisely. Nonetheless, because they

Figure 5.3: Numerous smart bracelets and watches burst onto the scene in recent years.

are placed around the wrist, the accelerations measured often suffer from the shake of arms in the great degree. In other words, these limb-mounted sensors cannot record the kinetic characteristics of the whole body faithfully. The oscillations of limbs affect the estimation for the velocity and distance severely, even though the cyclic property of these oscillations could also be made full use of to count the steps. To some extent, the smart bracelets or watches could at most serve as a kind of efficient assistant equipment in a QS system. They are not adequate for the complete functions of a fitness and sports application in any way.

In 2013 the researchers in KTH developed a sort of whole new digital positioning shoes [71]. They are used to track firemen's position during the rescue missions. The working depth reaches 25 meters underground. As shown in Fig. 5.4, the sensor nodes are installed at the heels of the shoes, which comprise accelerometers, gyroscopes and pressure transducers. By a wireless module placed on the firemen's shoulder, the acquired data are transmitted to their command center. As a result, the commander is able to learn their firemen's position as well as moving trajectory in real-time. Because this system relies on no GPS signal, in certain extreme scenarios the firemen would be guided and organized in a more safe and efficient way, so that they could save more lives in accidents. As a newly emerged wearable device, this kind of digital shoes are expected to be widely applied among police, medics, militaries and athletes. In view of the usability that the digital shoes could work underground, this system would also be serviceable in mine. In the case of an accident the miners could be immediately targeted by their shoes.

According to a few discussions [72] [73], the practical value of the digital shoes might outweigh that of the smart watches. Firstly and foremost, ordinarily the time that people in shoes is longer

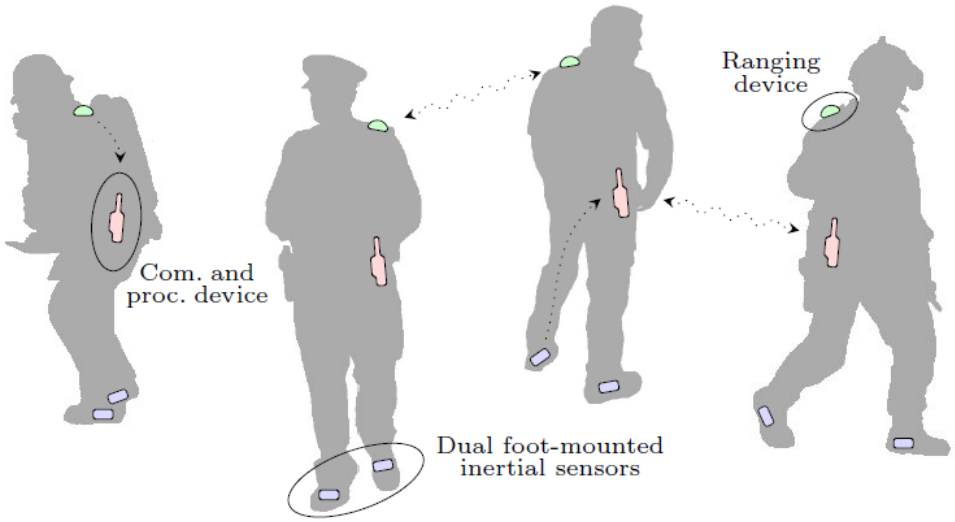

Figure 5.4: The illustration of the digital shoes system. With the feet-mounted IMU the positions of firemen are tracked in real-time.

than people wear watches. Office workers are usually reluctant to wear their watch all the time. Thus the digital shoes play a more important role in humans' daily lives. Besides, similar to the smart bracelets, all sorts of sensors in the digital shoes are able to monitor the manifold biometrical parameters for users as well. But the sensors are mounted at the feet of pedestrian rather than the wrist, and either walking or running is performed by the lower limbs. Consequently the counting for steps and the estimation for moving distance as well as energy expenditure are instinctively more accurate and reliable than by the wrist-mounted devices. Furthermore, in several prototypes of digital shoes, according to the equipped IMU, certain dangerous activities which lead to potential injuries could be recognized and warned in time.

However, the digital shoes are not without their disadvantages. In the first place the difficult and cost of developing and producing such a kind of custom shoes is certainly higher than that of smart watch and smartphone which are based on current available platforms. Moreover, with respect to the design of the commercial digital shoes, there are numerous nontechnical factors have to be taken into consideration, such as fashion, style, waterproof, compression strength, and other specialty characteristics. Additionally most of users are not willing to wear the same shoes invariably. Unlike the watch or mobile phone that there is no remarkable distinction between the business use and sports oriented style, the shoes are more likely to be the multi-optional products. In a word the universality of the digital shoes is eventually a challenge. The scheme whether designing a kind

of special sport shoes or merely producing a digital shoe module which could be easily applied in all the shoes of various styles is remains in suspense. In conclusion, the commercialization and popularization of the digital shoes still need a great deal of attempts as well as time.

According to the discussions above, a strategy based on smartphone is currently the first choice because the development platform is ubiquitous. Purchasing new equipment is not necessary so that the spreading of the application is naturally advantaged. Moreover, the corresponding algorithms and models are comparative mature.

5.2 Running Step Length Estimation Model

As described in Eq. 4.1-4.8, a series of mathematical models were developed for the step length estimation. Although most of the current models already show their conveniences, they are instinctively walking-oriented. When it comes to more varied and complicated running gaits, the effect is barely satisfactory. For more accuracy of step length estimation as well as positioning, a novel mathematical model special for running is investigated in this chapter.

The mathematical model introduced in Section 4.2 shows satisfying accuracy when pedestrian is walking. In spite of this, as far as running is referred to, the existing model is not capable any more. Moreover, the running gait could not be ignored among the daily activities, not only because of a few sport-related applications, but also for indoor positioning scenarios. When people pay all attention to their walking without distraction, the gait could be regarded as a simple and constant pattern. Nevertheless, when a pedestrian are talking with a companion or just wandering, the walk speed would decrease. In contrast, when a person is in hurry s/he might start running suddenly and this phenomenon is also quite common in human behaviors. The kinetic characteristics in the running gait are totally different from those of walking. Solely adjusting the user specified parameter is obviously not enough. In order to improve the accuracy of step length estimation, the running gait is analyzed and a wide range of experiments in terms of various step lengths as well as diverse frequencies are implemented once more. Thereafter an original mathematical model special for running step length estimation is developed in this section.

To develop a mathematical model that the step length could be expressed by the measured kinetic data when pedestrian is running, a multitude of experiments are implemented further. As mentioned in Section 4.2, this is the second stage of the experiments.

The collected items are similar to those in the first stage, including: the magnitude of the accelerations, the peak value, the trough value, the variance and the frequency of that step. But the sampling dimensions are changed partially. The running step length is set from 0.5 to 1.0 m, every

0.1 *m* a group, and 6 groups in all (not 0.4 to 0.9 *m*, every 0.05 *m* anymore). The step frequency varies from 120 to 240 *spm*, every 10 *spm* a group, and 13 groups in all. Thus there are 78 combine groups altogether, far less than the data size in the first stage which was 275 groups. According to the experiences of the first stage, after confirmed through a few tests, the module of accelerations in y- and z directions ($\sqrt{y^2 + z^2}$) are also not involved in the data collection anymore due to the overly irregularity in that item. In spite of this, the experiments for the running data sampling last for more than 2 weeks. Because running with a preselected step length and a fixed frequency is more difficult for volunteer than when walking (the adjusting methods are the same as those illustrated in Fig. 4.2 and 4.3). All of the experiments are implemented by one volunteer as well, and every combine group with the same gait is required to be repeated at least 10 times, in order to reduce the random errors. Due to the poor operability of the running experiments, sometimes the volunteer had to run with a certain gait many times to sample one set of qualified data successfully. The higher the frequency is, the greater challenge the volunteer may have.

As an instance, Fig. 5.5 shown a set of acceleration data collected from one running experiment.

In this group the volunteer is required to run for 24 steps, with each step length 1.0 *m* and the step frequency 160 *spm*. The total walking distance is 24 *m*. The upper figure of Fig. 5.5 is the acceleration signal sampled in y direction, while the bottom figure is in z direction. Both of the acceleration signals have been filtered. According to the results obtained from the experiments, the modules of y and z acceleration are rather disordered and this phenomenon was also verified in the walking experiments. Hence the item of yz module would not be displayed and analyzed any more. The starting and end points of the valid walking phase are indicated by the dashed lines. According to the algorithm introduced in Section 3.4.1, the vertical vibrations at the beginning (around the time points 150 to 200) are rejected from the valid signal because during the same time the corresponding valid wave in y direction is not yet detected. Besides, all of the valid peaks and troughs on both of the waves are extracted and marked. Compared with the data in z direction, the y data are rather instable and shows less regularity. As illustrated in the upper figure of Fig. 5.5, even the adjacent peak values differ greatly. This situation is similar to that in the walking experiments. The confusion is caused by the tendency that every 2 adjacent peaks on y wave are merging gradually (as analyzed in Fig. 4.11). Thus only z data related items would be referred to in the development of the running model.

Furthermore, in order to compare the influence of the 3 physical items (the magnitude, the difference between the peak and trough values, the variance of the vertical accelerations), the variation trends between these items and the step frequency are shown in Fig. 5.6, 5.7 and 5.8. These relations are demonstrated according to the different step lengths separately. Each of the figures comprises 2

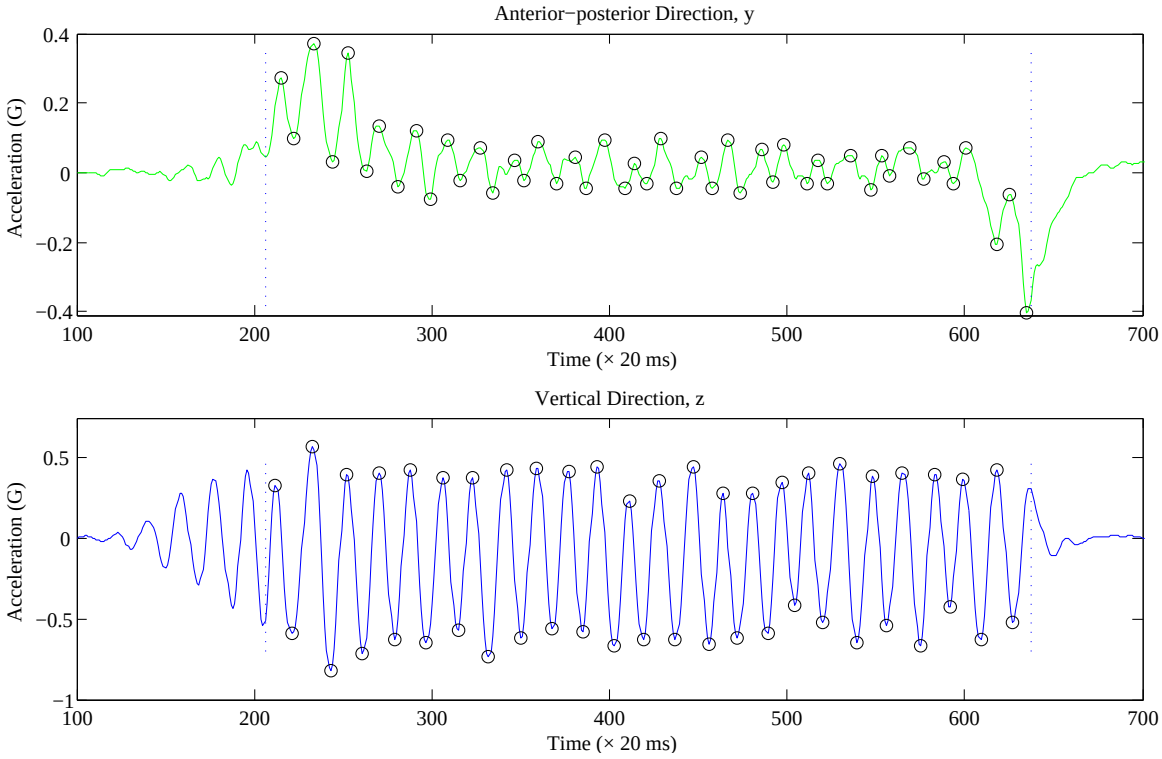

Figure 5.5: For each of the 78 running experiments, the accelerations in y and z-directions are recorded and processed. This is one of the samples when step length is 1.0 m and frequency 160 spm.

step length groups and all of the 6 running step length groups, from 0.5 m to 1.0 m, are compared altogether.

From these 3 figures, the relations between the 3 items and the step frequency are monotone, unlike the variation trends shown in the walking experiments, which are piecewise. There is a conspicuous trend that along with the increasing of the frequency, the motion of body in z direction is less and less intense. The possible reason is that when the frequency is higher, the barycenter of body is more likely to make a uniform motion, so that the vertical oscillation would be calmer.

According to these figures, it could be assumed that, there are quadratic relations among these 3 items and the step frequency. For the 6 step length groups and the 3 items, there are hence 18 quadratic equations theoretically. Furthermore all of these 18 equations are fitted and their curves are contrasted in Fig. 5.9 as well.

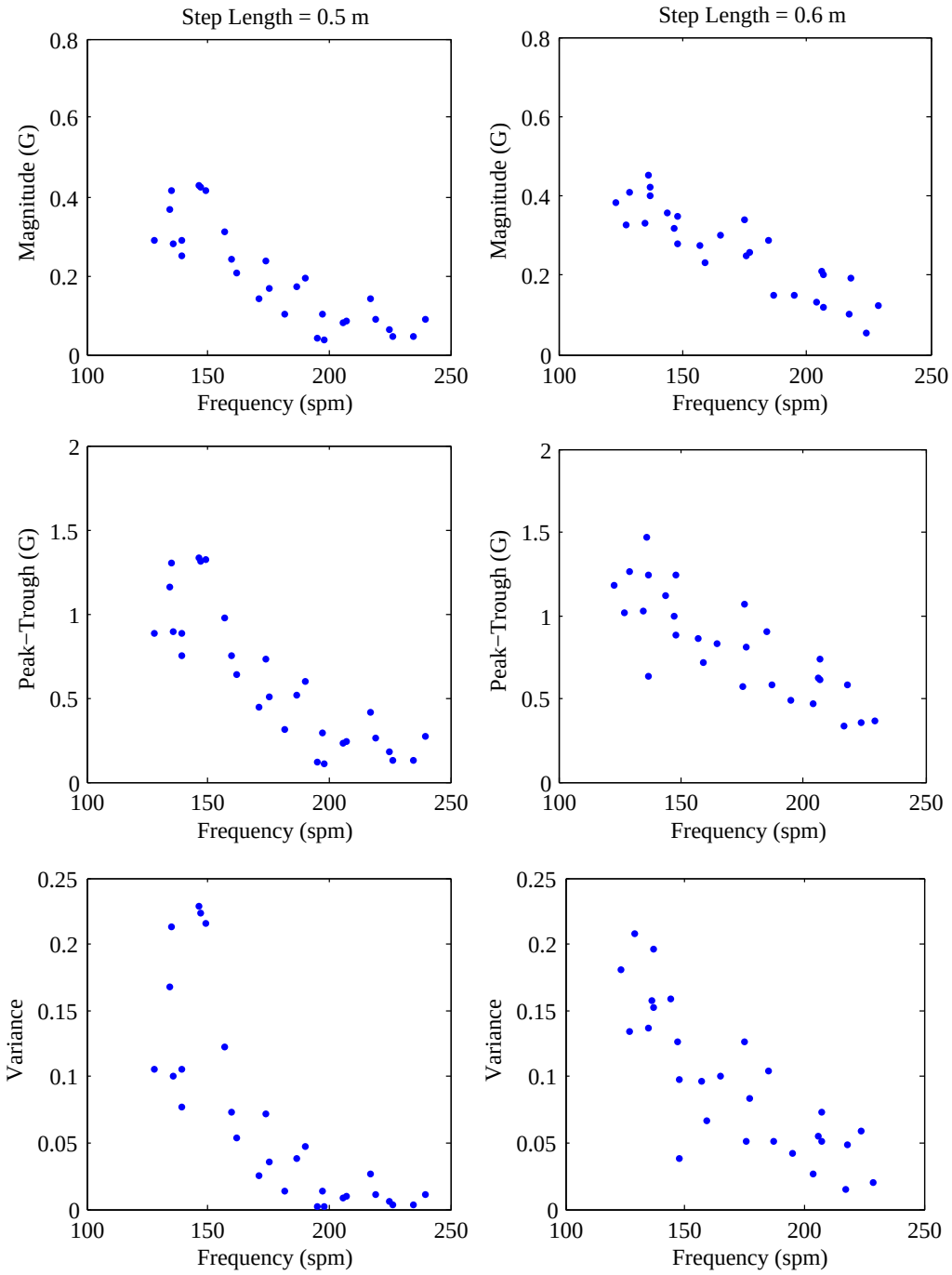

Figure 5.6: With 0.5 and 0.6 *m* as the step length, the 3 items (the magnitude, the peak-trough difference, the variance) vary with the step frequency.

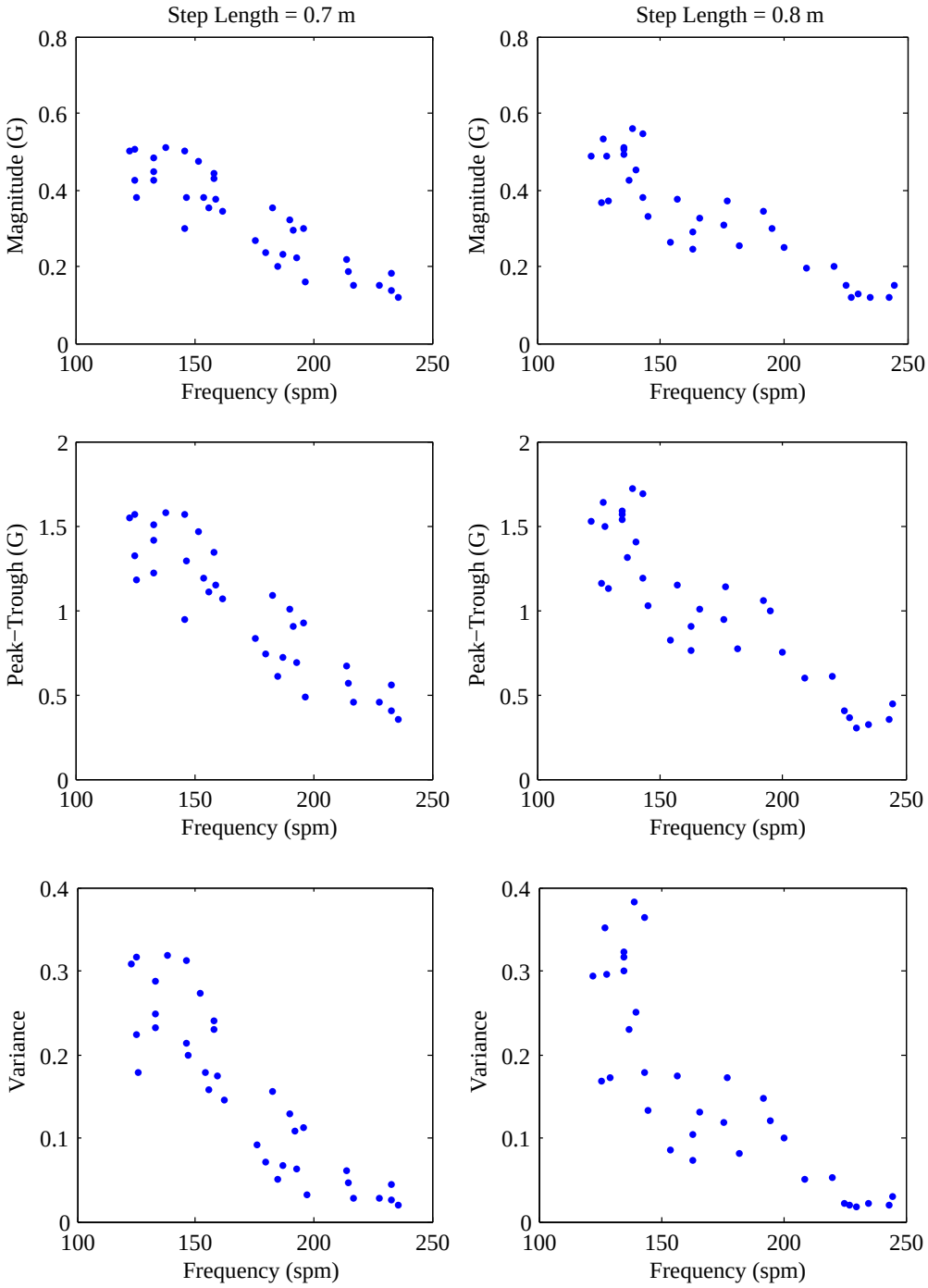

Figure 5.7: With 0.7 and 0.8 *m* as the step length, the 3 items (the magnitude, the peak-trough difference, the variance) vary with the step frequency.

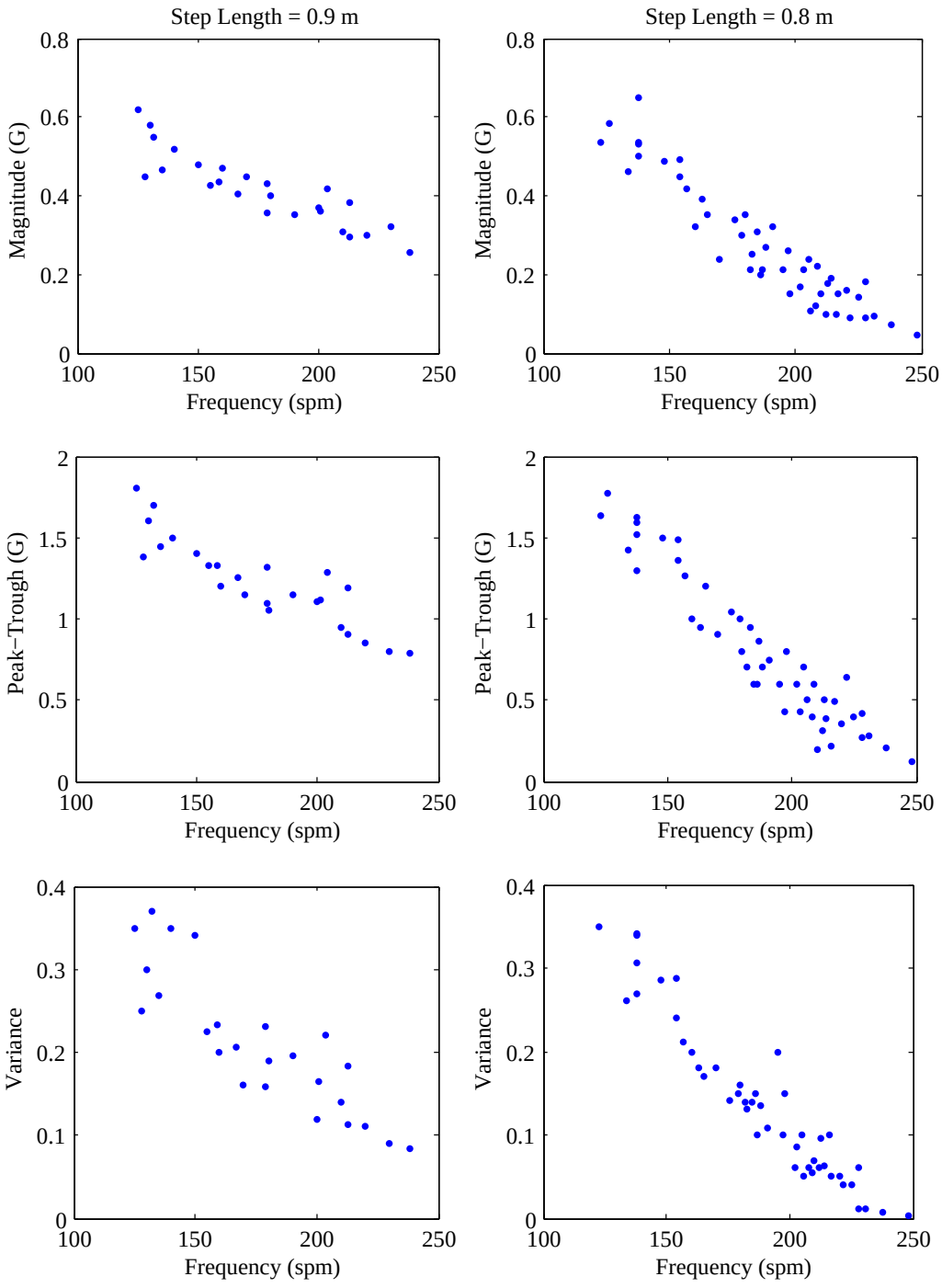

Figure 5.8: With 0.9 and 1.0 *m* as the step length, the 3 items (the magnitude, the peak-trough difference, the variance) vary with the step frequency.

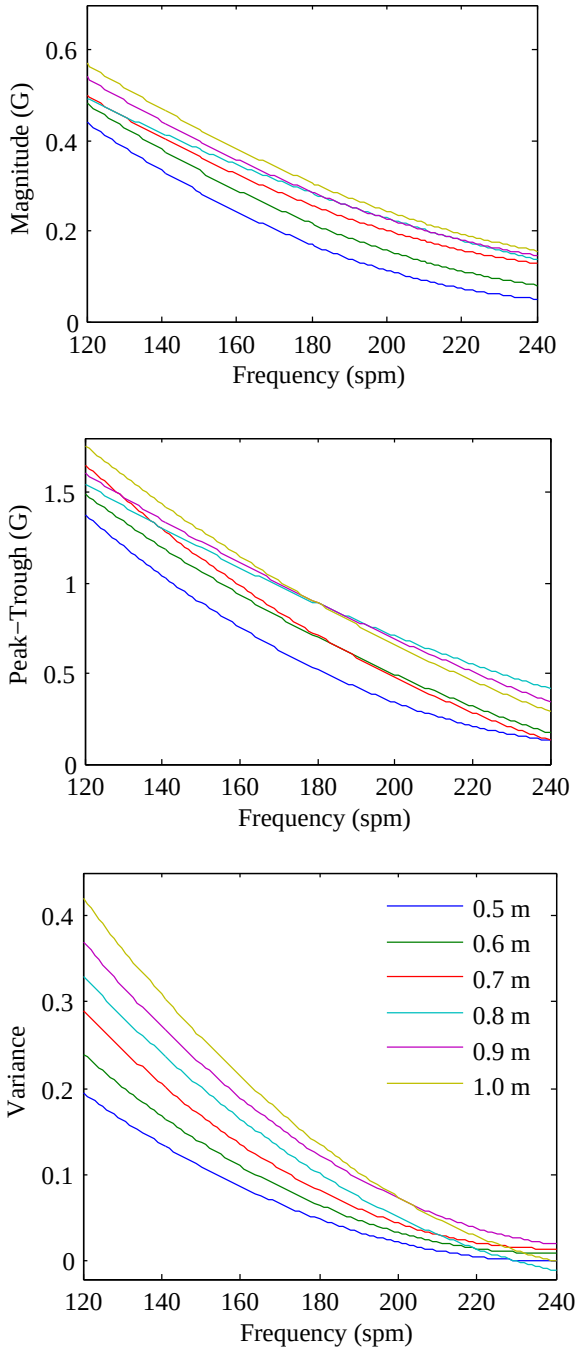

Figure 5.9: The fitting curves of the relations between the step frequency and the 3 items (the magnitude, the peak-trough difference, the variance) are demonstrated according to the different step lengths.

As a result the item *variance* is chosen as the independent variable in the prospective model for running step length estimation. Because from Fig. 5.9, the curves in the bottom figure vary most regularly and clearly. Among these 3 items, *variance* shows the most remarkable relation with *step length*. Consequently the mathematical model is supposed to be in the form that *step length* is a function of *variance* and $frequency$.

The relation between $frequency$ and *variance* with certain *step length* can be obtained from the fitting curve. As shown in Fig. 5.10, this example is the $f - v$ figure when *step length* is 1.0 m. This figure is similar to the sub-figures in the lower right corner of Fig. 5.8.

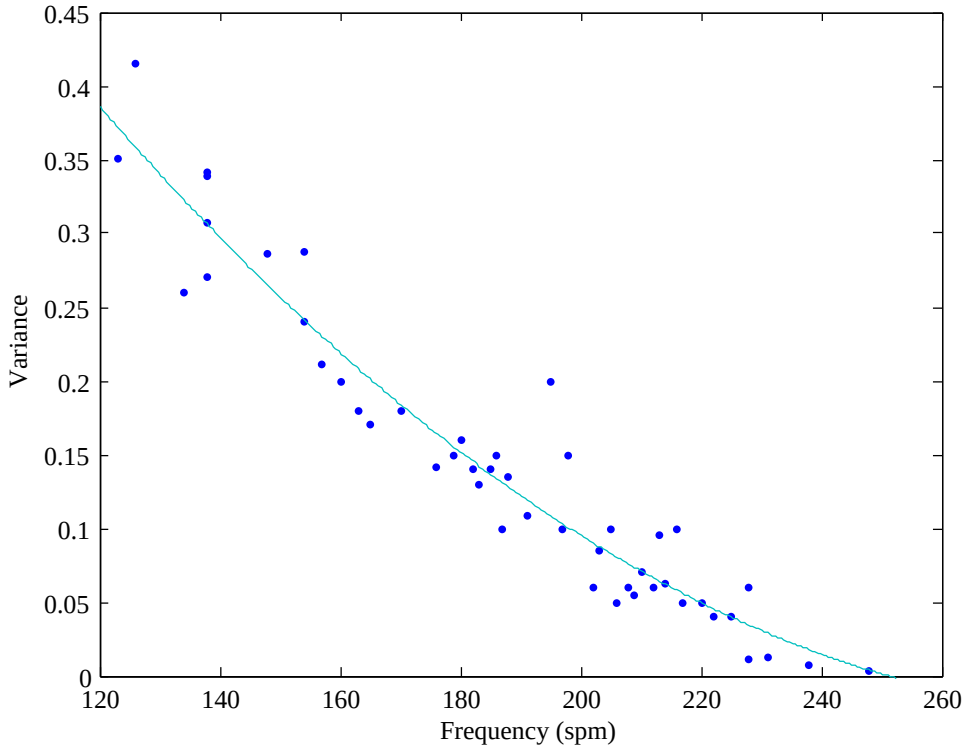

Figure 5.10: When the running step length is 1.0 m, the relation between the step frequency and the variance is illustrated. Accordingly a quadratic function is fitted.

Thereupon the relation between $frequency$ (f) and *variance* (v) when *step length* = 1.0 m is indicated by a quadratic function:

$$v = 0.00002056f^2 - 0.0109f + 1.432. \tag{5.1}$$

Along with the increasing $frequency$, the vibration in vertical direction would be calmer and

calmer. Similarly, the relations at other *step length*s are fitted as well and the equations are listed in Table 5.1.

Table 5.1: The $frequency - variance$ relations at different *step length*s

step length (m)	$frequency - variance$ Relations
0.5	$v = 0.000015678f^2 - 0.0073817f + 0.86991$
0.6	$v = 0.000016527f^2 - 0.007867f + 0.946$
0.7	$v = 0.0000194916f^2 - 0.0093086f + 1.12636$
0.8	$v = 0.000016167f^2 - 0.008653f + 1.1356$
0.9	$v = 0.000019944f^2 - 0.010096f + 1.2944$
1.0	$v = 0.00002056f^2 - 0.0109f + 1.432$

The $s - v$ relation could be indicated in form

$$v = as^2 + bs + c, \tag{5.2}$$

where s denotes *step length*; the coefficients a, b, c are supposed to be calculated by the least square method:

$$\begin{bmatrix} c \\ b \\ a \end{bmatrix} = \begin{bmatrix} 6 & \sum_{i=1}^{6} s_i & \sum_{i=1}^{6} s_i^2 \\ \sum_{i=1}^{6} s_i & \sum_{i=1}^{6} s_i^2 & \sum_{i=1}^{6} s_i^3 \\ \sum_{i=1}^{6} s_i^2 & \sum_{i=1}^{6} s_i^3 & \sum_{i=1}^{6} s_i^4 \end{bmatrix}^{-1} \begin{bmatrix} \sum_{i=1}^{6} v_i \\ \sum_{i=1}^{6} s_i v_i \\ \sum_{i=1}^{6} s_i^2 v_i \end{bmatrix} \tag{5.3}$$

where s_i are [0.5, 0.6, ..., 1.0], the 6 step length values; v_i are the 6 equations explicated in Table 5.1.

Consequently,

$$\begin{bmatrix} a \\ b \\ c \end{bmatrix} = \begin{bmatrix} 0.000019125f^2 - 0.0107575f + 0.9815 \\ -0.00002525f^2 + 0.01183f - 0.6472 \\ 0.000023375f^2 - 0.0105675f + 0.9455 \end{bmatrix}. \tag{5.4}$$

From Eq. 5.2,

$$s = k \cdot \frac{-b + \sqrt{b^2 - 4a(c - v)}}{2a}. \tag{5.5}$$

Eq. 5.5 together with Eq. 5.4 constitutes the main ingredients of the mathematical model for running step length estimation. Ultimately *step length* is a function of $frequency$ and *variance*. Compared with the estimation model for walking (Section 4.2), the running model is not piecewise function according to $frequency$ any more.

However, all of the sampled data are sourced from one volunteer. Theoretically the developed

model above is merely suitable for that specified volunteer exclusively. When a pedestrian runs slightly, with the same step length a comparative lower acceleration variance would be measured. On the contrary, when the feet strike ground harshly, a relative higher variance tends to be detected. Even the different gesture or position holding smartphone could also influence the variance greatly. Similar to the walking model, a user specified parameter k is supposed to be proposed in order to generalize the model.

(a) (b)

Figure 5.11: The screenshots of the beta app "Running Recorder". With this app based on iPhone 6, the developed running step length estimation model is tested. In particular, the adjustment for the user specified parameter is performed by the slider designed at the bottom. Because this app implements merely a part of function of PDR and the algorithm for distinguishing the activities between walking and running is not added up, this app is not submitted to App Store until been perfected.

One or more test running is expected to be performed for the parameter calibration. The distance could be estimated with the initial $k = 1$, and compared with the real distance observed by user. Eq. 5.6 is used to set the individual parameter.

$$k = \frac{d_{real}}{d_{estimated}}, \tag{5.6}$$

where $d_{estimated}$ denotes the distances estimated with the initial parameter $k = 1$; while d_{real} indicates the real distance during the test walking.

Adding with Eq. 5.6, the model is completed for running step length estimation.

Practically this customized parameter is implemented with a slider (exactly as that in Fig. 5.11): users may adjust the slider by themselves according to the initial estimation results.

5.3 Evaluation for the Model

In order to test the accuracy of the developed mathematical model for running step length estimation, 10 different volunteers (male and female, height from 1.60 m to 1.80 m, weight from 60 kg to 75 kg) are required to run for a distance at least 30 meters with smartphone held in different gestures (except swinging or changing between gestures). They are encouraged to run with their normal and abnormal step lengths as well as frequencies.

Afterwards, the accuracies of the estimation results from all of the available models are calculated and compared in Table 5.2 and 5.3. The accuracy is measured by 2 indexes: the Average Deviation Rate and the Root Mean Squared Error (RMSE).

Table 5.2: The comparison of Average Deviation Rates among all of the available models

Step length domains (m)	**0.50-0.59**	**0.60-0.69**	**0.70-0.79**	**0.80-0.89**	**0.90-0.99**	**1.00-1.09**	**All**
Weinberg Model	41.93%	30.43%	18.84%	10.70%	8.26%	16.92%	**25.33%**
Kim Model	41.59%	36.28%	21.70%	14.28%	8.66%	15.45%	**26.27%**
Scarlett Model	46.39%	21.77%	15.69%	14.66%	16.26%	20.81%	**22.15%**
Xu Model	47.45%	35.80%	34.19%	28.29%	18.14%	28.89%	**35.33%**
Frequency related Model	174.60%	115.09%	75.72%	42.74%	32.54%	54.78%	**82.79%**
Shin Model	80.69%	55.67%	37.76%	35.58%	22.79%	30.32%	**45.59%**
Bylemans Model	42.89%	31.00%	19.74%	10.64%	8.13%	15.44%	**22.83%**
My Model	24.98%	23.92%	19.06%	18.83%	15.30%	18.34%	**19.66%**

The deviation rate is calculated by

$$deviation\_rate = |\frac{s_{estimated} - s_{real}}{s_{real}}| \times 100\% \tag{5.7}$$

where $s_{estimated}$ denotes the step length estimated by different models, while s_{real} is the real observed value.

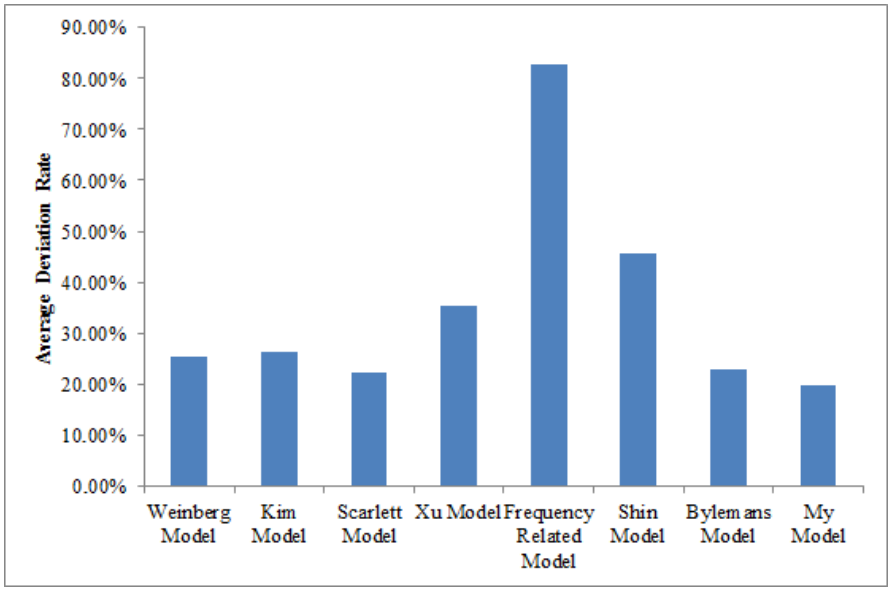

Figure 5.12: The comparison of the Average Deviation Rates among all of the available models

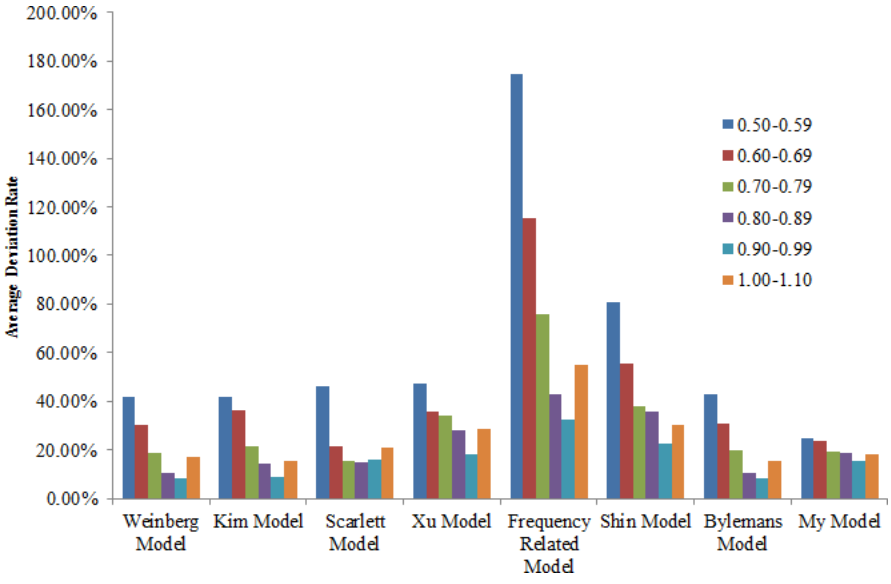

Figure 5.13: The comparison of the Average Deviation Rates in different step lengths among all of the available models

The Average Deviation Rates of the estimation results from all of the available models are compared in Fig. 5.12 as well. In terms of the different step length groups, the Average Deviation Rates of all of the available models are compared in Fig. 5.13.

The RMSE of the estimation results from part of the available models are listed in Table 5.3.

Because the comparatively poor performance in the frequency related models, their RMSE are not compared in Table 5.3 anymore. In addition, as analyzed in Section 4.3, the Average Deviation Rate is a more reasonable index than RMSE for a PDR scheme.

Table 5.3: The comparison of Average Deviation Rates among part of the available models

Step length domains (m)	**0.50-0.59**	**0.60-0.69**	**0.70-0.79**	**0.80-0.89**	**0.90-0.99**	**1.00-1.09**	**All**
Weinberg Model	0.24767	0.22100	0.15271	0.09992	0.04411	0.23380	**0.18940**
Kim Model	0.25140	0.23164	0.17805	0.13393	0.05913	0.25212	**0.20064**
Scarlett Model	0.23337	0.19333	0.14260	0.14076	0.18716	0.21012	**0.19239**
Xu Model	0.29675	0.28381	0.28874	0.27141	0.18513	0.35039	**0.27311**
Bylemans Model	0.24925	0.22895	0.15857	0.10005	0.03505	0.22245	**0.19091**
My Model	0.13547	0.13142	0.15928	0.22592	0.18755	0.19066	**0.17363**

The RMSE is defined as

$$RMSE = \sqrt{\frac{\sum (s_{estimated} - s_{real})^2}{n}}. \tag{5.8}$$

where $s_{estimated}$ denotes the estimated step length, while s_{real} is the real observed value.

The RMSE of the estimation results from part of the available models are compared in Fig. 5.14. In terms of the different step length groups, the RMSE of part of the available models are compared in Fig. 5.15.

From the results demonstrated in Tables and Figures above, Weinberg and Scarlett Models are both based on the difference between the peak and trough values. Their accuracies are on the similar level. Scarlett Model has even accuracies toward different step lengths but Weinberg Model performs better in 0.9 to 1.0 m length domain in which pedestrians usually run. The frequency related models show less accuracy in the experiments. The reason has been analyzed before, they are only suitable for the most common gaits (step length 0.8-1.0 m, frequency 160-180 spm), but here abnormal gaits are involved. Shin Model also refers to the variance, so its performance is better than solely frequency based models. Finally my model is more accurate than all of models above. The Average Deviation Rate for each step is 19.66%. Take the fact into consideration that it is only the average accuracy, this model is promising. In terms of the most general step length groups, the deviations are even lower.

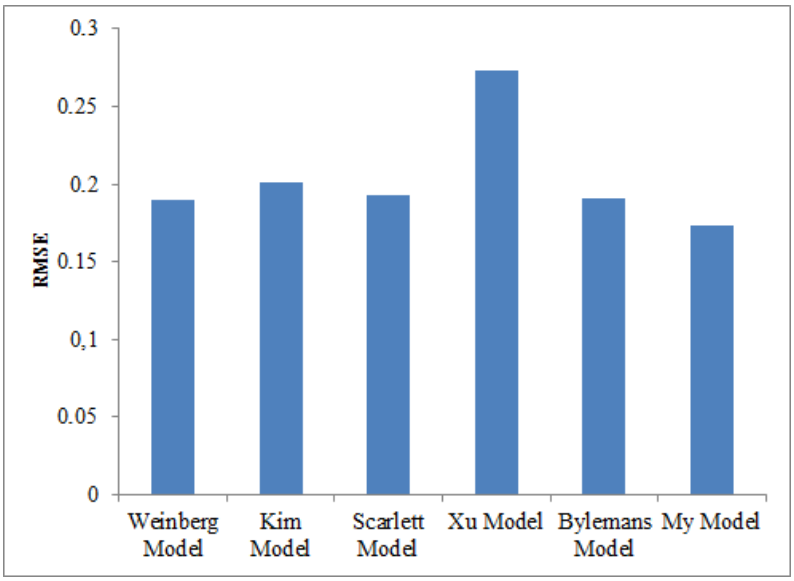

Figure 5.14: The comparison of RMSE among part of the available models

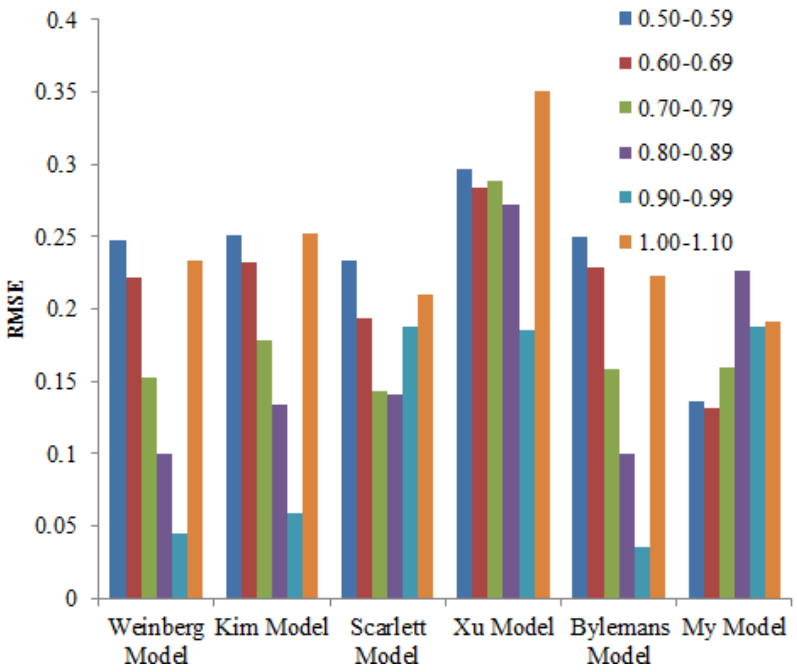

Figure 5.15: The comparison of RMSE in different step lengths among part of the available models

Recap

Special for running, a step length estimation model is developed in this chapter. On the basis of the experiments the relation among the acceleration variance, the step frequency and the step length is discovered and summarized. Accordingly the step length would be estimated from the accelerations measured by IMU. In the evaluations this new approach is proved to be more accurate than the previous works. With this new mathematical model the pedestrians' positions are able to be tracked even when they are occasionally running in a building. Because the running behavior is not processed by general walking oriented methods but the specialized model, the accuracy as well as stabilization of the entire positioning system is supposed to be promoted correspondingly.

Chapter 6

Particle Filter

According to the PDR method, the 2D position of a pedestrian after the ith step is:

$$\begin{cases} x[i] = x[i-1] + step\_length[i]\ cos(heading[i]) \\ y[i] = y[i-1] + step\_length[i]\ sin(heading[i]) \end{cases} \tag{6.1}$$

where $heading[i]$ is the average heading angles during the ith step, which results from the fusion of the gyroscope and magnetometer data (Section 3.4.2). On the basis of Eq. 6.1, the current location of a pedestrian is continually updated and the function of a positioning system is performed.

Although with a few calibration approaches the Step and Heading System (SHS) are able to abate the influence from the drift of inertial sensors to some extent, ultimately the position tracking for pedestrians has to cooperate with certain external measurements and environment information in order to acquire the long term stability as well as effectiveness. Specifically, the building layout is an impactful complementarity to improve the positioning accuracy.

6.1 Background

Particle Filter, which is also denoted as Sequential Monte Carlo (SMC) algorithm, are a series of genetic type particle Monte Carlo methodologies to tackle the filtering problem [74]. The term "particle filters" was first coined in 1996 by Del Moral in reference to mean field interacting particle methods [75].

If the transition model is based on the Markov Chain (MC), it is also named Markov Chain Monte Carlo (MCMC) method. Particle filter is a recursive Bayesian filter using the MC simulations [76]. The particle filtering methodology is used to solve Hidden Markov Model (HMM) and nonlinear,

non-Gaussian filtering problems arising in signal processing and Bayesian statistical inference.

The filtering problem consists in estimating the internal states in dynamical systems when partial observations are made, and random perturbations are present in the sensors as well as in the dynamical systems. The objective is to compute the conditional probability (also known as posterior distributions) of the states of some Markov process, given some noisy and partial observations [77]. This method allows researchers to approximate the joint posterior distribution using Sequential Importance Sampling (SIS).

Particle filters implement the prediction-updating transitions of the filtering equation directly by using a genetic type mutation-selection particle algorithm [78]. The samples from the distribution are represented by a set of particles (also denoted as samples, individuals); each particle has a likelihood weight assigned to it that represents the probability of that particle being sampled from the Probability Density Function (PDF). Weight disparity leading to weight collapse is a common issue encountered in these filtering algorithms; however it can be mitigated by including a resampling step before the weights become too uneven. Several adaptive resampling criteria are supposed to be used, including the variance of the weights and the relative entropy with respect to the uniform distribution. In the resampling step, the particles with negligible weights are replaced by new particles in the proximity of the particles with higher weights [79].

6.2 Map Matching

In an indoor positioning system, the applications of particle filter lie in 2 aspects: on one hand, commonly the applying of a filter would further improve the precision of the estimation results. Similar to the various signal processing algorithms adopted or not adopted in this dissertation, particle filter is expected to meliorate the sampled data and reproduce the true features of the original information to a certain extent. As the assumptions proposed in the development of the step length estimation models in Chapter 4 and 5, during the experiments and tests the volunteers are required to hold the smartphones constantly in their hands. Although the holding gestures are not restricted (taking the phone in front of the face or next to the chest, horizontally or slantwise, is all encouraged), swinging hand or changing between gestures is not allowed. Because it would make the analysis of the kinetic characteristics excessively complicated. However, in the real scenarios the holding gestures of smartphone are extremely diverse. Apart from that, pedestrians might not only take their phones in hands but also put them in pockets or bags. In case of those situations, solely adjusting the user specified parameter is barely enough, because even for the identical pedestrian, the changeful holding gestures would lead to totally different model parameters.

Fundamentally the mathematical models developed in Chapter 4 and 5 are both based on the kinetic characteristics of the human body's barycenter. In other words, according to the barycenter's accelerations features the step length when pedestrian is walking or running is estimated. Obviously there is definitely an assumption, or a premise: the built-in IMU in smartphone can record the acceleration information of the body's barycenter faithfully and exactly. If the holding gesture is not specified but unvaried, this criterion is fairly met. But if the relative motion between the smartphone and the body is uncertain or keeps changing, undoubtedly the effectiveness of the 2 models would reduce greatly.

Nevertheless, continually attempting other gestures and analyzing the kinetic characteristics for more human postures in order to develop an absolute universal mathematical model which is applicable to all of the situations are neither imperative nor feasible. Practically, by means of certain statistical theories, to reckon the final position where has the largest probability rather than calculate an absolute result, is supposed to be a more reasonable strategy.

Thereupon particle filter is an advisable solution. The positioning result of each step is determined by both the current measurement and the prediction from the last state. The unfavorable influences from gesture changing and device swinging may still exist. However, in the long term these perturbations could be conquered and mitigated to a great extent. As a result the robustness and stability of the system would be promoted substantially.

Moreover, as stated at the beginning of this section, the second function of particle filter in a positioning system rests on that it is serviceable to match the pedestrian's trajectory to the real building map. Practically the estimated position as well as trajectory must be constrained to lie on the corridors, lobbies or rooms within a building. In other words, the unreachable positions for pedestrians must be eliminated from the estimated result, such as walls, pillars, desks, cabinets etc. Particle filter is an ideal choice for this requirement. As described in Section 6.1, particle filter is a numerical approximation to a Bayesian filter. It is able to deal with the nonlinear, non-Gaussian noises may present in the estimation for step length and heading direction. The major procedures of particle filter consist of important sampling, weight calculation and resampling. Firstly, a set of "particles" are randomly produced. Each particle represents a possible 2D displacement and a heading angle which correspond to the length and azimuth of a step. They are produced on the basis of the posterior PDF of the state, so that each particle contains a weight which represents its probability for the new step. Subsequently, the state is estimated according to the particles and associated weights. As the amount of particles becomes quite large, the represented PDF is equivalent to the usual continuous posterior PDF. When the new step is made, the weights of all the particles are updated and this procedure is called resample. After several iterative in which resampling is involved, the final position is derived.

Theoretically this position has the largest probability and therefore is supposed to be a more reliable result [80]. In reality, the particles would only be initially produced at the accessible positions in the real architectural space. Consequently, the acquired moving trajectory is naturally coincident with the physical surroundings.

In this dissertation, every system state of a step consists of 2 items: the length of the *i*th step *step_length*[*i*] and the heading angle during the *i*th step *heading*[*i*]. The particle filter follows the procedures below.

Step 1: Initially, the first state (*step_length*[0] and *heading*[0]) are output, because no previous state could be used for predicting;

Step 2: Using the current position and the state of the last step (*step_length*[$i-1$] and *heading*[$i-1$]) the position after the *i*th step is predicted, according to Eq. 6.1;

Step 3: With this predicted position as *Expectation* and 1 meter as *Standard deviation*, 1000 random particles are produced (all must conform to the physical surroundings of the building);

Step 4: Taking the current state *step_length*[*i*] and *heading*[*i*] as *a posteriori* estimate, the weights of every particle are calculated. Based on these weights (importance) resampling is implemented. On the basis of new particles, an optimal estimated position is resulted (weighted sum). According to this position the state of the *i*th step is output and the trajectory is updated. The weight of every particle is calculated by Eq. 6.2:

$$weight[p] = normalizing(max\_deviation - deviation[p] + 1), \tag{6.2}$$

where *weight*[*p*] denotes the weight of the *p*th particle; *deviation*[*p*] indicates the distance between the *p*th particle and *a posteriori* position; *max_deviation* represents the maximum among all of *deviation*[]s; *normalizing*() is indicative of the function for normalizing.

Step 5: Turn to **Step 2** and operate iteratively, until no more step state within this walking segment is found.

6.3 Evaluation

In order to test the effect of particle filter in an indoor positioning system, a group of experiments are implemented. The most typical scenario is the corridor in the first floor of my institute (as Fig. 6.1). The experiments are performed by 10 different volunteers (male and female, height from 1.65 *m* to 1.80 *m*, weight from 60 *kg* to 75 *kg*). All of the volunteers are required to take the smartphone in hand and walk through the corridor from the door at the up-left corner to the door at the up-right corner. They are encouraged to walk with their preferred gaits. There are totally 12 breakpoints

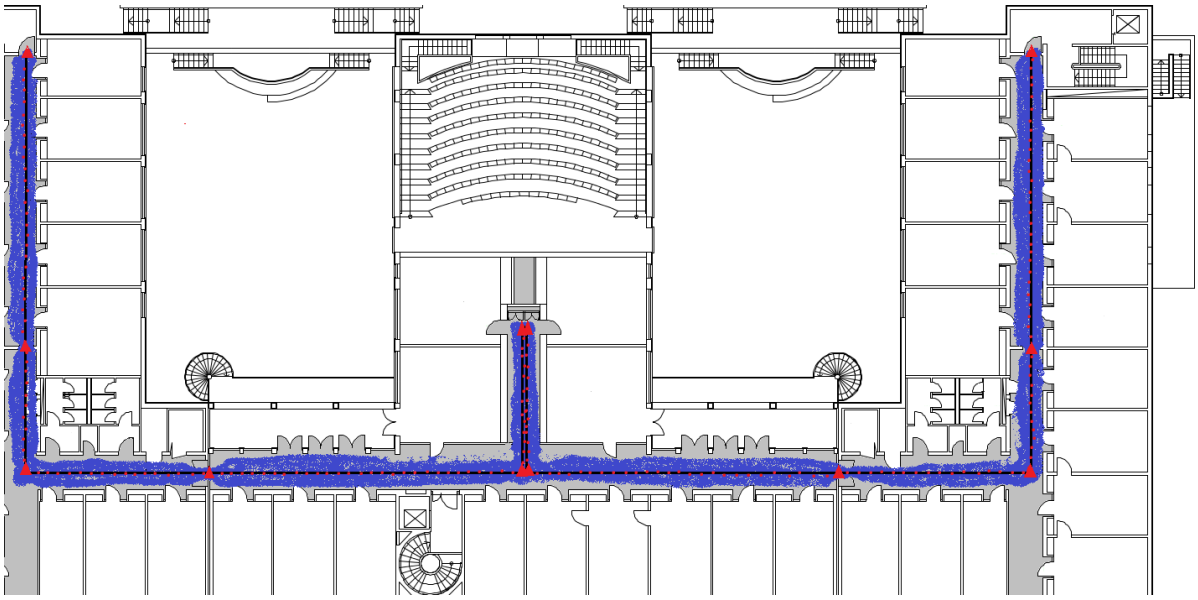

Figure 6.1: An instance for the application of particle filter in the indoor positioning system. In this experiment a pedestrian walked from the door at the up-left corner to the door up-right (black line is the real route). In the process he stopped 6 times (include at the start and end points) and turned 6 times. Every red triangle represents a breakpoint and the whole walking process is divided into 10 segments. The substantial blue points are the particles being produced. Every positioning result after a step is indicated by a red point. The total distance for walking is 136 m. It takes this volunteer 194 steps with the average step length 0.70 m.

consist in the whole route, with 6 stop points and 6 turning points. Each of these breakpoints is highlighted with a red triangle. At the breakpoints the volunteers are allowed to change their gesture holding the smartphone. Fig. 6.1 demonstrates the result of one instance.

According to the results of the experiments, the changing of the gesture could be handled well by the particle filter. During the walking, a few volunteers occasionally raise the smartphones to check the their kinetic data in real time, or put their smartphones into pockets around the breakpoints, but the unfavorable impact from gesture changing and device swinging is relatively limited and can be rectified by the neighboring step states. For comparison a few control groups are set, in which the absolute schemes solely by the estimation models are employed. In contrast, in the test scenario of Fig. 6.1, with the advantage of particle filter the average deviation of the final point declined from 1.96 meters to 1.21 meters, by 38.27%. Obviously the improvement in the positioning accuracy is attributed to the map matching.

Recap

In this chapter a complementary method is introduced. Because the mathematical models developed before apply basically to an absolute situation that the relative position between the smartphone and the body is unvaried. When the gesture changed the estimation accuracy would degrade. Thereupon particle filter is employed in this chapter. With this probabilistic method the system is able to maintain its performance in case of gesture changing and other eventualities. Furthermore the map matching problem is accordingly solved as well. As a result the serviceability of the whole system is improved greatly.

Chapter 7

Enhancement of the Functions

While designing an indoor positioning system of high intelligence, there are two more factors have to be taken into consideration: firstly, the behavior recognition for pedestrians is supposed to be involved in the system. Particularly, the activities between walking and running are required to be further distinguished [81], so that different mathematical models catering for variant situations could be utilized with more efficiency. Secondarily, regarding a multi-storied building which is quite common in the real application scenarios, the determination of users' floor is also an indispensable part in the Pedestrian Navigation System (PNS). For an indoor positioning system of full functions, solely the location information in terms of 2D layout is barely comprehensive in anyway. Therefore the solutions toward these pragmatic problems are discussed in this chapter.

7.1 Distinguish between Walking and Running

The step length of pedestrians is able to be estimated according to the mathematical models developed in Chapter 4 and 5. However, the differentiation rule between both behaviors is not yet referred to. Intuitively the body motion when pedestrian is running is more intense than when walking. Whether the intensity of body motion could serve as a discriminator between both of the activities, and if so, which parameter is the most appropriate and distinctive indicator to measure that intensity? In order to clarify these rules, the data collected during the previous experiments are analyzed once more in this section.

Fig. 7.1 are the statistics of various parameters in the case of walking as well as running.

From the comparison in Fig. 7.1, it is remarkable that the acceleration variance is the indicator showing the largest discriminability among the 4 parameters. Between walking and running,

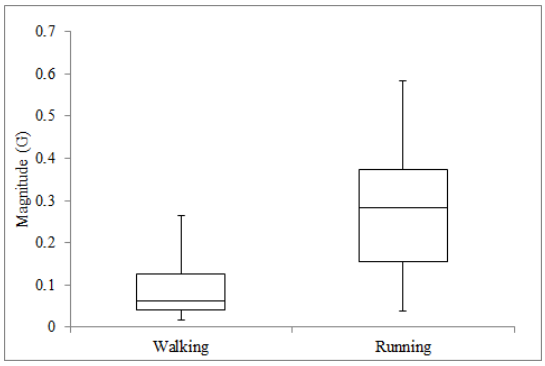

(a) Magnitude (in G)

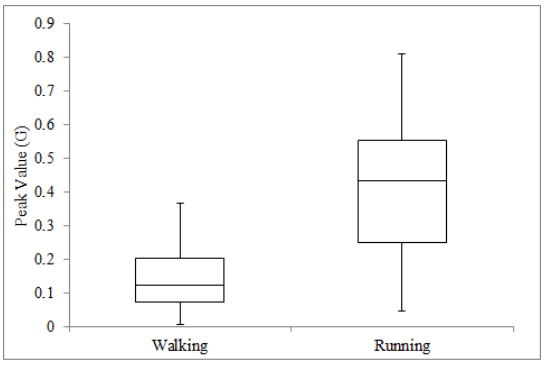

(b) Peak value (in G)

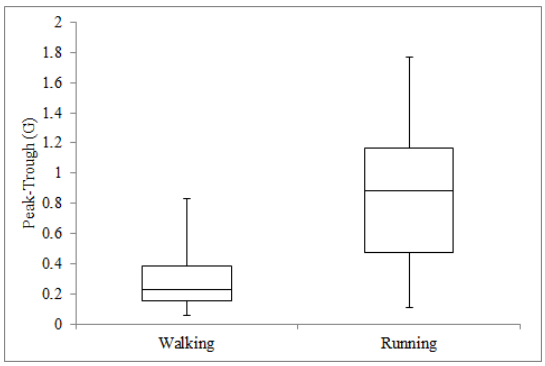

(c) Peak-Trough (in G)

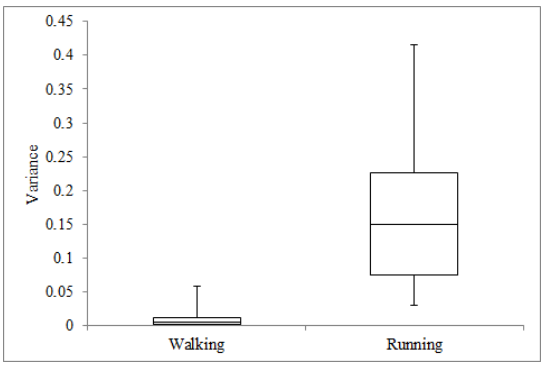

(d) Variance

Figure 7.1: The Box-whisker Plots of 4 parameters with reference to 2 different human behaviors. Obvious is it that the intensities of body motion when walking and running are rather dissimilar. In the 4 figures above, the magnitude, the peak value, the peak-trough difference, and the variance are used as 4 different indicators for the motion intensity, in order to search the right parameter which plays the most crucial role in the differentiation between walking and running.

the overlap region of the variance values is the smallest. Consequently the variance is chosen for distinguishing both of the behaviors.

On the basis of the sampled data from all of the experiments (10 volunteers), when the threshold for variance is set as 0.0397, the misrecognition rate reaches the minimum which is 2.52%. It has to be emphasized that this statistics result comes from the entire test experiments which quite a few abnormal gaits are also included, such as fast walking and slow running. With respect to the general situations this rule for distinguishing is convincingly effective.

7.2 Altitude Detection

As the popularization of the indoor positioning techniques, the requirement for altitude information has burst onto the scene as well. Along with the growing development of the Location Based Service (LBS), the multi-storied applications become increasingly imperative and indispensable in the realistic scenarios. Without the floor detection for a comprehensive and intelligent indoor positioning system it is barely satisfactory.

7.2.1 Related Works

With regard to the schemes acquiring the floor information, several investigations were fulfilled by the previous researchers [82] [83]. The majority employed WLAN based approaches which use Wi-Fi fingerprint or signal trilateration to estimate the client's location in 3D space [84]. The strength rests on the precision and users do not need to identify their initial storey because the positioning results are absolute heights [85]. Their shortcomings are also similar to those of all the WLAN related schemes, that the full coverage of the wireless signal is decidedly necessary. In case of the deficiency of the infrastructures these methods are naturally incapacity.

In terms of the solutions using IMU, there are also quite a few positive efforts were ever made [86] [87]. However, the key equipment is the inertial sensors placed at lower limbs. With the shoe-mounted sensors and the corresponding inertial mechanization theories, the vertical displacements between adjacent steps are directly integrated. Zero Velocity Updates (ZUPTs) would compensate the drift at each foot standstills [88]. Furthermore, more impressive attempts were never suspended. For instance demonstrated in Fig. 7.2, using a series of IMUs stuck close to the hip joints, knee joints and ankle joints to record and analyze the full activities of the lower limbs [89]. By mean of the data from every sensor node and the Personal Area Network (PAN), all of the motion details of both legs are reproduced while pedestrian is climbing a stair.

The advantage lies in their absolute accuracies. Relying on the Wireless Sensor Network (WSN) and the precise biometrical models, all of the kinetic characteristics of human's lower limbs would be completely captured [90]. The effect is similar to those of the vision-based surveillance systems. With the exhaustive details of the mechanical motions of both legs, the behaviors of stair ascent and descent are expected to be exactly recognized. Subsequently the function of floor detection is therefore implemented. By contrast, the inconvenience of these schemes is evident as well: the fully equipped WSN is definitely requisite. Obviously for an indoor positioning system solely based on the built-in sensors in smartphone, these brilliant schemes are excessively sophisticated and demanding.

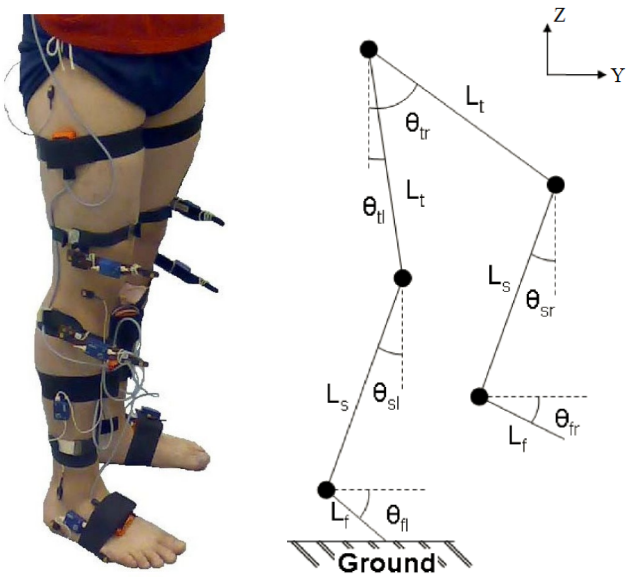

(a) (b)

Figure 7.2: An instance using the inertial sensors network around the lower limbs to recognize the human behaviors of stair ascent and descent

(a) The zigzag staircase (b) The spiral staircase

Figure 7.3: The staircases of 2 forms in the building of my institute. In each of the 2 staircases, ascending and descending, a series of the experiments are implemented to seek the appropriate approach for floor detection.

7.2.2 Accelerometer based Solution

In order to verify the feasibility of recognizing the stair ascent and descent by inexpensive IMUs of smartphone, a set of experiments are performed in the staircases of my institute. Fig. 7.3 illustrates the scenes. For the zigzag staircase, between the ground floor and the first floor, the lower half have 10 stairs, the upper half have 11 stairs; while for the spiral staircase, between the ground floor and the first floor, the lower half have 7 stairs, the upper half have 14 stairs.

Similar to the experiments in the previous chapters, one volunteer is required to ascend and descend both of the staircases for 10 times (40 times altogether). Each step corresponds to 1 stair singly. The step frequency is not pre-assigned anymore. The volunteer is able to adopt his preferred speed. Four sets of acceleration data selected from each of four groups of the experiments are demonstrated from Fig. 7.4 to 7.7.

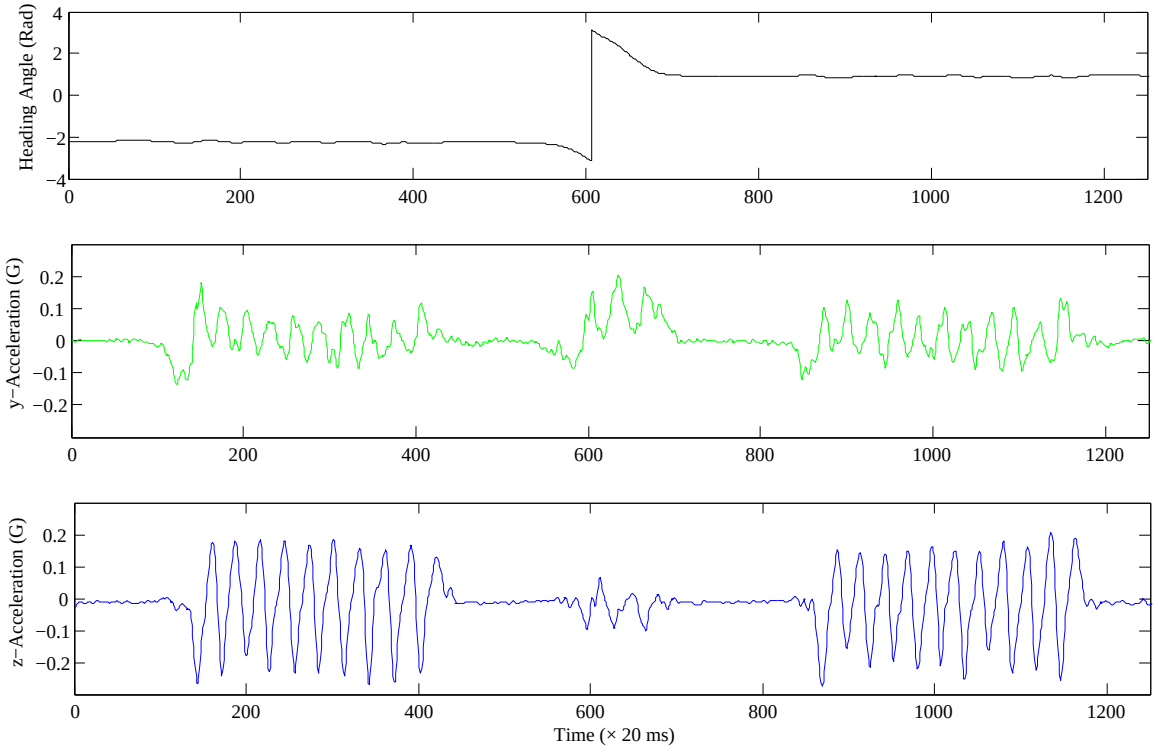

Figure 7.4: A set of data collected while the volunteer goes upstairs in the zigzag staircase (the scenes in Fig. 7.3 (a))

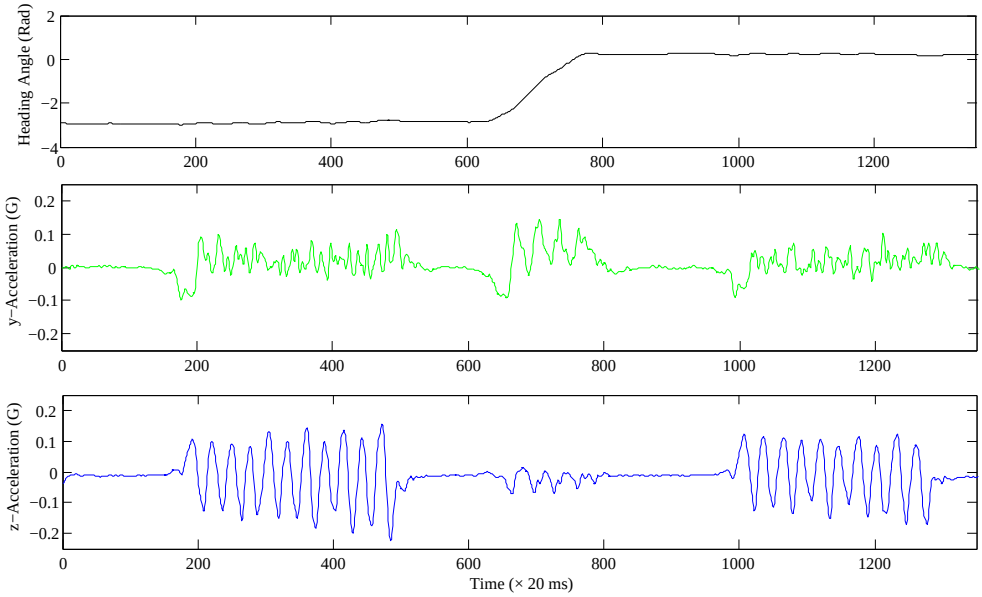

Figure 7.5: A set of data collected while the volunteer goes downstairs in the zigzag staircase (the scenes in Fig. 7.3 (a))

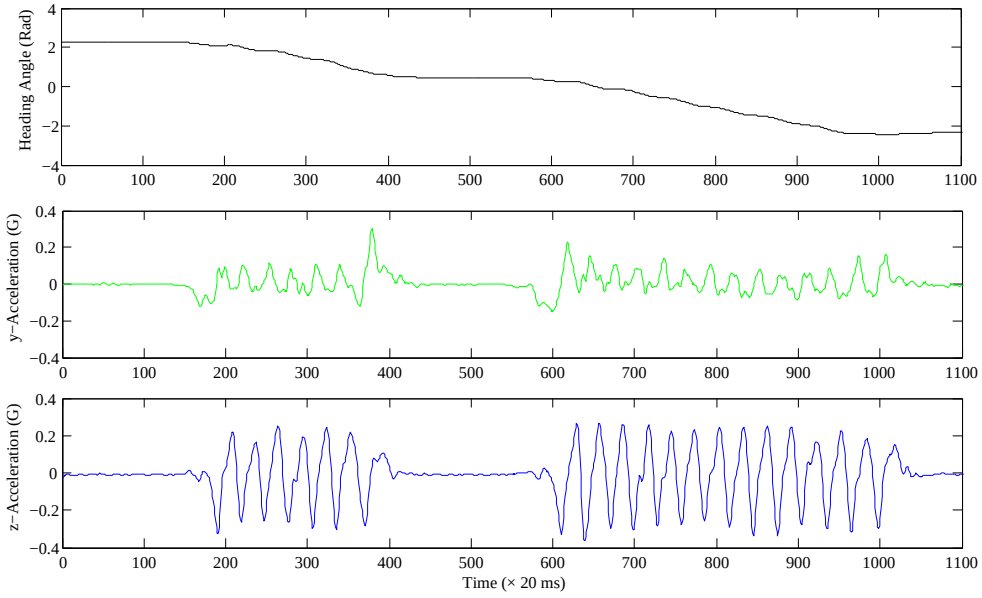

Figure 7.6: A set of data collected while the volunteer goes upstairs in the spiral staircase (the scenes in Fig. 7.3 (b))

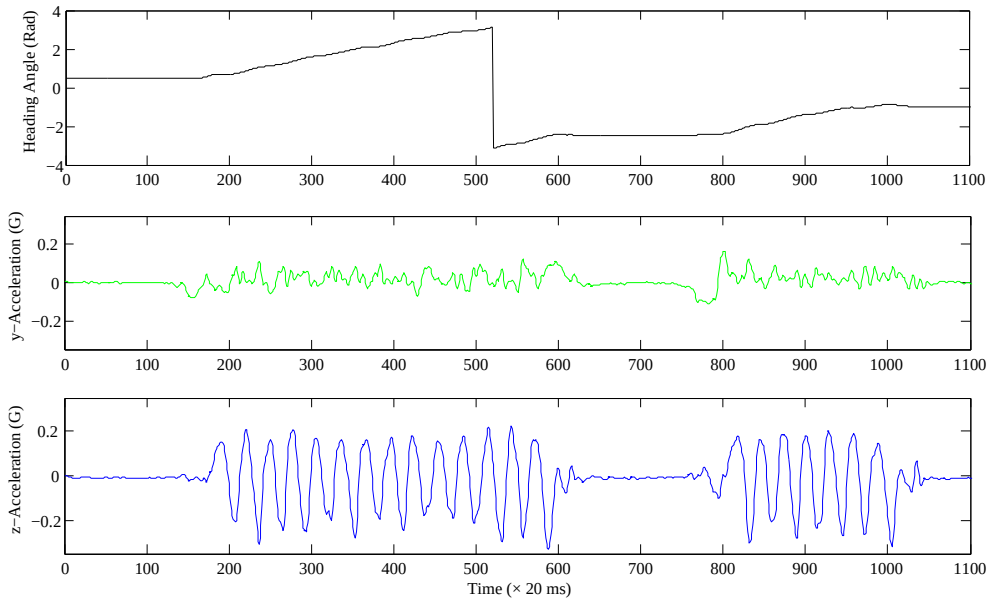

Figure 7.7: A set of data collected while the volunteer goes downstairs in the spiral staircase (the scenes in Fig. 7.3 (b))

The data demonstrated in Fig. 7.4 to Fig. 7.7 include: the heading angle (black curve, according to the data fusion algorithm introduced in Section 3.4.2), the acceleration in anterior-posterior direction (y, green), and the acceleration in vertical direction (z, blue). Both of the acceleration signals are processed by the multi filters described in Chapter 3.

From the acquired azimuth data, the turning in the staircases is indicated distinctly. In the zigzag staircase there is a sharp transition when the volunteer is turning at the corner; while in the spiral staircase, due to the rotating route the heading angles are more likely to vary progressively.

Similar to the data from the walking and running experiments, the y accelerations are instable as before: not only the amplitudes are uncertain but also the impulses are rather confused. In contrast, the z data show their regularity and legibility as they always are: the number of stairs is able to be explicitly counted (for Fig. 7.4 and 7.5 they are 10 and 11 stairs; while Fig. 7.6 and 7.7 are 7 and 14).

In order to seek a feature indicator in the z accelerations, which associates with certain physical property of stair ascent and descent, the average peak values, average trough values, average peak-trough differences, and average variance are compared in Fig. 7.8. Because the variance has proved to be the most crucial parameter to indicate the motion intensity (in Section 7.1), another related parameter— the magnitude is not involved here.

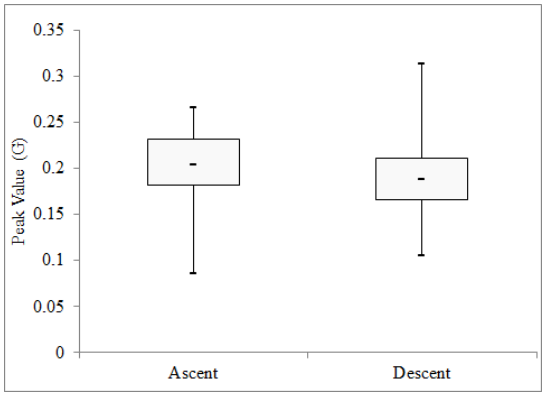

(a) Average peak value (in G)

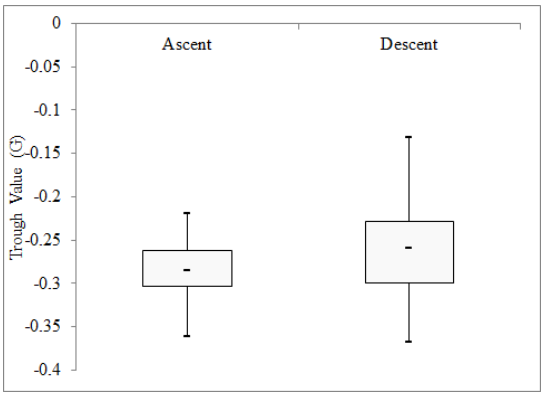

(b) Average trough value (in G)

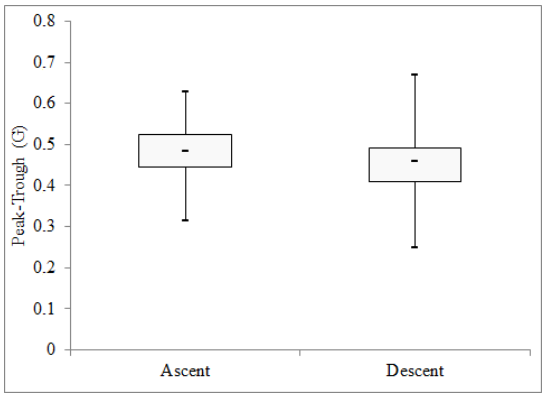

(c) Average peak-trough difference (in G)

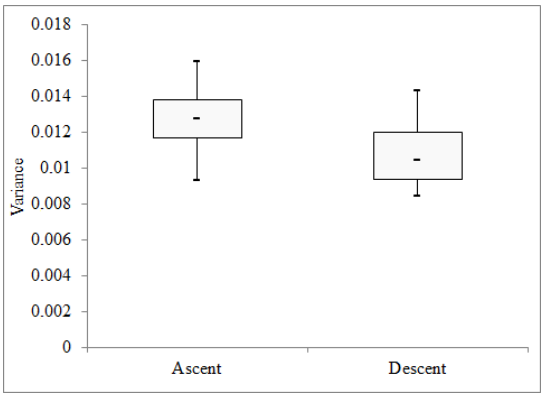

(d) Average variance

Figure 7.8: The Box-whisker Plots of 4 indicators with reference to stair ascent and descent are compared. It is postulated that certain parameter would show remarkable disparity towards stair ascent and descent. In the 4 figures, the average peak values, average trough values, average peal-trough differences, and average variances, together with their statistical distributions are compared. Unfortunately from the 4 parameters analyzed above, there is no significant difference between both behaviors.

All of the parameters demonstrated in Fig. 7.8 are sourced from the statistics of the data sampled in both staircases. Form the figures none of the 4 parameters is able to differentiate both behaviors of stair ascending and descending. There is merely an approximate phenomenon that the motion of ascent is slightly more intense than that of descent. However, that is hardly adequate to serve as a feature indicator. Since the effect is negative, further experiments by more diverse volunteers are not performed any more.

Theoretically that was not how it was expected to happen. When pedestrian is ascending the

stairs, on the whole the accelerations upward are supposed to be larger than downward, and then the barycenter could therefore rise; vice versa. Nevertheless the absolute value of the average peak value is less than that of average trough value, which is the same as the situation of descent. Moreover, there is nothing but marginal difference between the acceleration waveforms generated when ascent and descent (the only distinction revealed by Fig. 7.4 to 7.7 is: during ascending, it is trough first and then peak; while descending, it peak first then trough. But that could not be regarded as a reliable criterion). One possible reason is that eventually the precisions of the built-in accelerometers are limited. The difference between ascent and descent is even less significant than the error level of drift in inertial sensors. On the other hand, concerning the stair climbing scenario, the smartphone held in hand might not be capable to record the motion characteristics of the body barycenter exactly. That is also why most of researchers are inclined to rely on the sensor network set at the lower limbs rather than sole handheld IMU in the subject of ascent & descent recognition.

7.2.3 Barometer based Solution

On the basis of the analysis in Section 7.2.2, in reality floor detection relying on handheld accelerometer is barely feasible. A new approach is required to be attempted. The emergence of MEMS barometer brings this problem new solution. Along with the unveiling of iPhone 6 / 6 plus and iPad Air in 2014, barometer bursts onto the scene for the first time as a component of smartphone [91]. Because barometer is primarily used to estimate the relative altitude according to atmospheric pressure, it is called digital altimeter as well. The advent of inexpensive built-in barometer makes a wide range of altitude-oriented applications possible.

According to the data sheet of Bosch BMP 280[1] which is a popular digital pressure sensor adopted by many consumer electronics producers, the relative altitude is calculated by the barometric formula described in Eq. 7.1:

$$altitude = 44330 \times [1 - (\frac{p}{p_0})^{\frac{1}{5.255}}], \tag{7.1}$$

where p denotes the measured atmospheric pressure; while p_0 indicates the pressure at sea level, which is considered 101.325 kPa.

[1] https://www.bosch-sensortec.com/en/homepage/products3/environmentalsensors1/bmp280/

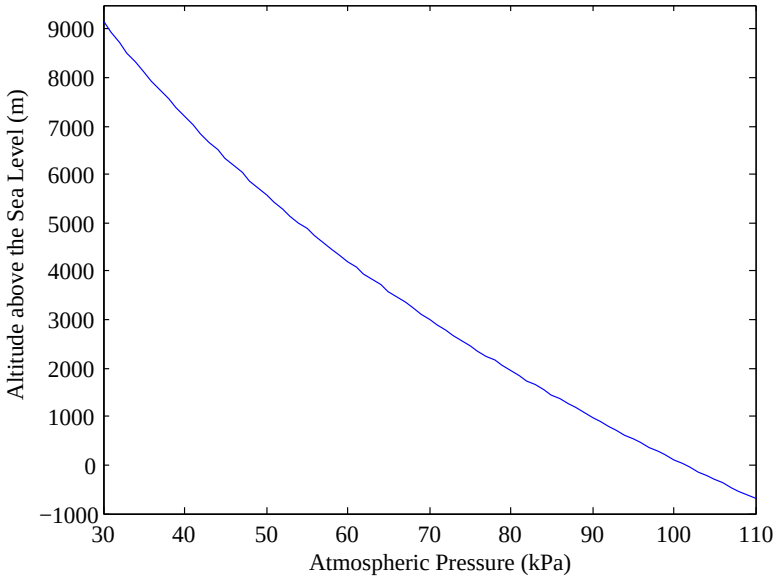

Figure 7.9: The relation between the varied atmospheric pressure and altitude

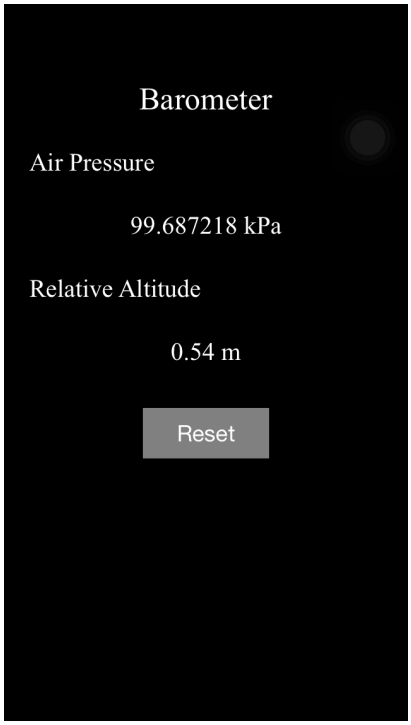

Figure 7.10: The screenshot of the app “Barometer”

As Fig. 7.9, along with the increasing of the measured atmospheric pressure, the altitude decreases gradually. Provided the pressure declines by 0.1 kPa at sea level, the altitude is supposed to rise by approximately 8.43 m.

However, the estimation result for altitude from atmospheric pressure is not stable at all. Because the reading from barometer is strongly influenced by the climate conditions, such as temperature, humidity, air density and other weather parameters. Even the environment of indoor or outdoor could impact on the measured pressure.

In order to verify the usability of the built-in barometer in the indoor positioning scenario, a test app is developed to record the atmospheric pressure in real time and calculate the relative altitude accordingly. The screenshot of the test app is demonstrated in Fig. 7.10.

With this app, the stair ascent and descent experiments are implemented once more in both of the staircase of my institute (as Fig. 7.3). Because the function of the app "Barometer" is too monotonous, it is not submitted to App Store.

Fig. 7.11 and 7.12 are 4 instances sampled from the experiments.

From the calculated results illustrated in Fig. 7.11 and 7.12, the variations in the altitude are able to be sensed evidently. Although the estimation values of altitude derived from atmospheric pressure are far from absolute accurate, and the results are not exactly in real-time as well, for the application of floor detection the precision and sensitivity is adequate. From the relative altitude curves in figures, even the platforms at the turning corners are demonstrated well.

Adding with the function of floor detection by the built-in barometer of smartphone, the serviceability and comprehensiveness of the indoor positioning system would be improved in the great degree.

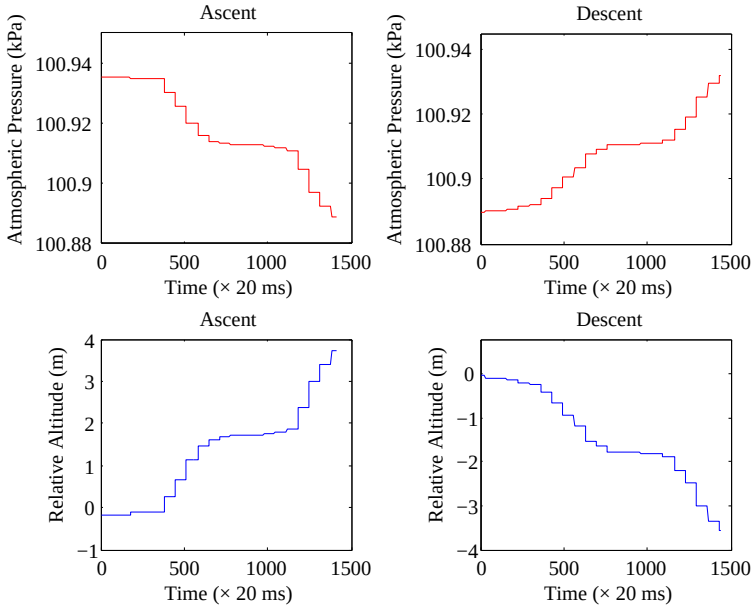

Figure 7.11: The sampled atmospheric pressures and calculated altitude information of the stair ascent and descent experiments in the zigzag staircase (Fig. 7.3 (a)).

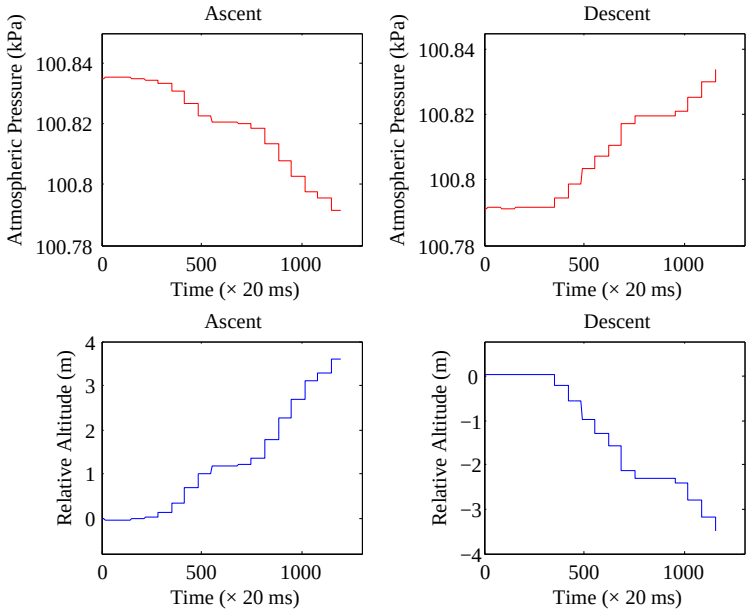

Figure 7.12: The sampled atmospheric pressures and calculated altitude information of the stair ascent and descent experiments in the spiral staircase (Fig. 7.3 (b)).

7.2.4 Evaluation

The utilization of barometer in floor detection shows the great convenience. However, in the experiments described in Fig. 7.11 and 7.12, as an altimeter the accuracy in real-time is far from prefect. According to the data sheet of Bosch BMP 280, the precision of this typical commercial digital barometer is $\pm 0.12\ hPa$ which is equivalent to $\pm 1\ m$ (with the environment temperature 25°C). Normally the height difference between 2 floors is approximately 2.8 to 3.5 m. For museum or exhibition hall it would be higher. Thus, this rough estimation of relative altitude is fairly capable of the low storied buildings. For example, in my institute there are only 2 floors above the ground. The pressure distinction between 2 floors in a short time is enough to distinguish between both. Nevertheless, with regard to the high-rise multi-storied buildings and in a comparative long period, could the barometer based solution still maintain a satisfactory performance?

In order to evaluate the long term accuracy and feasibility of the barometer scheme, a further test experiment is designed. Because the precision of the methods using WLAN or WSN around lower limbs approaches to 100%, the absolute accuracies are not compared in this section.

The experiment is performed in a six storied building, in which the floor heights are all 3.2 m. The Relative Altitude (RA) on the ground floor is initialized as 0 m. If

$$3.2n - 1.6 \leqslant RA < 3.2n + 1.6, \tag{7.2}$$

the current floor number is regarded as n. During this experiment n is supposed to be $0, 1, \ldots, 5$. In this dissertation the counting of the floor number conforms to the European standard by which the floor index begins from 0 (by contrast in North America and Asia it starts at 1).

The volunteer is required to take a smartphone and climb through the 6 floors, upward and downward, circularly. When he reaches a new floor, after the reading of the barometer is stable, the RA is recorded. Once the determined floor number is wrong according to Eq. 7.2, the experiment is ended. Finally the experiment was terminated at the 2th floor when the volunteer was going upstairs. At that time, the volunteer had finished 42 storeys and spent 665 seconds. In other words, after 11 *min* 5 *s*, the deviation of RA is around 3.2 m. This phenomenon is similar to the drift in accelerometer and gyroscope. After more than 10 *min*, the measured data is so offset that it needs to be calibrated. In order to eliminate the accidental factors, this experiment was repeated twice on other days, once it was rainy. And the first error occurred after 43 and 48 storeys respectively, which means the effectiveness of the barometer based solution for floor detection is able to maintain 11 to 13 *min*. Within this period, the acquired results could be deemed reliable and valid. However, in the longer term certain calibration strategies are necessary as well.

Recap

In this chapter two practical functions are implemented additionally. Firstly, the behaviors of walking and running are distinguished so that the choice of the mathematical models would be more targeted. Secondarily, for the requirement of stair ascent and descent recognition, various solutions are attempted and compared. Finally the scheme using barometer is proved to be the most operable and feasible. With the advantage of the newly emerged built-in barometer within smartphone, the indoor positioning system is extended to the multi-storied scenarios.

Chapter 8

Conclusion and Future Works

8.1 Contributions and Conclusion

In this dissertation the complete operating process of an indoor positioning strategy is described. By means of the built-in micro sensors of smartphone, the latest standpoint and the moving trajectory of pedestrian are calculated. Fundamentally the sampled data from accelerometer, gyroscope and magnetometer are meliorated by a series of filters. Basing on the fused data from gyroscope and magnetometer, the heading angles are determined. From the processed acceleration signals, the kinetic characteristics of pedestrian's body are extracted accordingly. Subsequently the length of each step is therefore estimated. With both the azimuth and length information of each step, the current position is supposed to be successively updated.

Particularly, two novel mathematical models for walking and running step length estimation are developed respectively. They are the key contributions in this dissertation. On the basis of the variance of the vertical accelerations, the horizontal displacement of each step is able to be reckoned. The average deviation rate of the walking model is 10.90% while the running model is 19.66%. In the same condition these accuracies are higher than all of the previous models. Although they are complicated and consist of 4 equations and 3 equations respectively (Eq. 4.12, 4.13, 4.14, 4.15 and Eq. 5.4, 5.5, 5.6), the computation cost towards smartphone is still feasible. Moreover, because my models refer to the variance of the vertical accelerations rather than the exact peak or trough values, they are able to promote the stabilization and robustness of the positioning system on the whole. Once any single peak or trough is misrecognized, it might lead to a series of disorders in the peak-trough pairs, which would cause meaningless result in the peak-trough based models. In contrast the variance is measured more safely and the unfavorable influence of the possible errors in step frequency is also comparatively limited. In other words, the fault-tolerant ability of the system

is enhanced to a certain extent.

Furthermore, particle filter is adopted to constrain the moving trajectory to the physical surroundings. Particle filtering methodology uses a genetic type mutation-selection sampling approach, with a set of particles to represent the posterior distribution of certain stochastic process given a few noisy and partial observations. The state-space model could be nonlinear and the initial state and noise distributions could take any form required. Particle filter techniques provide a well-established methodology for generating samples from the required distribution without requiring assumptions about the state-space model or the state distributions. In the experiment scenario by employing particle filter, the accuracy is improved by 38.27%. With the physical layout information, the positioning result would be rectified as well.

Eventually with reference to the problem of distinguishing the behaviors of walking and running, the variance related criteria is discussed in Chapter 7. Besides, the digital barometer is utilized for floor detection so that the positioning system is extended to multi-storied scenarios. According to the evaluation the reliability and validity of the floor numbers estimated by barometer can maintain for more than 10 minutes. In most of scenarios with certain calibration approaches this solution is convenient but adequate.

8.2 Future Works

The aim of my endeavors is to develop an autonomic indoor positioning system. In the view of the research in this dissertation, there are 4 problems require to be further engaged:

(1) It is not difficult to realize that an initial standpoint of pedestrian is foremost necessary, which is also an imperative premise for PDR methods. In all the experiments involved in this dissertation, the starting positions are either pre-assigned or input by users themselves. However, this is impractical for a realistic application. For this drawback, the collaboration between other positioning schemes is highly appreciated because the initial state may be acquired from other alternative information sources.

(2) As the literature [92], the accuracy of the barometer based floor detection would be promoted by WLAN signals as well. By the trilateration the searching zone is reduced and the more reliable floor number is therefore output. In reality the association of multi-techniques is supposed to be constantly encouraged because the entire performance would be improved by the advantage of every component. Besides, as the introduction in this dissertation, due to the instinctive drift problem, the scheme relying on solely inertial sensors is hardly able to perform perfectly in the long term. Combining other positioning techniques (such as WLAN, Bluetooth related methods) may be more

reasonable and advisable. Thereupon how to make full use of all the data sources, how to implement the task about sensors fusion, is pretty promising and definitely requires a considerable quantity of research as well as experiments.

Figure 8.1: The arrangements of the ceiling lamps can be used for walking speed estimation

(3) Other brilliant inspiring ideas occur continually, such as [93] that the ceiling lamps in a corridor are serviceable as well. Since a few latest smartphones are equipped with the ambient light sensor, the rhythmic property of the light intensity above (as Fig. 8.1) may be detected and applied to estimate the walking speed and certain special positions. Moreover, this sort of fantastic hardware is expected to be taken full advantage of in order to discover any possibility to improve the accuracy of positioning. The similar thoughts are ceaseless: for example, using barometer or thermometer to sense the particular locations such as opened windows or entrance between outdoor and indoor environments. Furthermore, if associating with numerous wearable devices, the application potentialities are considerable. Ultimately the knowledge about the big data becomes increasingly imperative.

Bibliography

[1] B. Hofmann-Wellenhof, H. Lichtenegger, and J. Collins, *Global positioning system: theory and practice*. Springer Science & Business Media, 2012.

[2] S. Bak, K.-H. Jung, C. Yu, and Y.-J. Suh, "Guided tour of handoff steering for bandwidth in indoor venues," in *Wireless Communications and Networking Conference (WCNC), 2015 IEEE*, pp. 1930–1935, IEEE, 2015.

[3] S. Jeon, Y.-J. Suh, C. Yu, and D. Han, "Fast and accurate wi-fi localization in large-scale indoor venues," in *Mobile and Ubiquitous Systems: Computing, Networking, and Services*, pp. 129–141, Springer, 2014.

[4] J. Liu, T. Chen, J. Bao, J.-U. Kim, and J. Wang, "Location technology-based mobile shopping service system," *International Journal of Hybrid Information Technology*, vol. 5, no. 4, pp. 133–142, 2012.

[5] M. A. Rashid, Z. Riaz, E. Turan, V. Haskilic, A. Sunje, and N. Khan, "Smart factory: E-business perspective of enhanced erp in aircraft manufacturing industry," in *Technology Management for Emerging Technologies (PICMET), 2012 Proceedings of PICMET'12:*, pp. 3262–3275, IEEE, 2012.

[6] K. Sun, Y. Yu, and J. Gu, "Efficient robot navigation for semi-structured indoor storehouse," in *Electrical and Computer Engineering (CCECE), 2015 IEEE 28th Canadian Conference on*, pp. 1313–1317, IEEE, 2015.

[7] W. Ge, R. T. Collins, and R. B. Ruback, "Vision-based analysis of small groups in pedestrian crowds," *Pattern Analysis and Machine Intelligence, IEEE Transactions on*, vol. 34, no. 5, pp. 1003–1016, 2012.

[8] S. S. Rautaray and A. Agrawal, "Vision based hand gesture recognition for human computer interaction: a survey," *Artificial Intelligence Review*, vol. 43, no. 1, pp. 1–54, 2015.

[9] J. Sampaio, R. Leser, A. Baca, J. Calleja-Gonzalez, D. Coutinho, B. Gonçalves, and N. Leite, "Defensive pressure affects basketball technical actions but not the time-motion variables,"

Journal of Sport and Health Science, 2015.

[10] S. Sivaraman and M. M. Trivedi, "Looking at vehicles on the road: A survey of vision-based vehicle detection, tracking, and behavior analysis," *Intelligent Transportation Systems, IEEE Transactions on*, vol. 14, no. 4, pp. 1773–1795, 2013.

[11] S. Han and S. Lee, "A vision-based motion capture and recognition framework for behavior-based safety management," *Automation in Construction*, vol. 35, pp. 131–141, 2013.

[12] J. M. Chaquet, E. J. Carmona, and A. Fernández-Caballero, "A survey of video datasets for human action and activity recognition," *Computer Vision and Image Understanding*, vol. 117, no. 6, pp. 633–659, 2013.

[13] M. Cristani, R. Raghavendra, A. Del Bue, and V. Murino, "Human behavior analysis in video surveillance: A social signal processing perspective," *Neurocomputing*, vol. 100, pp. 86–97, 2013.

[14] A. Möller, M. Kranz, R. Huitl, S. Diewald, and L. Roalter, "A mobile indoor navigation system interface adapted to vision-based localization," in *Proceedings of the 11th International Conference on Mobile and Ubiquitous Multimedia*, p. 4, ACM, 2012.

[15] H. Yucel, T. Ozkir, R. Edizkan, and A. Yazici, "Development of indoor positioning system with ultrasonic and infrared signals," in *Innovations in Intelligent Systems and Applications (INISTA), 2012 International Symposium on*, pp. 1–4, IEEE, 2012.

[16] C. Medina, J. C. Segura, and A. De la Torre, "Ultrasound indoor positioning system based on a low-power wireless sensor network providing sub-centimeter accuracy," *Sensors*, vol. 13, no. 3, pp. 3501–3526, 2013.

[17] S. S. Saad and Z. S. Nakad, "A standalone rfid indoor positioning system using passive tags," *IEEE Transactions on Industrial Electronics*, vol. 58, no. 5, pp. 1961–1970, 2011.

[18] M. Moreno-Cano, M. A. Zamora-Izquierdo, J. Santa, and A. F. Skarmeta, "An indoor localization system based on artificial neural networks and particle filters applied to intelligent buildings," *Neurocomputing*, vol. 122, pp. 116–125, 2013.

[19] H. Liu, H. Darabi, P. Banerjee, and J. Liu, "Survey of wireless indoor positioning techniques and systems," *Systems, Man, and Cybernetics, Part C: Applications and Reviews, IEEE Transactions on*, vol. 37, no. 6, pp. 1067–1080, 2007.

[20] A. W. S. Au, C. Feng, S. Valaee, S. Reyes, S. Sorour, S. N. Markowitz, D. Gold, K. Gordon, and M. Eizenman, "Indoor tracking and navigation using received signal strength and compressive sensing on a mobile device," *Mobile Computing, IEEE Transactions on*, vol. 12, no. 10, pp. 2050–2062, 2013.

[21] H. Leppäkoski, J. Collin, and J. Takala, "Pedestrian navigation based on inertial sensors, indoor

map, and wlan signals," *Journal of Signal Processing Systems*, vol. 71, no. 3, pp. 287–296, 2013.

[22] Z. Yang, C. Wu, and Y. Liu, "Locating in fingerprint space: wireless indoor localization with little human intervention," in *Proceedings of the 18th annual international conference on Mobile computing and networking*, pp. 269–280, ACM, 2012.

[23] Y. Luo, O. Hoeber, and Y. Chen, "Enhancing wi-fi fingerprinting for indoor positioning using human-centric collaborative feedback," *Human-centric Computing and Information Sciences*, vol. 3, no. 1, pp. 1–23, 2013.

[24] Y. Zhao, Y. Yang, and M. Kyas, "Likelihood adaptation of particle filter for target tracking using wireless sensor networks," in *Global Communications Conference (GLOBECOM), 2013 IEEE*, pp. 3323–3328, IEEE, 2013.

[25] Y. Yang, Y. Zhao, and M. Kyas, "A statistics-based least squares (sls) method for non-line-of-sight error of indoor localization," in *Wireless Communications and Networking Conference (WCNC), 2013 IEEE*, pp. 2299–2304, IEEE, 2013.

[26] S. Liu, Y. Jiang, and A. Striegel, "Face-to-face proximity estimation using bluetooth on smartphones," *Mobile Computing, IEEE Transactions on*, vol. 13, no. 4, pp. 811–823, 2014.

[27] S. Li, Y. Lou, and B. Liu, "Bluetooth aided mobile phone localization: a nonlinear neural circuit approach," *ACM Transactions on Embedded Computing Systems (TECS)*, vol. 13, no. 4, p. 78, 2014.

[28] P. D. Groves, *Principles of GNSS, inertial, and multisensor integrated navigation systems*. Artech House, 2013.

[29] R. Harle, "A survey of indoor inertial positioning systems for pedestrians," *IEEE Communications Surveys & Tutorials*, no. 15, pp. 1281–1293, 2013.

[30] A. Jimenez, F. Seco, C. Prieto, and J. Guevara, "A comparison of pedestrian dead-reckoning algorithms using a low-cost mems imu," in *Intelligent Signal Processing, 2009. WISP 2009. IEEE International Symposium on*, pp. 37–42, IEEE, 2009.

[31] A. R. J. Ruiz, F. S. Granja, J. C. Prieto Honorato, and J. I. G. Rosas, "Accurate pedestrian indoor navigation by tightly coupling foot-mounted imu and rfid measurements," *Instrumentation and Measurement, IEEE Transactions on*, vol. 61, no. 1, pp. 178–189, 2012.

[32] Y. Jin, H.-S. Toh, W.-S. Soh, and W.-C. Wong, "A robust dead-reckoning pedestrian tracking system with low cost sensors," in *Pervasive Computing and Communications (PerCom), 2011 IEEE International Conference on*, pp. 222–230, IEEE, 2011.

[33] Y. Sun, Y. Zhao, and J. Schiller, "An autonomic indoor positioning application based on smartphone," in *Wireless Communications and Networking Conference (WCNC), 2014 IEEE*,

pp. 3326–3331, IEEE, 2014.

[34] L. Pei, R. Guinness, R. Chen, J. Liu, H. Kuusniemi, Y. Chen, L. Chen, and J. Kaistinen, "Human behavior cognition using smartphone sensors," *Sensors*, vol. 13, no. 2, pp. 1402–1424, 2013.

[35] Y. Jin, W.-S. Soh, M. Motani, and W.-C. Wong, "A robust indoor pedestrian tracking system with sparse infrastructure support," *Mobile Computing, IEEE Transactions on*, vol. 12, no. 7, pp. 1392–1403, 2013.

[36] L. Atzori, T. Dessi, and V. Popescu, "Indoor navigation system using image and sensor data processing on a smartphone," in *Optimization of Electrical and Electronic Equipment (OPTIM), 2012 13th International Conference on*, pp. 1158–1163, IEEE, 2012.

[37] Z. Sun, X. Mao, W. Tian, and X. Zhang, "Activity classification and dead reckoning for pedestrian navigation with wearable sensors," *Measurement Science and Technology*, vol. 20, no. 1, p. 015203, 2009.

[38] I. Bylemans, M. Weyn, and M. Klepal, "Mobile phone-based displacement estimation for opportunistic localisation systems," in *Mobile Ubiquitous Computing, Systems, Services and Technologies, 2009. UBICOMM'09. Third International Conference on*, pp. 113–118, IEEE, 2009.

[39] A. R. Pratama, R. Hidayat, *et al.*, "Smartphone-based pedestrian dead reckoning as an indoor positioning system," in *System Engineering and Technology (ICSET), 2012 International Conference on*, pp. 1–6, IEEE, 2012.

[40] J. Lötters, J. Bomer, A. Verloop, E. Droog, W. Olthuis, P. Veltink, and P. Bergveld, "Design, fabrication and characterization of a highly symmetrical capacitive triaxial accelerometer," *Sensors and Actuators A: Physical*, vol. 66, no. 1, pp. 205–212, 1998.

[41] J. Söderkvist, "Micromachined gyroscopes," *Sensors and Actuators A: Physical*, vol. 43, no. 1, pp. 65–71, 1994.

[42] F. Ferraris, U. Grimaldi, and M. Parvis, "Procedure for effortless in-field calibration of three-axial rate gyro and accelerometers," *Sensors and Materials*, vol. 7, no. 5, pp. 311–330, 1995.

[43] D. Titterton and J. L. Weston, *Strapdown inertial navigation technology*, vol. 17. IET, 2004.

[44] F. Li, C. Zhao, G. Ding, J. Gong, C. Liu, and F. Zhao, "A reliable and accurate indoor localization method using phone inertial sensors," in *Proceedings of the 2012 ACM Conference on Ubiquitous Computing*, pp. 421–430, ACM, 2012.

[45] J. W. Kim, H. J. Jang, D.-H. Hwang, and C. Park, "A step, stride and heading determination for the pedestrian navigation system," *Positioning*, vol. 1, no. 08, p. 0, 2004.

[46] "Method for pedestrian step size estimation and dead reckoning," Nov. 27 2013. CN Patent

App. CN 201,310,388,466.

[47] J.-S. Wang, Y.-L. Hsu, and C.-L. Chu, "Online handwriting recognition using an accelerometer-based pen device," in *2nd International Conference on Advances in Computer Science and Engineering*, pp. 229–232, 2013.

[48] P. G. Weyand, M. Kelly, T. Blackadar, J. C. Darley, S. R. Oliver, N. E. Ohlenbusch, S. W. Joffe, and R. W. Hoyt, "Ambulatory estimates of maximal aerobic power from foot-ground contact times and heart rates in running humans," *Journal of Applied Physiology*, vol. 91, no. 1, pp. 451–458, 2001.

[49] S. Grzonka, A. Karwath, F. Dijoux, and W. Burgard, "Activity-based estimation of human trajectories," *Robotics, IEEE Transactions on*, vol. 28, no. 1, pp. 234–245, 2012.

[50] M. Frank, "Positioning refinement algorithm," Sept. 18 2001. US Patent 6,292,751.

[51] F. Seco, J. Prieto, J. Guevara, *et al.*, "Indoor pedestrian navigation using an ins/ekf framework for yaw drift reduction and a foot-mounted imu," in *Positioning Navigation and Communication (WPNC), 2010 7th Workshop on*, pp. 135–143, IEEE, 2010.

[52] R. E. Kalman, "A new approach to linear filtering and prediction problems," *Journal of Fluids Engineering*, vol. 82, no. 1, pp. 35–45, 1960.

[53] R. E. Kalman and R. S. Bucy, "New results in linear filtering and prediction theory," *Journal of Fluids Engineering*, vol. 83, no. 1, pp. 95–108, 1961.

[54] S. Shin, C. Park, J. Kim, H. Hong, and J. Lee, "Adaptive step length estimation algorithm using low-cost mems inertial sensors," in *Sensors Applications Symposium, 2007. SAS'07. IEEE*, pp. 1–5, IEEE, 2007.

[55] E. Bishop and Q. Li, "Walking speed estimation using shank-mounted accelerometers," in *Robotics and Automation (ICRA), 2010 IEEE International Conference on*, pp. 5096–5101, IEEE, 2010.

[56] S. Yang, C. Mohr, and Q. Li, "Ambulatory running speed estimation using an inertial sensor," *Gait & posture*, vol. 34, no. 4, pp. 462–466, 2011.

[57] X. Zhu, F. Xu, E. Novak, C. C. Tan, Q. Li, and G. Chen, "Extracting secret key from wireless link dynamics in vehicular environments," in *INFOCOM, 2013 Proceedings IEEE*, pp. 2283–2291, IEEE, 2013.

[58] X. Zhu, Q. Li, and G. Chen, "Apt: Accurate outdoor pedestrian tracking with smartphones," in *INFOCOM, 2013 Proceedings IEEE*, pp. 2508–2516, IEEE, 2013.

[59] D. Alvarez, R. C. González, A. López, and J. C. Alvarez, "Comparison of step length estimators from weareable accelerometer devices," in *Engineering in Medicine and Biology Society, 2006. EMBS'06. 28th Annual International Conference of the IEEE*, pp. 5964–5967, IEEE,

2006.

[60] Y. Hatano, "Use of the pedometer for promoting daily walking exercise," *International Council for Health, Physical Education, and Recreation*, vol. 29, no. 4, pp. 4–8, 1993.

[61] H. Weinberg, "Using the adxl202 in pedometer and personal navigation applications," *Analog Devices AN-602 application note*, 2002.

[62] J. Scarlett, "Enhancing the performance of pedometers using a single accelerometer," *Application Note, Analog Devices*, 2007.

[63] V. Renaudin, M. Susi, and G. Lachapelle, "Step length estimation using handheld inertial sensors," *Sensors*, vol. 12, no. 7, pp. 8507–8525, 2012.

[64] R. Levi and T. Judd, "Dead reckoning navigational system using accelerometer to measure foot impacts," Dec. 10 1996. US Patent 5,583,776.

[65] S.-W. Lee and K. Mase, "Recognition of walking behaviors for pedestrian navigation," in *Control Applications, 2001.(CCA'01). Proceedings of the 2001 IEEE International Conference on*, pp. 1152–1155, IEEE, 2001.

[66] Y. Sun, Y. Zhao, and J. Schiller, "An indoor positioning system based on inertial sensors in smartphone," in *Wireless Communications and Networking Conference (WCNC), 2015 IEEE*, pp. 2221–2226, IEEE, 2015.

[67] G. Wolf, A. Carmichael, and K. Kelly, "The quantified self. ted," 2010.

[68] P. Carmona, D. Nunes, D. Raposo, D. Silva, J. S. Silva, and C. Herrera, "Happy hour-improving mood with an emotionally aware application," in *Innovations for Community Services (I4CS), 2015 15th International Conference on*, pp. 1–7, IEEE, 2015.

[69] M. Swan, "The quantified self: Fundamental disruption in big data science and biological discovery," *Big Data*, vol. 1, no. 2, pp. 85–99, 2013.

[70] J. Rooksby, M. Rost, A. Morrison, and M. C. Chalmers, "Personal tracking as lived informatics," in *Proceedings of the 32nd annual ACM conference on Human factors in computing systems*, pp. 1163–1172, ACM, 2014.

[71] J.-O. Nilsson, D. Zachariah, I. Skog, and P. Händel, "Cooperative localization by dual foot-mounted inertial sensors and inter-agent ranging," *arXiv preprint arXiv:1304.3663*, 2013.

[72] J. Majumder, I. Zerin, C. P. Tamma, S. Ahamed, R. O. Smith, *et al.*, "A wireless smart-shoe system for gait assistance," in *Biomedical Conference (GLBC), 2015 IEEE Great Lakes*, pp. 1–4, IEEE, 2015.

[73] A. Bränzel, C. Holz, D. Hoffmann, D. Schmidt, M. Knaust, P. Lühne, R. Meusel, S. Richter, and P. Baudisch, "Gravityspace: tracking users and their poses in a smart room using a pressure-sensing floor," in *Proceedings of the SIGCHI Conference on Human Factors in Com-*

puting Systems, pp. 725–734, ACM, 2013.

[74] A. Smith, A. Doucet, N. de Freitas, and N. Gordon, *Sequential Monte Carlo methods in practice*. Springer Science & Business Media, 2013.

[75] P. Del Moral, "Non-linear filtering: interacting particle resolution," *Markov processes and related fields*, vol. 2, no. 4, pp. 555–581, 1996.

[76] Z. Khan, T. Balch, and F. Dellaert, "An mcmc-based particle filter for tracking multiple interacting targets," in *Computer Vision-ECCV 2004*, pp. 279–290, Springer, 2004.

[77] M. Klaas, N. De Freitas, and A. Doucet, "Toward practical n2 monte carlo: the marginal particle filter," *arXiv preprint arXiv:1207.1396*, 2012.

[78] P. Del Moral, A. Doucet, A. Jasra, *et al.*, "On adaptive resampling strategies for sequential monte carlo methods," *Bernoulli*, vol. 18, no. 1, pp. 252–278, 2012.

[79] I. M. Rekleitis, "A particle filter tutorial for mobile robot localization," *Centre for Intelligent Machines, McGill University, Tech. Rep. TR-CIM-04-02*, 2004.

[80] J. Hightower and G. Borriello, "Particle filters for location estimation in ubiquitous computing: A case study," in *UbiComp 2004: Ubiquitous Computing*, pp. 88–106, Springer, 2004.

[81] S. H. Shin and C. G. Park, "Adaptive step length estimation algorithm using optimal parameters and movement status awareness," *Medical engineering & physics*, vol. 33, no. 9, pp. 1064–1071, 2011.

[82] Z. Tian, X. Fang, M. Zhou, and L. Li, "Smartphone-based indoor integrated wifi/mems positioning algorithm in a multi-floor environment," *Micromachines*, vol. 6, no. 3, pp. 347–363, 2015.

[83] A. Farshad, J. Li, M. K. Marina, and F. J. Garcia, "A microscopic look at wifi fingerprinting for indoor mobile phone localization in diverse environments," in *Indoor Positioning and Indoor Navigation (IPIN), 2013 International Conference on*, pp. 1–10, IEEE, 2013.

[84] R. S. Campos, L. Lovisolo, and M. L. R. de Campos, "Wi-fi multi-floor indoor positioning considering architectural aspects and controlled computational complexity," *Expert systems with applications*, vol. 41, no. 14, pp. 6211–6223, 2014.

[85] N. Marques, F. Meneses, and A. Moreira, "Combining similarity functions and majority rules for multi-building, multi-floor, wifi positioning," in *Indoor Positioning and Indoor Navigation (IPIN), 2012 International Conference on*, pp. 1–9, IEEE, 2012.

[86] E. Foxlin, "Pedestrian tracking with shoe-mounted inertial sensors," *Computer Graphics and Applications, IEEE*, vol. 25, no. 6, pp. 38–46, 2005.

[87] W. T. Faulkner, R. Alwood, D. W. Taylor, and J. Bohlin, "Altitude accuracy while tracking pedestrians using a boot-mounted imu," in *Position Location and Navigation Symposium*

(PLANS), 2010 IEEE/ION, pp. 90–96, IEEE, 2010.

[88] S. Beauregard, "Omnidirectional pedestrian navigation for first responders," in *Positioning, Navigation and Communication, 2007. WPNC'07. 4th Workshop on*, pp. 33–36, IEEE, 2007.

[89] J. H. Bergmann, R. E. Mayagoitia, and I. C. Smith, "A portable system for collecting anatomical joint angles during stair ascent: a comparison with an optical tracking device," *Dynamic Medicine*, vol. 8, no. 1, p. 3, 2009.

[90] A. Protopapadaki, W. I. Drechsler, M. C. Cramp, F. J. Coutts, and O. M. Scott, "Hip, knee, ankle kinematics and kinetics during stair ascent and descent in healthy young individuals," *Clinical Biomechanics*, vol. 22, no. 2, pp. 203–210, 2007.

[91] T. Waber, W. Pahl, M. Schmidt, G. Feiertag, S. Stufler, R. Dudek, and A. Leidl, "Flip-chip packaging of piezoresistive barometric pressure sensors," in *SPIE Microtechnologies*, pp. 87632D–87632D, International Society for Optics and Photonics, 2013.

[92] D. Banerjee, S. K. Agarwal, and P. Sharma, "Improving floor localization accuracy in 3d spaces using barometer," in *Proceedings of the 2015 ACM International Symposium on Wearable Computers*, pp. 171–178, ACM, 2015.

[93] Q. Xu, R. Zheng, and S. Hranilovic, "Idyll: indoor localization using inertial and light sensors on smartphones," in *Proceedings of the 2015 ACM International Joint Conference on Pervasive and Ubiquitous Computing*, pp. 307–318, ACM, 2015.

List of Figures

1.1 According to the real-time video, the sport assistance software SIMI Scout records the player's position as well as moving trajectory, in order to provide the reliable data support for the coach when tactics analysis and decision making. This is an instance of the vision-based positioning approach. 2

1.2 The comparison of accuracy among different positioning schemes 3

1.3 The effect of double integrals of the acceleration measured by commercial IMU. The red square is the real walking path whose side-length is 10 meters; the other 4 curves are the trajectories calculated by double integral. The drifts are rather serious. 5

1.4 The raw acceleration recorded by IMU when pedestrian is walking. A volunteer holds the accelerometer in hand and walks for 10 steps. The plotted data is the module of the accelerations in all 3 axes. It is remarkable that each impulse is corresponding to a single step. 6

2.1 The general view of the positioning system 10

2.2 The workflow of developing the positioning system. Foremost it is the preparation stage to make acquainted with the current positioning methods and theories. The most crucial stage is developing the novel mathematical models for step length estimation so that the accuracy for positioning could be improved substantially. Lastly a set of real-time software based on smartphones is implemented as the final products. 11

2.3 The accelerometer samples data in its own coordinate system (red). The raw data need to be transformed to the earth coordinate (blue). 12

2.4 The positive directions of 3 axes of smartphone. 13

2.5 A simplified schematic diagram for a single axial mechanical accelerometer. The magnitude of acceleration in the sensitive direction can be calculated by the variation in the spring's length. The principle in the electronic accelerometer is similar. . . . 14
2.6 A simplified schematic diagram for a tri-axial accelerometer 15
2.7 A simplified schematic diagram for a MEMS gyroscope in 2D view 16
2.8 The app "Meine Sensors" is used for recording the data from the sensors in iOS devices. 19
2.9 An example to illuminate what the correct rotation angles are, when smartphone tilts 20
2.10 A screenshot of the test app which is used for measuring and calculating the proper accelerations of smartphone. It measures the accelerations in the device's own current coordinate system and transforms them to the standard earth-fixed coordinate system. The 3 values with 3 colors on the screen indicate the tri-axial accelerations after coordinate transform and elimination from the gravitational component. The 3 curves below are plotted from them. The directions of the 3 axes are previously explained in Fig. 2.4. During test, when the smartphone spins freely, as long as its barycenter doesn't move, the displayed accelerations' values and their curves would never vary sharply. Because the function of this test app is rather deficient, it is not publicized in App Store. 22

3.1 To determine which component of acceleration plays the most crucial role in the step recognition. A group of experiments are designed. While the volunteer is walking, the inertial sensor is held in hand and attached on shoe respectively in order to observe the different acceleration components according to the different attach positions. The results are compared in Fig. 3.2. 24
3.2 Comparison between holding inertial sensor in different positions. The upper figure is taking it in hand, from curves it is obvious that the acceleration in vertical direction (z, blue) are more remarkable; the lower figure is sticking it on shoe that the signal in anterior-posterior direction (y, green) counts more. 24
3.3 The operation of Zero Velocity Compensation (ZVC) 26
3.4 The screenshot of the test app for 3 filters 27
3.5 The effect of the Moving Average Filter in off-line simulation. The vertical accelerations while pedestrian is walking are recorded. With the Moving Average Filter the jitters in raw data have been eliminated to some extent. 29
3.6 The effects of Moving Average Filter 30

3.7 Searching the breakpoints by Moving Variance Analysis. The active domains for vertical (blue) and anterior-posterior (green) accelerations are calculated by the variance analysis respectively. Then the valid phase for pure walking is determined by their intersection set. Therefore not only the disordered data when walking pattern transforms can be eliminated, but also the abnormal gaits such as marking time and lateral shift could be differentiated from normal walking because their accelerations in both directions are not coincide. 32

3.8 The effect of Sensors Fusion in terms of heading angle 35

3.9 Identifying the turning points by Moving Variance Analysis 35

3.10 The flow chart for azimuth measurement and turn action recognition. Usually the azimuth results from the data fusion of gyroscope and magnetometer. If the EMI is too severe, gyroscope would support the azimuth system independently. When magnetometer is stable, the output can provide an initial orientation and offset the drift of gyroscope timely. 36

3.11 The map of the corridor in our institute. A pedestrian walks along the green line, from the door at up-right corner (Point 1) through the corridor to the door at up-left corner (Point 8). In this 136 meters long distance, totally 8 breakpoints are involved: 6 stop points with red sign (including start and end points) and 2 turning points with blue sign. 38

3.12 By mean of the data measured by the magnetometer and the gyroscope, the breakpoints results from turn actions are searched (as Point 3 and 6 in Fig. 3.11) according to Moving Variance Analysis. 39

3.13 The effect of the breakpoints searching 40

3.14 The oscillation in the vertical acceleration is generated by walking. Each step corresponds to a cycle of wave. When one foot strikes the ground with the most force, the wave reaches its peak; a trough is detected when a foot swings over the contralateral leg. 41

3.15 An instance of acceleration data after prophase filters. It is still rather difficult to recognize every single step accurately. Certain further processes are still necessary. 42

3.16 The schematic diagram for Kalman Filter The squares represent matrices. The ellipses represent multivariate normal distributions (with the mean and covariance matrix enclosed). The unenclosed values are vectors. 44

3.17 The flow chart of the Kalman Filter 46

3.18 A segment of acceleration signals are processed by the Kalman Filter. The input signal is after the Moving Average Filter, while the output is after the Kalman Filter 47
3.19 The effects of Moving Average Filter 47
3.20 The peak and trough of the ith step are identified by the dynamic thresholds 49
3.21 The flow chart of the algorithm for removing potential double peaks within a single step wave cycle; for troughs is similar. 51
3.22 When a jitter happens, double peaks may be recorded within a single wave cycle. The arrays *peak*[] and *trough*[] store the indexes of every peak and trough detected. (a) is for the situation, peak first, then trough; while (b) is for trough first and then peak. 52
3.23 The screenshot of the demo app for step recognition 53
3.24 The effect of Model Wave Simulation Algorithm 55

4.1 The relation between step length and frequency. According to the experiment results from [44], the step length is proportional to the step frequency, which can be applied to estimate the step length. 59
4.2 To develop the step length model, a large number of experiments are implemented by volunteer. The step length and frequency are calibrated by measuring tape and metronome. The acceleration data are collected by smartphone. 63
4.3 The step lengths are adjusted by the tags on the measuring tape. 63
4.4 The sampled data during the experiments 64
4.5 With the step length 0.4 m, the 8 items vary with the different frequencies 65
4.6 With the step length 0.5 m, the 8 items vary with the different frequencies 66
4.7 With the step length 0.6 m, the 8 items vary with the different frequencies 66
4.8 With the step length 0.7 m, the 8 items vary with the different frequencies 67
4.9 With the step length 0.8 m, the 8 items vary with the different frequencies 67
4.10 With the step length 0.9 m, the 8 items vary with the different frequencies 68
4.11 Even with the identical gait (the same step length and frequency, the waveforms in the anterior-posterior direction change uncertainly. There is an obvious tendency that 2 adjacent peaks are merging gradually. 69
4.12 The relations between *magnitude*, *peak−trough difference*, *variance* and *step length* are demonstrated according to different *frequency* groups. 70
4.13 The fitting curves of *magnitude*, *peak − trough difference*, *variance* to *step length* are illustrated with different *frequency* ranges. 72

4.14 When step length is 0.7 m, the relation between $frequency$ and *variance* is demonstrated. Two quadratic functions can be fitted accordingly. 73
4.15 The comparison of RMSE among all of the available models 76
4.16 The comparison of RMSE in different step lengths among all of the available models 77
4.17 The comparison of the Average Deviation Rates among all of the available models . 78
4.18 The comparison of the Average Deviation Rates in different step lengths among all of the available models 79
4.19 The screenshot of the app "Walk Recorder". According to the mathematical model developed in this chapter, the length of each step is estimated and the whole walking distance is therefore calculated. Pedestrians can use the slider at the bottom to adjust their specified parameter. For the concision of the interface, the curves of the raw data (brown line) and the variance (white) could be hidden temporarily as the right figure. 80
4.20 The QR code and the launch image of the app "Walk Recorder" 81

5.1 All sorts of fitness tracker devices enable people to quantify their exercises. 84
5.2 A popular fitness app names Runtastic. It tracks runner by GPS. 85
5.3 Numerous smart bracelets and watches burst onto the scene in recent years. 86
5.4 The illustration of the digital shoes system. With the feet-mounted IMU the positions of firemen are tracked in real-time. 87
5.5 For each of the 78 running experiments, the accelerations in y and z-directions are recorded and processed. This is one of the samples when step length is 1.0 m and frequency 160 spm. 90
5.6 With 0.5 and 0.6 m as the step length, the 3 items (the magnitude, the peak-trough difference, the variance) vary with the step frequency. 91
5.7 With 0.7 and 0.8 m as the step length, the 3 items (the magnitude, the peak-trough difference, the variance) vary with the step frequency. 92
5.8 With 0.9 and 1.0 m as the step length, the 3 items (the magnitude, the peak-trough difference, the variance) vary with the step frequency. 93
5.9 The fitting curves of the relations between the step frequency and the 3 items (the magnitude, the peak-trough difference, the variance) are demonstrated according to the different step lengths. 94
5.10 When the running step length is 1.0 m, the relation between the step frequency and the variance is illustrated. Accordingly a quadratic function is fitted. 95

5.11 The screenshots of the beta app "Running Recorder". With this app based on iPhone 6, the developed running step length estimation model is tested. In particular, the adjustment for the user specified parameter is performed by the slider designed at the bottom. Because this app implements merely a part of function of PDR and the algorithm for distinguishing the activities between walking and running is not added up, this app is not submitted to App Store until been perfected. 97

5.12 The comparison of the Average Deviation Rates among all of the available models . 99

5.13 The comparison of the Average Deviation Rates in different step lengths among all of the available models 99

5.14 The comparison of RMSE among part of the available models 101

5.15 The comparison of RMSE in different step lengths among part of the available models 101

6.1 An instance for the application of particle filter in the indoor positioning system. In this experiment a pedestrian walked from the door at the up-left corner to the door up-right (black line is the real route). In the process he stopped 6 times (include at the start and end points) and turned 6 times. Every red triangle represents a break-point and the whole walking process is divided into 10 segments. The substantial blue points are the particles being produced. Every positioning result after a step is indicated by a red point. The total distance for walking is 136 m. It takes this volunteer 194 steps with the average step length 0.70 m. 107

7.1 The Box-whisker Plots of 4 parameters with reference to 2 different human behaviors. Obvious is it that the intensities of body motion when walking and running are rather dissimilar. In the 4 figures above, the magnitude, the peak value, the peak-trough difference, and the variance are used as 4 different indicators for the motion intensity, in order to search the right parameter which plays the most crucial role in the differentiation between walking and running. 110

7.2 An instance using the inertial sensors network around the lower limbs to recognize the human behaviors of stair ascent and descent 112

7.3 The staircases of 2 forms in the building of my institute. In each of the 2 staircases, ascending and descending, a series of the experiments are implemented to seek the appropriate approach for floor detection. 112

7.4 A set of data collected while the volunteer goes upstairs in the zigzag staircase (the scenes in Fig. 7.3 (a)) 113

7.5 A set of data collected while the volunteer goes downstairs in the zigzag staircase (the scenes in Fig. 7.3 (a)) 114
7.6 A set of data collected while the volunteer goes upstairs in the spiral staircase (the scenes in Fig. 7.3 (b)) 114
7.7 A set of data collected while the volunteer goes downstairs in the spiral staircase (the scenes in Fig. 7.3 (b)) 115
7.8 The Box-whisker Plots of 4 indicators with reference to stair ascent and descent are compared. It is postulated that certain parameter would show remarkable disparity towards stair ascent and descent. In the 4 figures, the average peak values, average trough values, average peal-trough differences, and average variances, together with their statistical distributions are compared. Unfortunately from the 4 parameters analyzed above, there is no significant difference between both behaviors. 116
7.9 The relation between the varied atmospheric pressure and altitude 118
7.10 The screenshot of the app “Barometer” 118
7.11 The sampled atmospheric pressures and calculated altitude information of the stair ascent and descent experiments in the zigzag staircase (Fig. 7.3 (a)). 120
7.12 The sampled atmospheric pressures and calculated altitude information of the stair ascent and descent experiments in the spiral staircase (Fig. 7.3 (b)). 120

8.1 The arrangements of the ceiling lamps can be used for walking speed estimation . . 125

List of Tables

3.1 Comparison between Gyroscope and Magnetometer 33
3.2 The Interpretation of the Magnetic Heading Angles 38

4.1 The fitting equations of *magnitude* (m) to *step length* (s) in terms of the different *frequency* ranges 70
4.2 The fitting equations of *peak – trough difference* (d) to *step length* (s) in terms of the different *frequency* ranges 71
4.3 The fitting equations of *variance* (v) to *step length* (s) in terms of the different *frequency* ranges 71
4.4 The *frequency – variance* relations at different *step length*s 74
4.5 The comparison of RMSE among all available models 76
4.6 The comparison of Average Deviation Rates among all available models 77

5.1 The *frequency – variance* relations at different *step length*s 96
5.2 The comparison of Average Deviation Rates among all of the available models . . 98
5.3 The comparison of Average Deviation Rates among part of the available models . . 100

List of Publications

Sun, Y., Zhao, Y, & Schiller, J. An Autonomic Indoor Positioning Application based on Smartphone. In *Proceedings of the Wireless Communications and networking Conference (WCNC '14)*. IEEE, 2014.

Sun, Y., Zhao, Y, & Schiller, J. An Indoor Positioning System based on Inertial Sensors in Smartphone. In *Proceedings of the Wireless Communications and networking Conference (WCNC '15)*. IEEE, 2015.

Sun, Y., Wu, H., & Schiller, J. A Running Step Length Estimation Model for Position Tracking. In *Positioning, Navigation and Communication (WPNC), 2015 12th Workshop on*. IEEE, 2015.

Sun, Y., Wu, H., & Schiller, J. A Step Length Estimation Model for Position Tracking. In *Localization and GNSS (ICL-GNSS), 2015 International Conference on*. IEEE, 2015.

Wu, H., **Sun, Y.**, & Wolter, K. Analysis of the Energy-Response Time Tradeoff for Delayed Mobile Cloud Offloading. *ACM SIGMETRICS Performance Evaluation Review*.43(2),33-35. ACM, 2015.

Wu, H., Seidenstücker, D., **Sun, Y.**, Nieto, C.M., Knottenbelt, W. J., & Wolter, K. An Optimal Offloading Partitioning Algorithm in Mobile Cloud Computing. *Submitted*, 2015.

Wu, H., **Sun, Y.**, & Wolter, K. Energy-Efficient Decision Making for Mobile Cloud Offloading. *Submitted*, 2015.

About the Author